PIPTIDES: A NEW PEPTIDOMIMETIC DESIGN FOR BIOMOLECULAR INTERACTIONS

A Dissertation

by

MARITESS NOELLE VICTORIA ARANCILLO

Submitted to the Office of Graduate and Professional Studies of
Texas A&M University
in partial fulfillment of the requirements for the degree of

DOCTOR OF PHILOSOPHY

Chair of Committee,	Kevin Burgess
Members,	David Barondeau
	Coran Watanabe
	Thomas R. Ioerger
Head of Department,	Simon North

May 2021

Major Subject: Chemistry

ABSTRACT

Small molecule probe development is pivotal in biomolecular science. Peptidomimetics are generally interesting if they resemble peptides or protein-fragments and display biological activities. To achieve this, it is desirable that they have parameters such as conformational rigidity (relative to analogs peptides of a similar length), proteolytic stability, and the ability to display natural pharmacophores, *i.e.* amino acid side-chains. They must also be easily prepared on a solid phase.

This dissertation presents a new peptidomimetic design that we call *piptides*. Advantages of the design include efficient and accessible synthesis of oligomers featuring most natural amino acid side-chains, atom spacings that correspond to peptide main-chains, and enhanced rigidity relative to α-peptides, β-peptides and peptoids.

Solution-phase syntheses of the monomers and solid-phase routes to piptides were developed. Its physiochemical properties, which includes predicted physiological parameters, pH and proteolytic stabilities, CD, and NMR were also elucidated.

Illustrative application of piptides against protein-protein interaction (PPI) targets, specifically EGF•EGFR and uPA•uPAR, were explored. The Exploring Key Orientations, EKO, strategy was used to evaluate piptide candidates for this. Compounds were found to have low micromolar values for IC_{50} and K_d for both studied PPI targets.

DEDICATION

To my family and friends who have continually encouraged and inspired me.

This is for all of you.

ACKNOWLEDGEMENTS

I would like to thank my research advisor, Dr. Kevin Burgess, for giving me the opportunity to work in his lab and for supervising me throughout the course of my Ph.D. study. I appreciate all the advice, encouragement, and patience with my research projects. I also want to thank my committee members Dr. David Barondeau, Dr. Coran Watanabe, and Dr. Thomas Ioerger, for their guidance and support throughout the course of this research.

To all my past and present colleagues from the Burgess group, thank you for the mentorship, collaborations, discussions, and support. Special thanks to Dr. Syed Muhammad Usama, Dr. Chen-Ming Lin, Dr. Zhengyang Jiang, Dr. Zhe Gao and Dr. Shaon Joy. Not only were they great colleagues, but they also turned into good friends whom I have relied on throughout this tumultuous journey.

Thanks to all my past professors and other department faculty and staff, whom I have encountered and worked with, for making my time at Texas A&M University a memorable experience. Special thanks to Jill Powers and Andrea Scott, for being patient, and for helping me with lab-related administrative work, and to Sandy Horton, for making my life as a graduate student a little bit easier.

Thanks to all the people I have befriended here in B/CS. Thanks to Isita, Trang, Hyeran, Sanjoy, Sayan and Elham for making my first few years of graduate school fun, interesting, and less stressful. Thanks to all the Filipino people I have met, especially to

Abby, Troy, Butch, KC, Kat, Aldrin, Samae, JC, Joan, Madz, and their respective kids, for the friendships, food, and the familiarity of home.

I am pleasantly surprised with the past friendships that I have maintained and for the new ones that blossomed throughout this time. To Octet and my undergraduate friends, thank you for the long-lasting friendships despite the distance. Thank you to my Shawol friends; I never would have thought that I would make friends online, living in different parts of the world, and yet, here we are. To Dawn, thank you for being my exercise buddy and for the endless conversations. And to my forever bff Celine, thank you for the unwavering and never-ending support, love, encouragement, and patience.

Lastly, thank you to Mommy, Papa, Ate Pepot and Alex, Ate Beng, Ate Mercy, and the rest of my family, for being patient and understanding, and for encouraging, inspiring, and believing in me.

CONTRIBUTORS AND FUNDING SOURCES

Contributors

This work was supervised by a dissertation committee consisting of Professor Kevin Burgess (advisor) and Professors David Barondeau and Coran Watanabe of the Department of Chemistry and Professor Thomas Ioerger of the Department of Computer Science & Engineering.

Development of the synthesis of piptides and synthesis of some pip acids in Chapter 2 were done with the help of Dr. Jaru Taechalertpaisarn. Synthesis of compounds **12** in Chapter 5 were accomplished by Dr. Chen-Ming Lin. The surface plasmon resonance studies were done in the protein interaction core at the Institute of Biosciences and Technology-Texas A&M University in Houston and were conducted by Dr. Xiaowen Liang for Chapter 4 and Dr. Kelly Churion for Chapter 5.

All other work conducted for the dissertation was completed by the student independently.

Funding Sources

This work was made possible by Texas A&M University (RP180875), the Robert A. Welch Foundation (A-1121), the Cancer Prevention and Research Institute of Texas (RP170144 and RP180875), the Department of Defense – Breast Cancer Research Program Breakthrough Award (BC141561), the National Institutes of Health (R01EY029695) and the National Science Foundation (CHE1608009). The NMR

instrumentation at Texas A&M University was supported by the Texas A&M University System and a grant from the National Science Foundation (DBI-9970232).

Its contents are solely the responsibility of the authors and do not necessarily represent the official views of Texas A&M University, the Robert A. Welch Foundation, the Cancer Prevention and Research Institute of Texas, the Department of Defense, the National Institutes of Health, or the National Science Foundation.

NOMENCLATURE

CD	Circular Dichroism
EGF	Epidermal Growth Factor
EGFR	Epidermal Growth Factor Receptor
EKO	Exploring Key Orientations
EKOS	Exploring Key Orientations on Secondary-structures
ELISA	Enzyme-Linked Immunosorbent Assay
ELSD	Evaporative Light Scattering Detector
FP	Fluorescence Polarization
HBTU	(2-(1*H*-Benzotriazol-1-yl)-1,1,3,3-tetramethyluronium hexafluorophosphate
HPLC	High-Performance Liquid Chromatography
IC_{50}	Half-maximal Inhibitory Concentration
K_i	Inhibitor Constant
K_d	Equilibrium Dissociation Constant
NMR	Nuclear Magnetic Resonance
PBS	Phosphate-Buffered Saline
PPI	Protein-Protein Interaction
RMSD	Root-Mean-Square Deviation
SPR	Surface Plasmon Resonance
TFA	Trifluoroacetic Acid

TGFα	Transforming Growth Factor Alpha
uPA	Urokinase-type Plasminogen Activator
uPAR	Urokinase-type Plasminogen Activator Receptor
UV	Ultraviolet

TABLE OF CONTENTS

Page

LIST OF FIGURES

Page

LIST OF TABLES

Page

1. INTRODUCTION

Small molecule probes that perturb biomacromolecular function are useful in medicinal science.[1-3] High throughput screening can be used to obtain such probes, but these strategies are not always fruitful, justifiable, or affordable.[4-5] Screening becomes more efficient if it features chemotypes that can be quickly, reliably, and inexpensively assembled into diverse libraries using combinatorial methods.[6] Such strategies are optimally useful if they can be performed by researchers possessing only basic synthetic skills. Further streamlining may be achieved using "privileged chemotypes" that have a bias to positively interact with the target biomacromolecules.[7]

1.1. Peptides

Peptides are privileged chemotypes because they interact with biomolecules using native pharmacophores (Figure 1-1a). Cyclization[8-9] and *N*-methylation[10-12] strategies can make them even better probes by rendering them more rigid, proteolytically stable, and cell permeable,[10, 13-14] but these modifications require more synthetic expertise.

Useful peptidomimetics, aside from being proteolytically stable should be easily accessible with all the side-chains corresponding to the natural α-amino acids, *i.e.* not just the ones that are easy to make. The atom correspondence to the oligoamide backbone of peptides, or *periodicity*, should be somewhat similar, and, ideally, the mimic should have more rigidity than α-peptides to reduce the entropic cost of binding protein it targets.

1.2. Peptoids

Two of the most common peptidomimetics today are peptoids and β-peptides. Peptoids were first developed by Zuckerman and co-workers (Figure 1-1b).[15] Side-chains in peptoids are connected to the main-chain nitrogen atoms instead of the Cα. This removes all the secondary amide hydrogens, hence the secondary structure motifs of peptides and peptoids must be different. Peptoids lack main-chain hydrogen bonding donors, and they are not easily denatured by solvent, temperature, and other agents. They also resist proteolysis and tend to be more cell permeable than peptides. Peptoids can be made easily using the submonomer method,[16] which introduces the side chains via primary amines; this is an attribute because a diversity of amines are available.[17]

Despite their indisputable popularity, there are problems using peptoids. However, they tend to be *more* flexible than peptides, which must lose more entropy to interact with a target, hence rarely bind with dissociation constants <1 μM.[18-21] Analogs with enhanced rigidity are known (*e.g.* cyclic[22-26] and ones with α-chiral centers[27]) but making them requires well-developed synthetic skills. Moreover, population of both *cis* and *trans* conformers of tertiary amide bonds, of which there are often many, complicate peptoid NMR spectra.

1.3. β-Peptides

β-Peptides, first studied by Seebach[28] and Gellman,[29] are oligomers of β-amino acids (Figure 1-1c). There are two main types of β-peptides: β^2-peptides that have the "side chain" next to the carbonyl group, and β^3-peptides with "side chains" next to the amine

group. Both types, like peptoids, are resistant to proteolysis, and synthetically accessible. Some β-peptides can form secondary structures due to the gauche conformation favored between the α- and β-carbons, *e.g.* stable helices in solution featuring hydrogen bonding in a favorable ring size. Disadvantages of these peptidomimetics involve harder synthesis, due to the various possible "side-chains" that could be bonded to the β-carbon and retaining chirality, and they tend to be more flexible than α-peptides. An exception is systems comprised of α,β-amino acids (*eg* cyclic systems), but these cannot be readily functionalized with the full complement of side chains corresponding to genetically encoded amino acids.[30-31]

Despite the limitations of peptoids and β-peptides, they are still widely used today, 20 years after conception. Nevertheless, we hypothesize, better designs with complementary properties can be developed for systems featuring piperazine-type amino acids, which will be referred to as *piptides* here (Figure 1-1d).

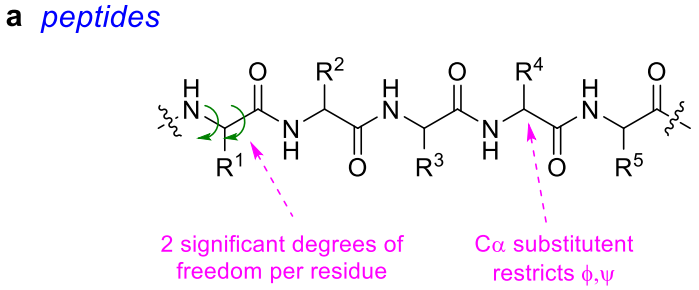

Figure 1-1. Comparison of **a** peptides, **b** peptoids, **c** β-peptides, and **d** piptides. Reprinted with permission from ref 112. Copyright 2020 Wiley-VCH Verlag GmbH & Co. KGaA, Weinheim.

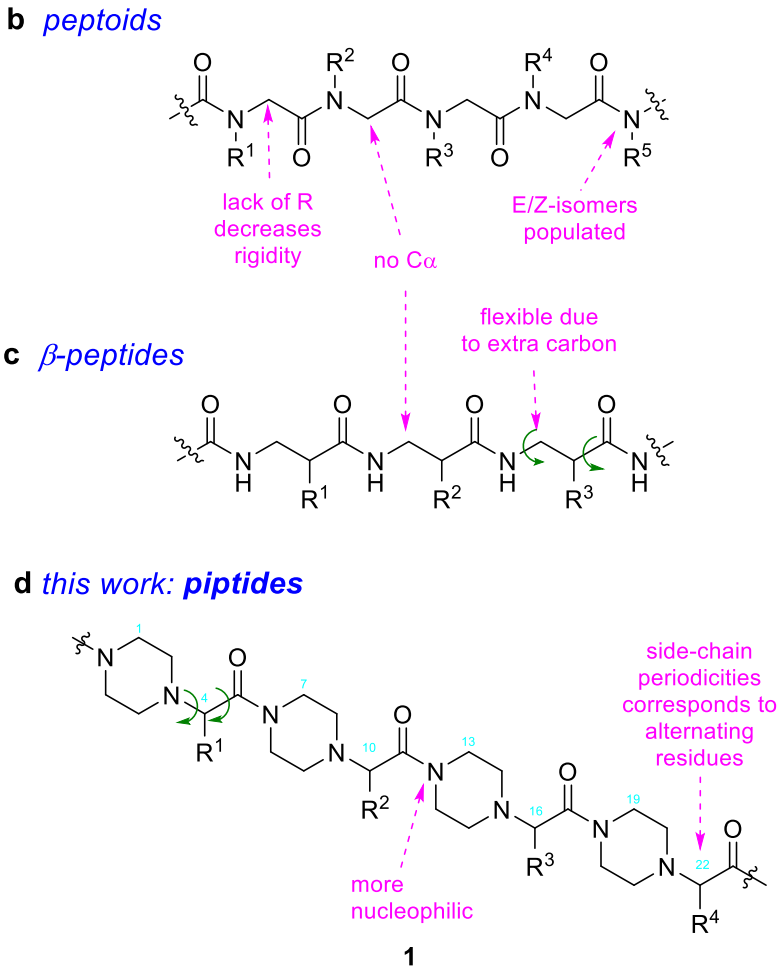

Figure 1-1. Continued.

1.4. Exploring Key Orientations

One compelling reason for our group to develop piptides is that they may be used as chemotypes in our method *Exploring Key Orientations (EKO)* to design molecules to perturb protein-protein interactions (PPIs).[32] EKO involves: (i) molecular dynamics on the scaffold with three methyl side chains (three amino acid side chains are sufficient to perturb PPIs[33]) to establish a large number of accessible conformations; (ii) expression of

the results as a database of side-chain orientations based on *C*α-*C*β vectors; (iii) formation of a similar database of side-chain orientations for one or more PPIs; and, (iv) data mining to determine if a conformer of the small molecule can present side-chains in an orientation that resembles three residues on a protein in a PPI. A hit, which implicates a conformation with highly superimposable orientations of side-chains with the target protein, indicates a candidate to perturb the PPI.

A related strategy that will also be used is called *Exploring Key Orientations on Secondary-structures (EKOS).*[34] It uses the same approach but with a database of side-chain orientations in ideal secondary structures rather than in PPIs. It is important to understand that the EKO strategy is performed using a scaffold with three methyl side-chains, which is a representative and may overlay on *C*α-*C*β vectors of any protein side-chain (except Gly), and an orientation enforced by the protein-binding partner in a PPI.

Overall, this dissertation describes the synthesis and development of piptides. General syntheses of pip acid monomers, piptides and analogues, and elucidation of their physiochemical properties are discussed in Chapter 2 and 3, respectively. The ability of piptides to disrupt protein-protein interactions in experiments guided by the EKO process developed in these laboratories were then discussed in Chapters 4 (EGF•EGFR) and 5 (uPA•uPAR).

2. SYNTHESES OF PIPTIDES*

2.1. Pip acid

Piptides can be constructed from fragments **2,** *pip acids* (Figure 2-1). Prior to our work there were only two synthetic strategies to a small number of pip acids, and both rendered only *racemic* material.[35-36]

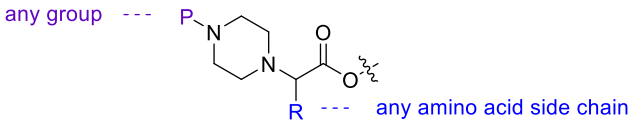

2
pip acid

Figure 2-1. Pip acid general structure **2**. Reprinted with permission from ref 112. Copyright 2020 Wiley-VCH Verlag GmbH & Co. KGaA, Weinheim.

Tri(4-nitrobenzene sulfonate) {tri-nosyl or tri-^{4}Ns} **3** had been reacted with primary arylamines under microwave conditions to give *N*-aryl,*N*-^{4}Ns-piperazines.[37] Compounds **3** could be converted into a variety of *N*-^{4}Ns-pip acid esters **4**, then selectively deprotected to their *C*-free *N*-protected forms **5** (and, under other conditions, to *C*-protected *N*-free analog **6**, *vide infra*; Scheme 2-1). These *N*-protected pip acids tend to be

*Reprinted with permission from "Piptides: New, Easily Accessible Chemotypes For Interactions With Biomolecules" by Maritess Arancillo, Jaru Taechalertpaisarn, Xiaowen Liang, and Kevin Burgess, 2020. *Angew. Chem., Int. Ed.*, DOI: 10.1002/anie.202015203, Copyright 2020 by Wiley-VCH Verlag GmbH & Co. KGaA, Weinheim.

solids. They can be made from amino acid building blocks with protected-functionalized side chains, *i.e.* exactly the ones commonly used in the FMOC approach to peptides,[38-39] and appropriate for solid-phase syntheses on trifluoroacetic acid (TFA)-sensitive resins. This is important because incorporation of functionalized side chains into peptidomimetic chemotypes can be time-consuming and experimentally tedious.

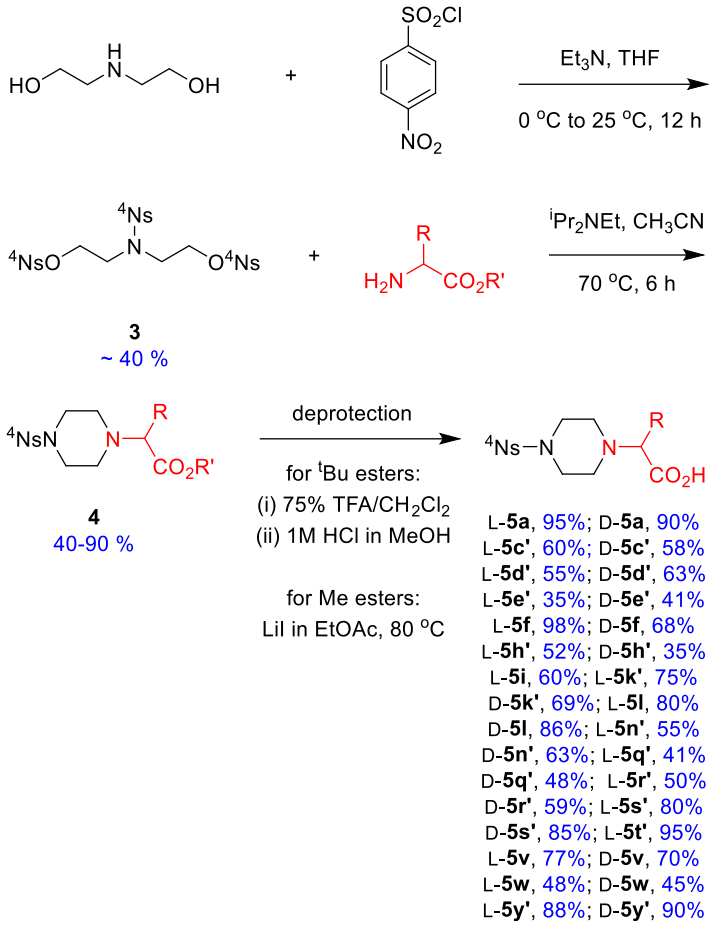

Scheme 2-1. Generalized syntheses of pip acids. Lower case one-letter codes are used to delineate amino acid side chains (R) and relate them to the closest amino acid; primed letters indicate protected side chains (*e.g.* d' for the $–CH_2CO_2{}^tBu$ of Asp and k' for the $–(CH_2)_4NHBoc$ of Lys). Reprinted with permission from ref 112. Copyright 2020 Wiley-VCH Verlag GmbH & Co. KGaA, Weinheim.

2.2. Solution phase syntheses

Denosylation of Phe- and Thr(O^{t}Bu)-derived pip acids L-**4f** and L-**4t'**, respectively, gave the piperazines **6** used to initiate trial solution phase syntheses. Several denosylation methods were investigated, and the conditions shown in Scheme 2-2 were the best found.

(2-(1*H*-Benzotriazol-1-yl)-1,1,3,3-tetramethyluronium hexafluorophosphate (HBTU)[40-42] was used to activate the *C*-free *N*-protected units **5** to give the *C*,*N*-diprotected dipiptides **7** then tripiptides **8** (Scheme 2-2a). Scheme 2-2b illustrates how piptides with repeating sequences can be made by dividing intermediates like **8**, selective deprotection of either terminus, then recombination.

2.3. Solid-phase syntheses

Solid-phase piptide syntheses may be guided by the following concepts. The protection strategy is similar to common peptide syntheses because side chain-protected amino acids appropriate for FMOC-peptide syntheses[38] are used to make the functionalized *N*-protected pip acid derivatives **5**. In that case, use of resins functionalized with TFA-sensitive handles allows successive couplings of side chain-protected pip acids with retention of their masking groups. Finally, cleavage of the target piptide with simultaneous side chain deprotection, could be achieved via treatment with scavenger cocktails containing TFA. Uncoupled, supported, piptide *N*-termini are better stained using the chloranil test[43] than via ninhydrin,[44-45] just as for peptides syntheses where Pro

is the *N*-terminal residue. Thus, visual chloranil tests indicate situations in which two or more coupling cycles are necessary to drive the reactions to completion. Denosylation of supported piptides (*cf* for supported peptides[46]), and the coupling reactions used to form them, may optionally be accelerated using microwave reactors (Scheme 2-3). Scheme 2-3 also illustrates how hybrids of piptides, and peptides can be produced easily by coupling α-amino acids to piptide *N*-termini, as in the synthesis of compounds **10** shown.

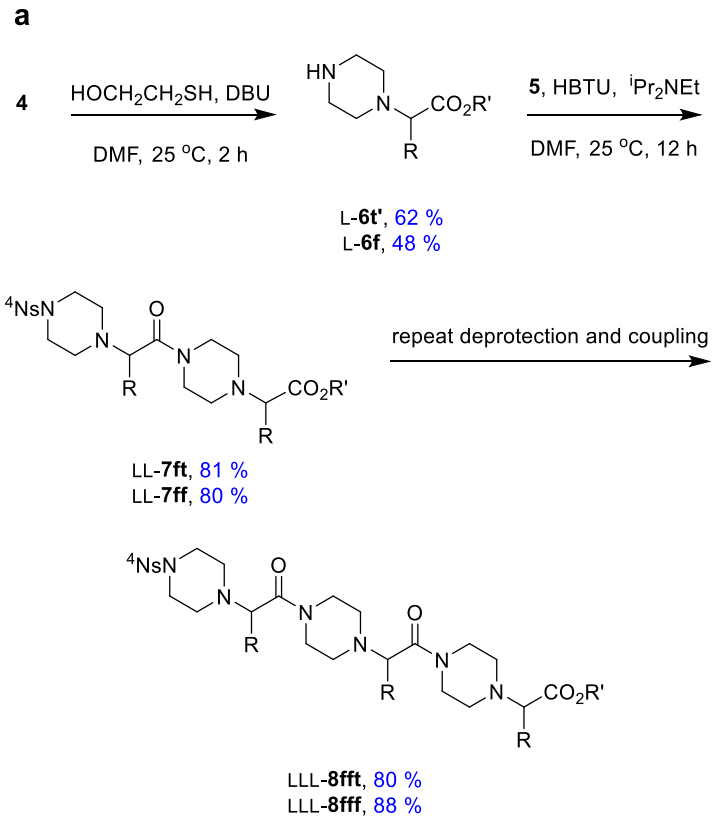

Scheme 2-2. a Linear, and **b** divergent-convergent solution phase syntheses of piptides. Reprinted with permission from ref 112. Copyright 2020 Wiley-VCH Verlag GmbH & Co. KGaA, Weinheim.

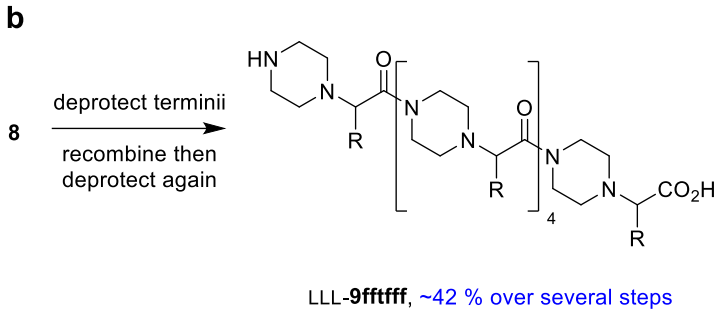

Scheme 2-2. Continued.

Isolated yields are indicated in Scheme 2-3, but these parameters are notoriously variable in solid-phase syntheses due to the small amounts of material cleaved from the support, losses in prep-HPLC purification, and because all yields based on support loading are hard to measure accurately. Analytical HPLC UV/ELSD analyses of crude materials from illustrative solid-phase syntheses are given in the Appendix; these data show that the purity of piptides cleaved from the resin is high. Moreover, solid-phase syntheses of piptides are not restricted to two or three repeat residues; Appendix Scheme A-1 shows preparation of a 9-mer piptide.

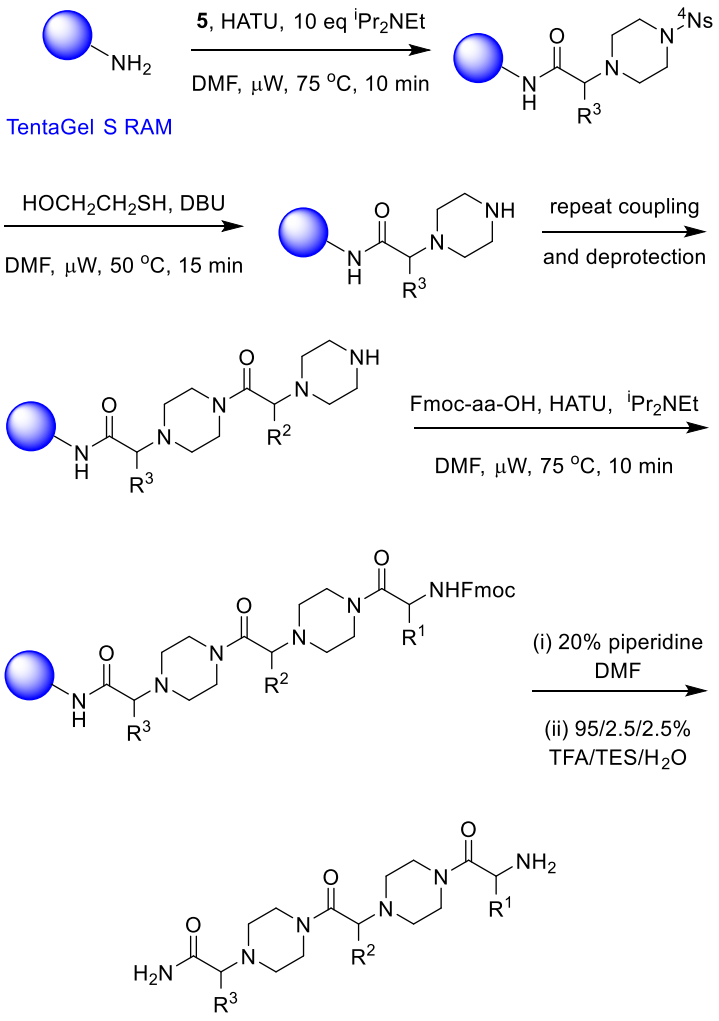

LLL-**10aaf**, 40%; LLL-**10aev**, 38%; LDL-**10eav**, 32%
LDL-**10vae**, 37%; LDL-**10ave**, 25%; DDD-**10eal**, 35%

Scheme 2-3. Illustrative solid-phase synthesis of piptides on TentaGel S-RAM resin (blue spheres). Reprinted with permission from ref 112. Copyright 2020 Wiley-VCH Verlag GmbH & Co. KGaA, Weinheim.

3. PHYSIOCHEMICAL PROPERTIES OF PIPTIDES*

3.1. Predicted Physiochemical Data

Table 3-1 shows predicted physiochemical data (QikProp)[47-48] for a structure LLL-**10aaa** (with all methyl side-chains). Physiochemical characteristics of piptides vary widely with their side-chain functionalities as expected, but LLL-**10aaa** represents the core framework, and this is relevant to application outlined below. That structure has a relatively low molecular mass and no rule-of-five violations. One of the attributes of amine pharmaceutical-candidates is that their equilibration between ammonium and free-base forms is conducive to cell permeation; similar equilibration might be expected for **10**. Moreover, there is also potential to optimize for cell permeability by varying the ammonium *N*-terminus.

Table 3-1. Predicted physiochemical properties of LLL-**10aaa** and its protonated form [LLL-**10aaa**]$^{3+}$ calculated using QikProp. Reprinted with permission from ref 112. Copyright 2020 Wiley-VCH Verlag GmbH & Co. KGaA, Weinheim.

parameter	*neutral*	*protonated*	*ideal for cell permeability*
MW	368.5	371.5	<500
log $P_{o/w}$	-3.8	-3.8	<5
rule-of-five violations	none	none	<5 HB donors; <10 HB acceptors
PSA (Å)	138.2	132.4	7-200
P Caco-2 (nm/s)	0.3	0.5	25-500

*Reprinted with permission from "Piptides: New, Easily Accessible Chemotypes For Interactions With Biomolecules" by Maritess Arancillo, Jaru Taechalertpaisarn, Xiaowen Liang, and Kevin Burgess, 2020. *Angew. Chem., Int. Ed.*, DOI: 10.1002/anie.202015203, Copyright 2020 by Wiley-VCH Verlag GmbH & Co. KGaA, Weinheim.

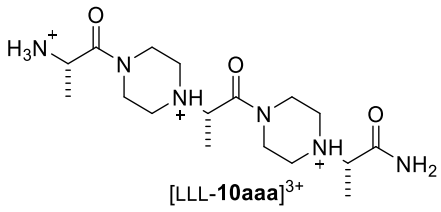

3.2. Protease and pH stability

Two experiments were performed to assess relative stabilities of piptides and peptides towards hydrolysis. To test enzymatic proteolysis, piptide LLL-**10fff** and the closely related peptide LLL-**11fff** (Figure 3-1a) were incubated at 37 °C in pH 7.4 PBS with Pronase® (a protease mixture used in proteomic studies).[49] The peptide degraded rapidly under these conditions ($t_{1/2}$ ~ 2 h), whereas the piptide showed no significant decomposition after 24 h (Figure 3-1b). To test for pH-mediated hydrolysis, the same piptide was maintained in aqueous media under acidic, basic, and neutral conditions; it showed essentially no decomposition at low pH but around 30 % decomposition was observed at pH 10 (Figure 3-1c).

Short piptide-containing sequences such as **10** would not be expected to fold into any preferred conformation in solution. Indeed, circular dichroism spectra collected for LLL-**10ysl** in methanol showed only very weak molar ellipticities, *i.e.* its CD spectrum was essentially flat (Appendix Figure A-1).

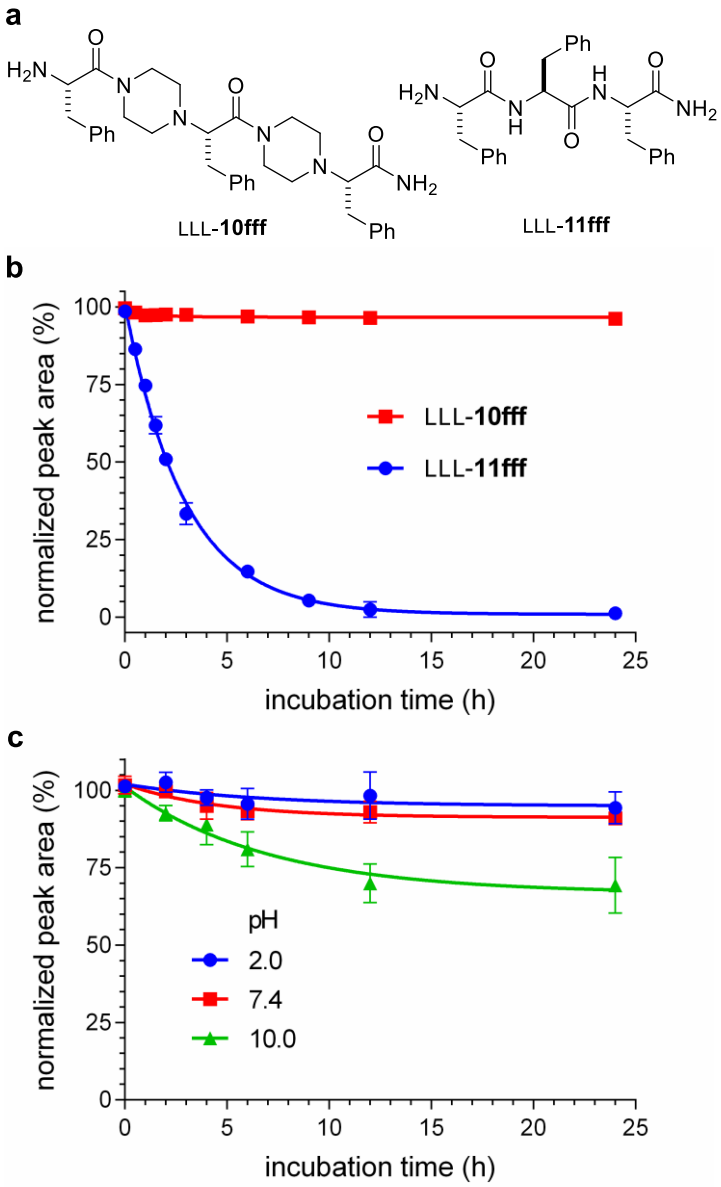

Figure 3-1. Hydrolytic stability of piptides. **a** Piptide **10fff** and peptide **11fff**. **b** Pronase®-mediated decomposition. **c** pH-dependent decomposition of **10fff** (HCl, PBS, and NaOH). Reprinted with permission from ref 112. Copyright 2020 Wiley-VCH Verlag GmbH & Co. KGaA, Weinheim.

Exploring Key Orientations on Secondary structures (EKOS)[34] was used to evaluate biases of preferred conformations of **10aaa**. In EKOS, conformations of the

mimic are simulated, preferred ones (within 3 kcal/mol of the lowest energy conformation identified) are systematically overlaid on ideal secondary structures according to their three *C*α – *C*β vectors, and the fit of the superimpositions are evaluated in terms of the root mean square deviations (RMSDs) of the six *C*α and *C*β coordinates involved. We have shown,[34, 50-51] superior secondary structure mimics overlay with RMSD values <0.5 Å. Figure 3-2 shows **10aaa** is an excellent mimic of strand-turn-strand, and parallel and antiparallel b-sheets. A Ramachandran plot (Appendix Figure A-2) shows preferred conformers of **10aaa** are concentrated in a narrow range of ϕ,ψ-bond angles, indicative of conformational rigidity.

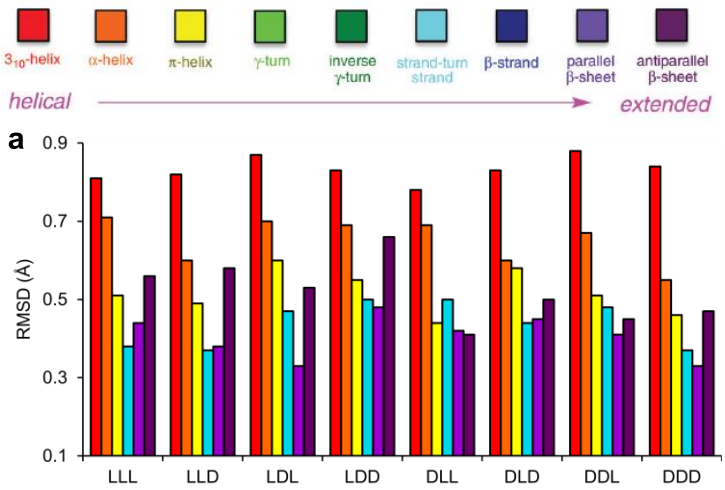

Figure 3-2. RMSD (Å) of the overlays of **10aaa** on each of the ideal secondary structures, organized **a** by stereochemistry or **b** by decreasing RMSD. No hits were observed for β-strands and γ-turns (regular or inverse), throughout. **c** Overlay of DDD-**10aaa** (gold) on a parallel β-sheet (blue), RMSD 0.34 Å. Reprinted with permission from ref 112. Copyright 2020 Wiley-VCH Verlag GmbH & Co. KGaA, Weinheim.

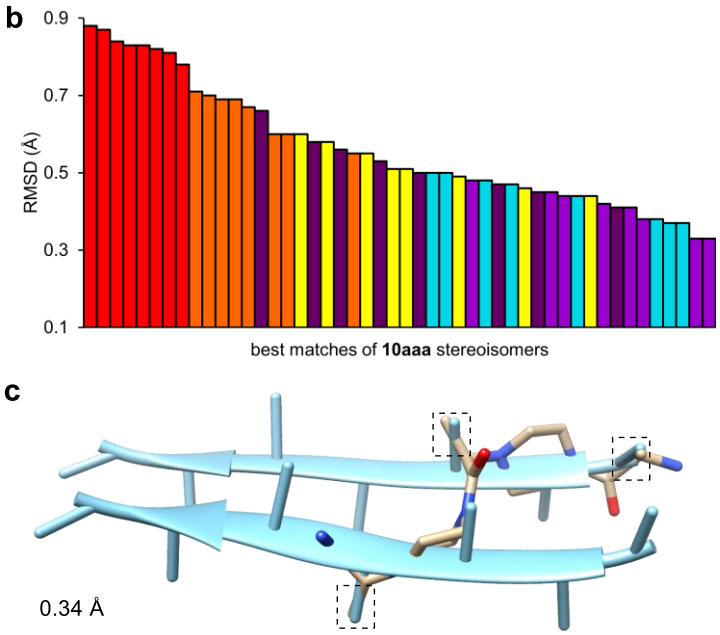

Figure 3-2. Continued.

4. PERTURBATION OF THE INTERACTION OF EGF WITH ITS RECEPTOR*

4.1. Introduction

Epidermal growth factor receptor (EGFR) is overexpressed at varying levels in most types of cancer cells.[52-55] High surface densities of EGFR favor dimerization, making cells overexpressing EGFR abnormally sensitive to stimulation by their complementary endogenous protein growth hormones (EGF and TGFα), hence promoting unconstrained cell growth.[56] For instance, secretion of TGFα is associated with various cancer types including breast, lung,[57] kidney, melanoma, liver,[58] and glioblastomas.[56] In general, there seems to be a causal link between increased EGF or TGFα expression and tumor development.[59] Conversely, blockade of EGFR suppresses tumor cell growth *in vitro* and *in vivo.*

EGFR antagonists used for cancer chemotherapy can be divided into "biologicals" (typically antibodies, *e.g.* cetuximab, panitumumab, and trastuzumab) that perturb ligand•EGFR interactions,[57, 60-64] and kinase inhibitors (*e.g.* gefitinib, erlotinib, lapatinib) that suppress signaling from the receptors.[61-62, 65-66] However, small molecule inhibitors of the EGF kinase domain are not ideal probes for EGFR-mediated signaling because they tend to inhibit other kinases. Furthermore, in the clinic, EGFR kinase inhibitors (and even humanized mAbs for this target) are vulnerable to intrinsic and acquired resistance.[63]

---

*Reprinted with permission from "Piptides: New, Easily Accessible Chemotypes For Interactions With Biomolecules" by Maritess Arancillo, Jaru Taechalertpaisarn, Xiaowen Liang, and Kevin Burgess, 2020. *Angew. Chem., Int. Ed.*, DOI: 10.1002/anie.202015203, Copyright 2020 by Wiley-VCH Verlag GmbH & Co. KGaA, Weinheim.

The non-ligated, "inactive" form of EGFR rests in an autoinhibited conformation. On introduction of TGFα or EGF, two of the same protein ligands bind two identical domains along the EGFR periphery causing conformational changes, but the EGFR•EGFR interface is maintained.[67-68] Mutagenesis of EGF and of TGFα have revealed key residues for interactions with EGFR. For instance, affinity between TGFα and EGFR seems to disproportionately rely on ^{42}Arg and ^{48}Leu of the ligand.[69] A molecular dynamics study[70] and X-ray crystallography (1MOX) has also revealed several residues of TGFα that are involved in hydrogen bonding and salt bridge formation with EGFR, including ^{44}Glu and ^{46}Ala.

In the current study, the EKO strategy[32] was used to evaluate piptide-based chemotypes for their potential to disrupt protein ligand•EGFR interactions. Briefly, EKO compares favored conformations of small molecules that present three amino acid sidechains, with PPI interface regions, based on degree of fit of side chain $C\alpha$ and $C\beta$ coordinates. Validation for the strategy has been reported in the context of the HIV-1 protease dimer,[32] the anti-thrombin dimer,[71] and PCSK9•LDLR.[72]

4.2. Results and Discussion

Here, EKO analyses indicated preferred conformers of chemotype **10** overlaid on EGF or TGFα at the TGFα•EGFR interface (Figure 4-1). Figures 4-1b – g illustrates different stereoisomers of **10aaa** overlaid well on ^{39}Val, ^{44}Glu, and ^{46}Ala, in both possible orientations (*i.e. N*-to-*C*, and *C*-to-*N*). Thus, Figure 4-1b shows the *C*-terminus of DLD-**10aaa** superimposed on ^{39}Val, whereas DDD-**10aaa** best matched its *N*-terminus on ^{39}Val

in Figure 4-1e. Observations such as these, where "*pseudo*-symmetrical" chemotypes, like **10,** overlay with either *N*-to-*C* polarity, are unsurprising because EKO considers *only* the side chain orientations and not the scaffold core.

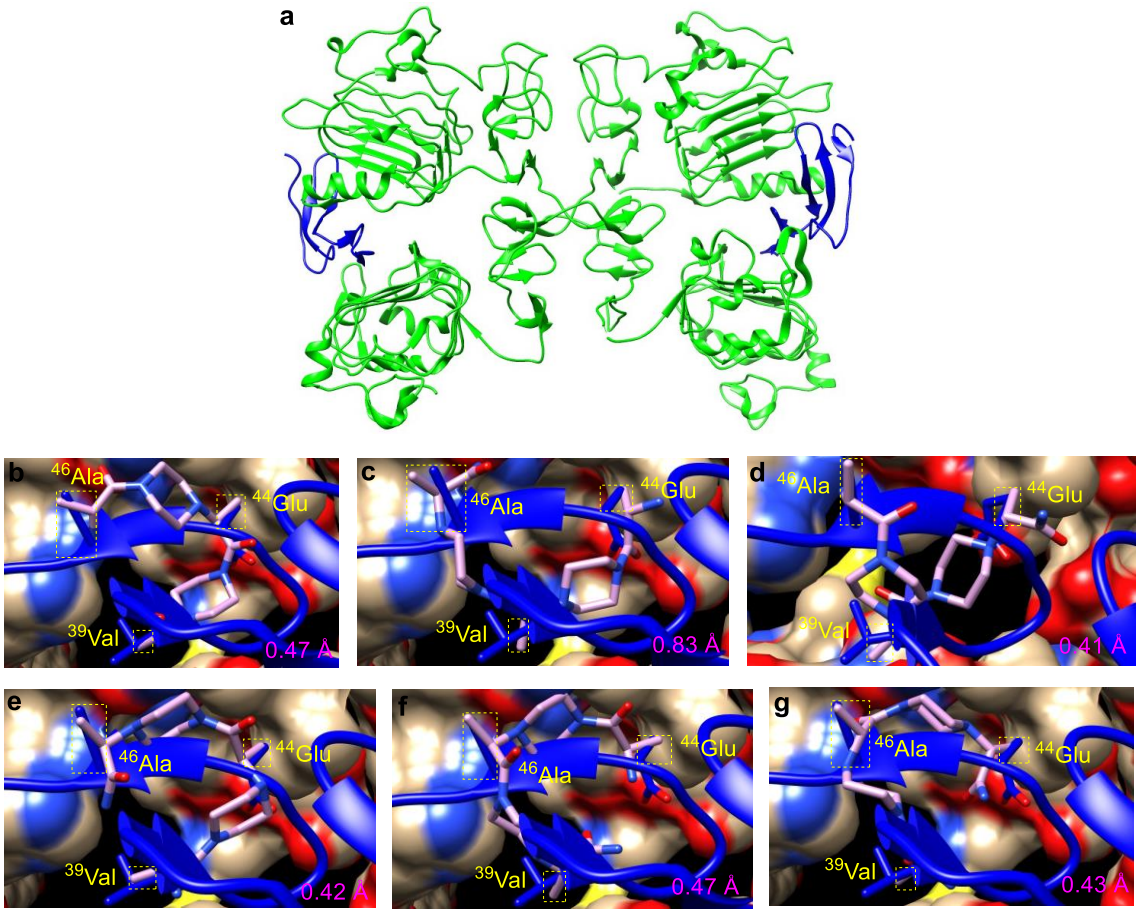

Figure 4-1. EKO analyses of piptide-based chemotypes on TGFα•EGFR. **a** TGFα•EGFR dimer interface (1MOX). **b-g** EKO implicated stereoisomers of **10aaa** overlaid on TGFα: ^{39}Val, ^{44}Glu, and ^{46}Ala. Note structure 1MOX indicates ^{44}Glu and ^{46}Ala are involved in *H*-bonding with EGFR. Figures in purple represent the root mean squared deviation of mimic and protein-ligand at the six Cα and Cβ coordinates involved. Reprinted with permission from ref 112. Copyright 2020 Wiley-VCH Verlag GmbH & Co. KGaA, Weinheim.

ELISA primary assays revealed five of the 14 EKO-implicated chemotypes perturbed EGF•EGFR at micromolar concentrations with satisfactory dose-response profiles. Figure 4-2 calibrates their inhibition of EGF•EGFR relative to a blank with no protein ligand (equivalent to 100% "inhibition" because there is no EGF binding to EGFR) and to 10 μM EGF-biotin (under these conditions EGF-biotin saturates the available EGFR hence "inhibition" is set to 0%). That graphic also includes data for LLL-**10faa**, which is a "partial control" insofar as it has the same chemotype core, but some of the side chains and stereochemistries are *not* ones predicted to be appropriate from the EKO analyses. Compound LLL-**10faa** also has hydrophobic sidechains, which could promote non-specific binding, and, indeed, in the event, that partial control showed only relatively low inhibition with no dose-response (Figure 4-2a). Concentrations of the three best inhibitors from the primary ELISA were varied at closer intervals to obtain IC_{50} values (μM throughout; Figure 4-2b): LDL-**10eav**, 30.5 ± 1.2; LLL-**10aev**, 33.3 ± 1.7; DDL-**10vae**, 35.8 ± 2.2.

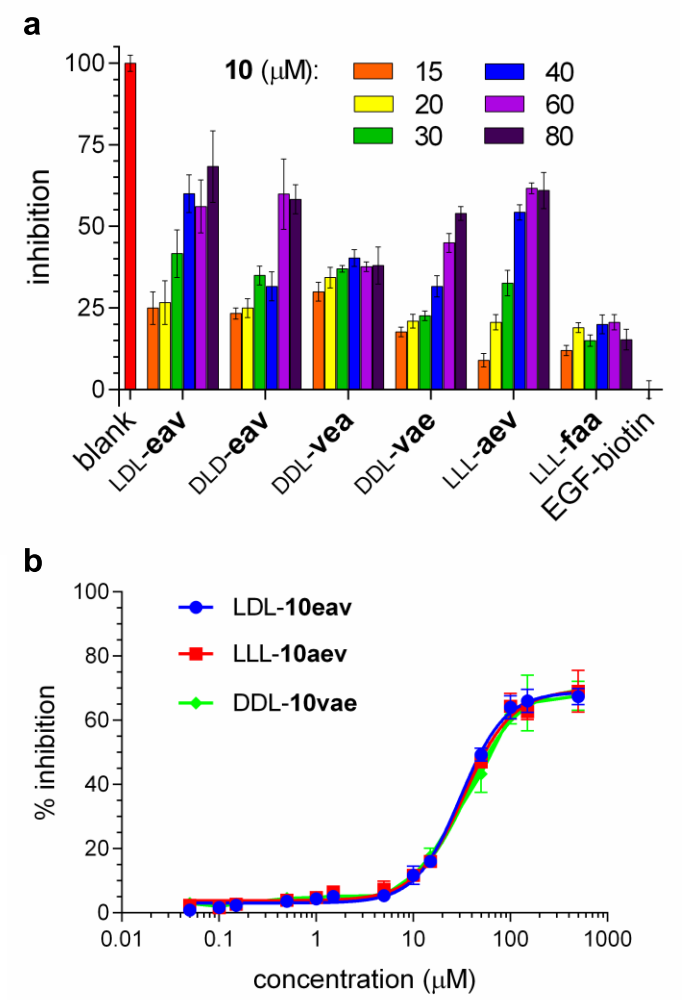

Figure 4-2. ELISA assays to a detect inhibition of binding 10 μM EGF-biotin to EGFR anchored to a microplate, and to b determine IC_{50} values. Reprinted with permission from ref 112. Copyright 2020 Wiley-VCH Verlag GmbH & Co. KGaA, Weinheim.

In SPR experiments, binding of LDL-**10eav** and DDL-**10vae** to EGFR was shown to be reversible as indicated by complete dissociation to baseline level. However, LLL-**10aev** showed more significant secondary binding and aggregation on the receptor surface, as indicated by incomplete dissociation after extended washing. The K_d values calculated from SPR were LDL-**10eav**, 41.1 ± 13.2; LLL-**10aev**, 50.6 ± 13.8; DDL-**10vae**,

30.7 ± 10.2 μM (Figure 4-3). Competition experiments were performed to complement these direct binding assays. In these, the compounds were tested in competition with 30 nM TGFα or 27 nM EGF on immobilized EGFR. Ratios of K_d values of EGF or TGFα for EGFR with and without the featured compounds were obtained; values greater than 1 indicate diminished binding of the natural protein ligands to EGFR. In the event, the compound predicted to have the lowest K_d for EGFR in the direct binding SPR studies, DDL-10vae, had the most negative impact on the binding of TGFα to EGFR in the competitive assay, as expected (Appendix Figure A-3c).

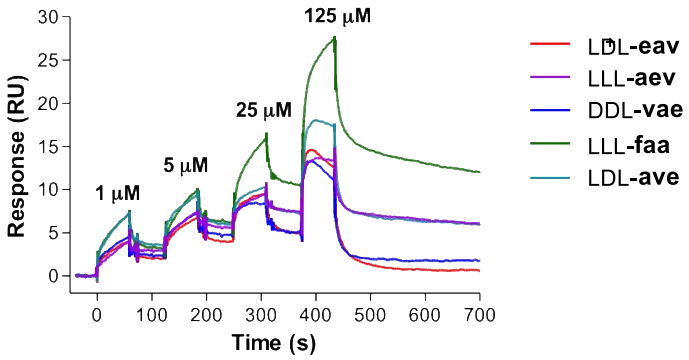

Figure 4-3. Direct binding of compounds **10** to EGFR immobilized on Biacore sensor chip surface (SPR) shown as a sensorgram. Reprinted with permission from ref 112. Copyright 2020 Wiley-VCH Verlag GmbH & Co. KGaA, Weinheim.

Cytotoxicity assays were performed on the five hit compounds featured in Figure 4-4a with the expectation that reduced viabilities would result if these bind EGFR. A549 human lung cancer cells were used in this study because they overexpress EGFR.[73-74]

Figure 4-4a shows all the five of these featured compounds reduced viability more than the partial negative control LLL-**10faa**, but less than gefitinib (a FDA-approved EGFR kinase inhibitor).[75-76] Compounds were also tested using HEK293 (EGFR-negative) cells and showed little to no cytotoxicity (Appendix Figure A-4).

Flow cytometry experiments indicated gefitinib and LDL-**10eav** caused cytotoxicity via early apoptosis (annexin V staining), more than necrosis (propidium iodide; Figure 4-4b and Appendix Figure A-5). Western blot assays were performed to determine if an illustrative piptide-based probe impedes EGF-induced pTyr at EGFR. Figure 4-4c illustrates that phosphorylation could be suppressed almost completely by LDL-**10eav** in competition with EGF.

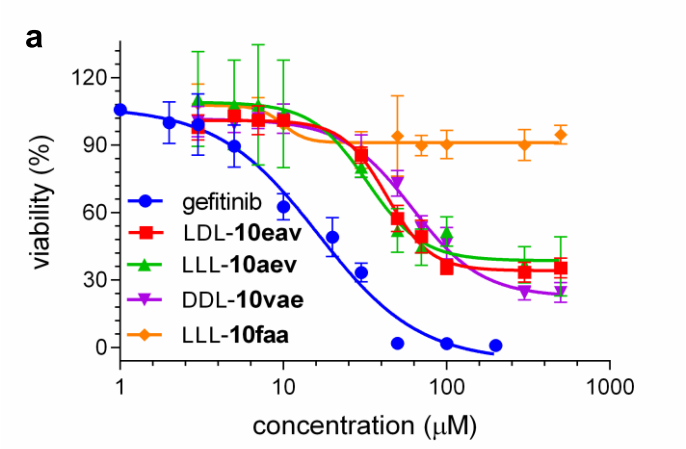

Figure 4-4. Cellular data for piptide-based chemotypes. **a** A549 cell viabilities as monitored using alamarBlue. **b** Flow cytometry data for A549 cells treated with either 15 μM gefitinib or 50 μM LDL-**10eav**. **c** Inhibition of EGFR pTyr for LDL-**10eav** at concentrations (μM) decreasing from 112.5, 75, 50, 25, 12.5 in competition with EGF (uniformly used at 50 ng/mL). Reprinted with permission from ref 112. Copyright 2020 Wiley-VCH Verlag GmbH & Co. KGaA, Weinheim.

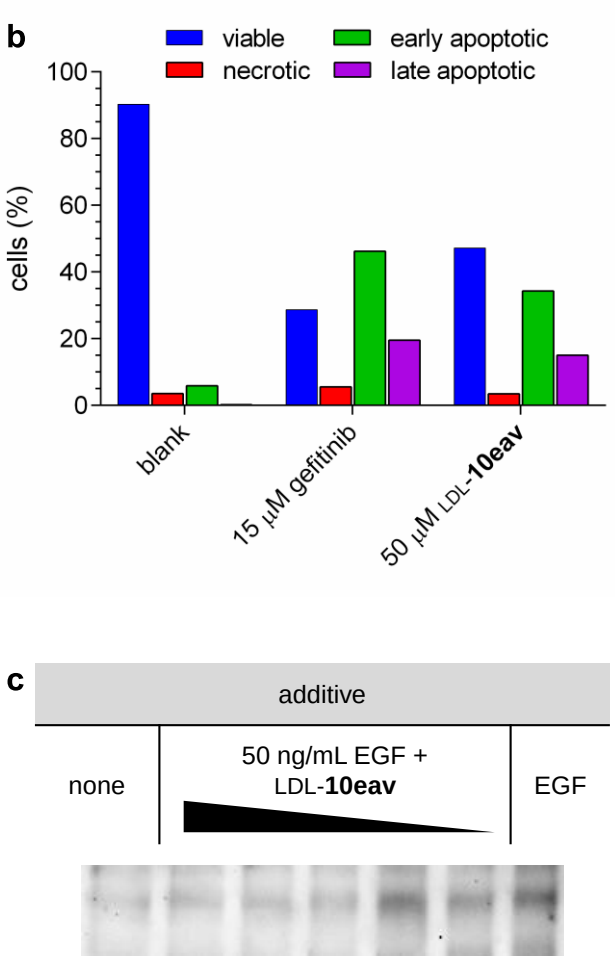

Figure 4-4. Continued.

4.3. Conclusions

Our data on EGFR indicate piptide-based chemotypes can be starting point probes for PPI targets. Five viable hits emerged from a library of only 14 molecules selected by evaluation with EKO; their K_d values (20 – 50 μM) are modest, but detection of any measurable binding is a notable success in studying small molecules to perturb PPIs, particularly because solubilized EGFR is probably not in a native conformation when

immobilized on a gold surface for SPR. Moreover, the best binders from these five hits were active in cellular assays (induce cytotoxicity via apoptosis and inhibit EGF-mediated phosphorylation of intracellular Tyr residues in EGFR).

5. PERTURBATION OF THE INTERACTION OF UROKINASE WITH ITS RECEPTOR

5.1. Introduction

Urokinase, also called urokinase-type plasminogen activator (uPA), has two functions.[77-78] First, uPA is a serine protease that becomes involved with degradation of the interstitial tissue in tumor growth and metastasis. Proteolytic activity of the protease is upregulated on binding the uPA receptor (uPAR), causing uPA to mediate hydrolysis of plasminogen to its active form, plasmin, which degrades extracellular matrix proteins such as fibronectin, vitronectin, and fibrin, which are essential processes in metastatic spread. Consequently, uPA is a marker for a poor prognosis of cancer patient survival.[79] Second, interaction of uPA and uPAR (Figure 5-1) at the cancer cell surface is critical in the pathogenesis of neoplastic growth and metastasis, mediating tissue remodeling, tumor cell invasion, adhesion, and proliferation.[80] Activated macrophages in the tumor-reactive stroma have high levels of uPAR, but expression on normal cells is low, in some cases undetectable, hence opportunities for off-target effects are not apparent. Upregulation of uPAR is also associated with activation by vascular endothelial growth factor (VEGF), which promotes development of vasculature to feed tumors. Overall, the anticipated *in vivo* effects of targeting this protein-protein interaction (PPI) are different from inhibiting the enzyme.[81-83] Research reported here relates to disruption of uPA•uPAR with small molecules.

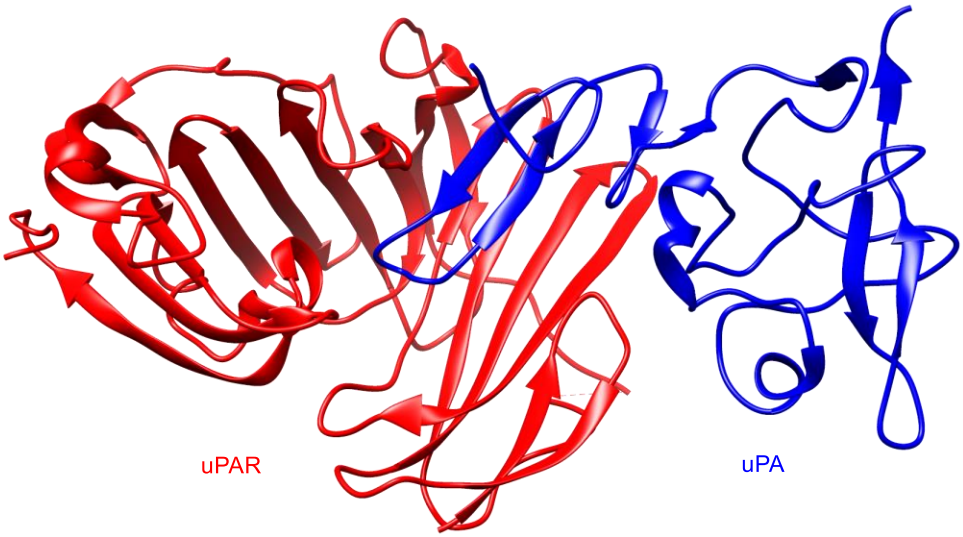

Figure 5-1. uPA•uPAR interaction (PDB: 3bt1).

Most molecules reported to disrupt uPA•uPAR are monoclonal antibodies (mAbs),[84-86] and peptides,[87] including AE105,[88] large cyclic peptides,[89-92] peptoids,[93-94] and recombinant uPA.[95-97] Only a few *small* molecules have been shown to perturb uPA•uPAR even though that interaction has been studied for three decades.[98-100] Reports of these small molecules include patents by pharmaceutical companies, including Roche[101] and Shering-Plough,[102] and, more recently, heterocyclic compounds initially discovered by Meroueh's group through screening.[103-105]

Our interest in uPA•uPAR as a target arose while using Exploring Key Orientations (EKO)[32, 34] to evaluate preferred conformations of peptidomimetics designed for similarity with side-chain orientations at PPI interfaces. One mode of use for EKO is this comparison for all the crystallographically characterized PPI interfaces in a single run; uPA•uPAR gave a good match when this was done. One of the chemotypes that emerged

as a virtual hit in these evaluations was based on *piptides* **10**. Another was chemotypes **12** that we colloquially refer to as "ladder-rung" mimics because they tend to overlay on sheet-turn-sheet motifs like rungs on a ladder.[106] Recently, we found select examples of molecules **12** do, in fact, impede the uPA•uPAR interaction. Those encouraging results led to the studies reported here for the piptide system **10**. Design, synthesis, and testing of chemotypes **13** and **14** are also reported here; these are chimeras of **10** and **12** (Figure 5-2).

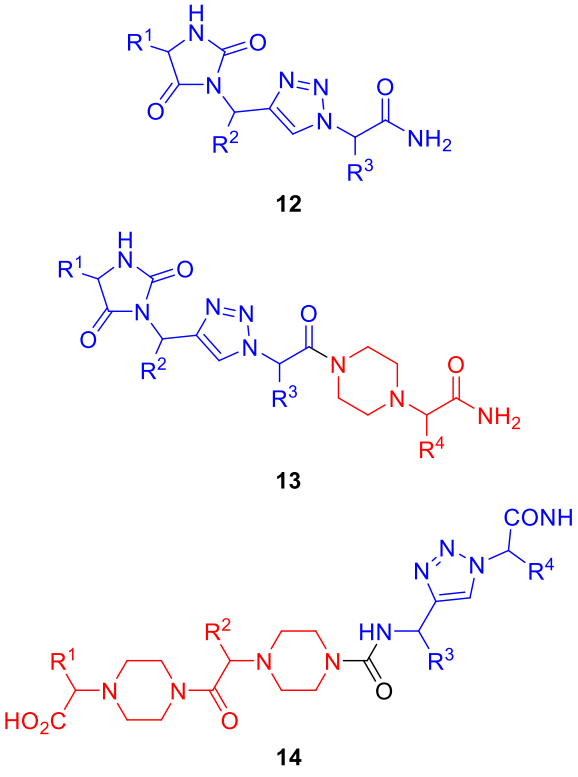

Figure 5-2. General structures of **12**-**14**.

5.2. Results and Discussion

Syntheses of the piptides **10** used in these studies have already been reported. Eighteen EKO-implicated compounds were prepared for this study. Our primary assay in this work was ELISA, augmented by fluorescence polarization (FP) and surface plasmon resonance (SPR) to confirm the dissociation constants of the key compounds from solubilized human uPAR. Wound healing, migration, and invasion assays were performed on selected compounds to assess their potential to retard tumor outgrowth and metastatic spread. Anticipated effects of compounds that putatively disrupt uPA•uPAR relate to formation of metastases, though not directly to cytotoxicity; nevertheless, cytotoxicities of the compounds were checked using MDA-MB-231[107] (a triple negative breast cancer cell line) to establish if they had characteristics that triggered unanticipated cell death (Appendix Figure B-3).

A competitive ELISA (uPAR anchored, uPA in solution) was used to monitor binding with uPAR. All 18 EKO-implicated structures prepared showed evidence for disruption of uPA-HRP •uPAR (HRP is horse radish peroxidase, Appendix Figure B-1) at 50 μM sample concentrations. Three of these were selected for determination of IC_{50} values: DDD-**10skf**, 3.06 ± 0.04; DDL-**10skf**, 6.88 ± 0.03; and DDD-**10fns**, 14.67 ± 0.05 μM, respectively (where errors quoted are standard deviations; Figure 5-3a).

FP assay was used to determine dissociation constants of the three lead compounds with respect to solubilized human uPAR (Figure 5-3b; FITC-AE105,[108] was used as a competitor). K_i values obtained from FP were between 2.75 and 13.2 μM, where DDD-**10skf** was retained most strongly (2.75 ± 0.06 μM**)**.

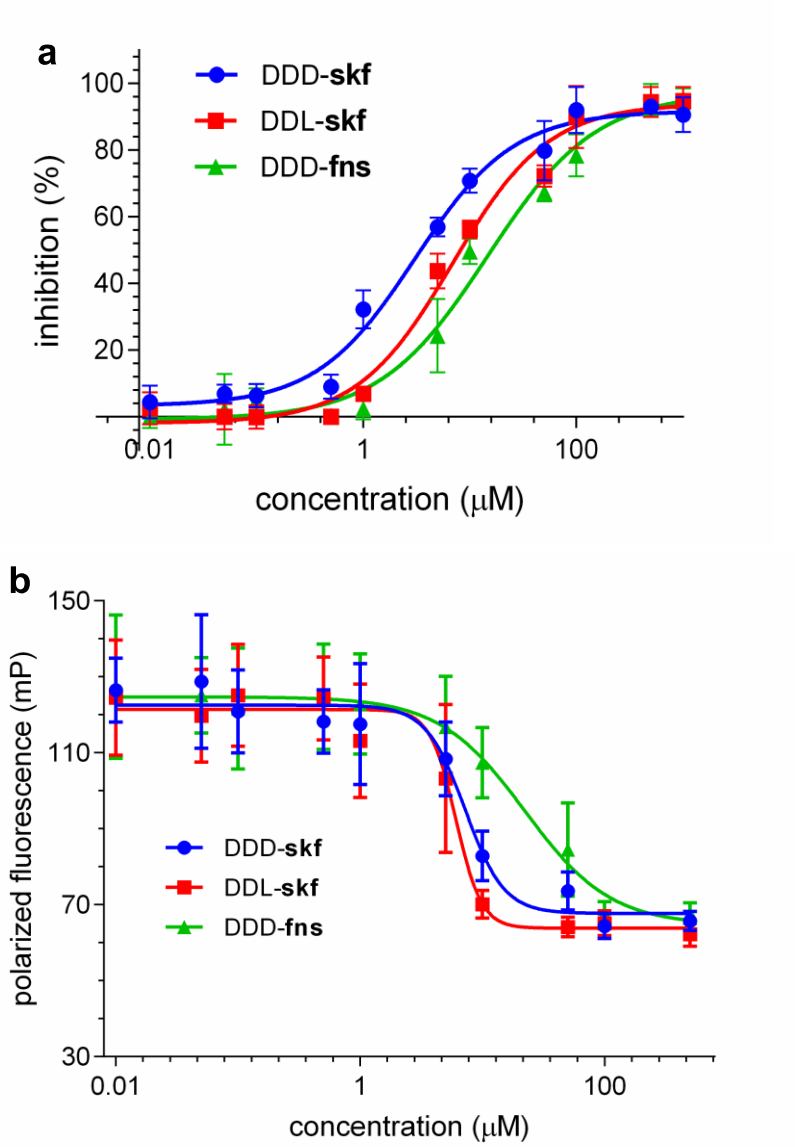

Figure 5-3. a IC_{50} determination through ELISA, and **b** fluorescence polarization assay of Compounds **10.**

These EKO analyses predict chemotypes **10** and **12** overlay different but overlapping regions of the strand-turn-strand motif of uPA in uPA•uPAR; Figure 5-4a show the chemotypes separately, and 5-4b depicts them superimposed. These observations

led to the hypothesis that hybrid molecules comprising fragments of both **10** and **12** also might be effective inhibitors of uPA•uPAR. Thus, compounds LDDL-**13sfks** and LLLL-**14kssi**, implicated as logical design targets, were prepared as shown in the schemes below.

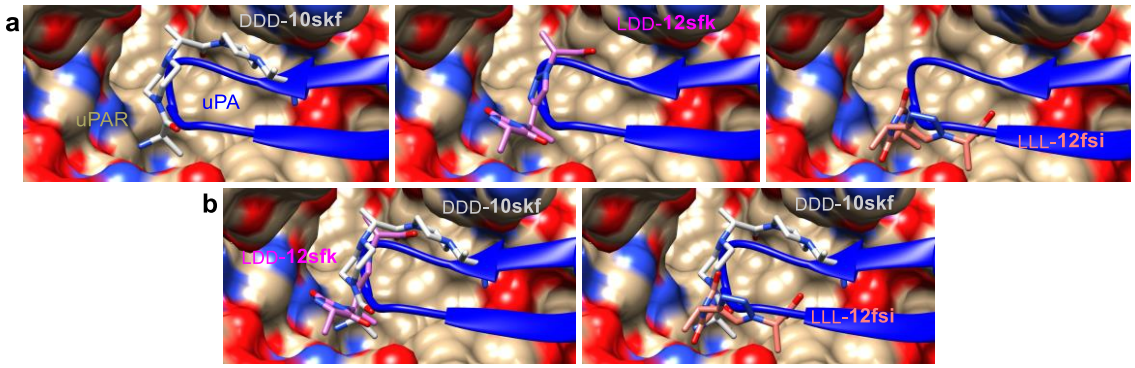

Figure 5-4. a Overlays of DDD-**10skf**, LDD-**12skf**, and LLL-**12fsi** on uPA (PDB: 3bt1). **b** Superimposed overlays of **10** and **12** used for the hybrid (**13sfks**, left, and **14kssi**, right) designs.

Solid-phase synthesis of LDDL-**13sfks** (Appendix Scheme B-1) featured coupling an azido acid to an anchored pip acid, then copper-mediated cycloaddition[109] of this to an allyl amine. This click product was coupled with another amino acid, and the two *C*-terminal residues were cyclized to a hydantoin using conditions previous developed in these labs to prepare compounds **12**.[106]

Synthesis of LLLL-**14kssi** (Appendix Scheme B-2) was more difficult than LDDL-**13sfks**. LLLL-**14kssi** was prepared from a dipiptide **15**, cleaved with retention of the side-chain protecting groups. The piperidine fragment of **15** was coupled with the supported

isocyanate to form a urea linkage,[110] then cleaved from the support, with simultaneous deprotection, to give the desired product.

ELISA and FP binding assays for the chimeras gave the following data (IC_{50} for the ELISA, and K_i for FP, respectively): LDDL-**13sfks**, 2.22 ± 0.09 and 1.99 ± 0.09; LLLL-**14kssi**, 2.52 ± 0.08 and 2.26 ± 0.08 μM (Figure 5-5).

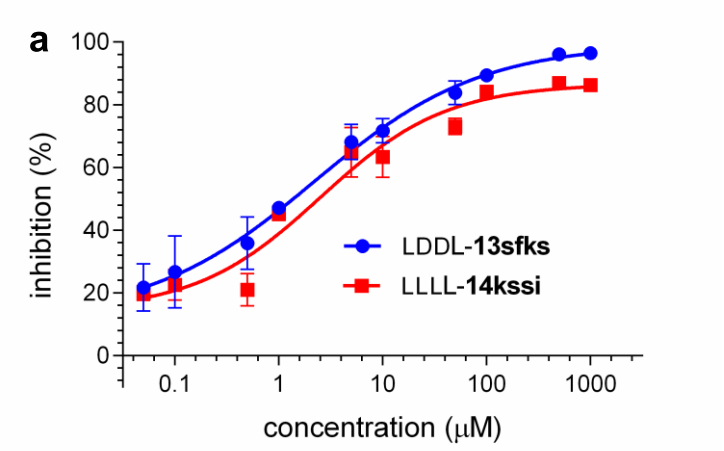

Figure 5-5. a IC_{50} from ELISA, and **b** K_i from FP, for LDDL-**13sfks** and LLLL-**14kssi**.

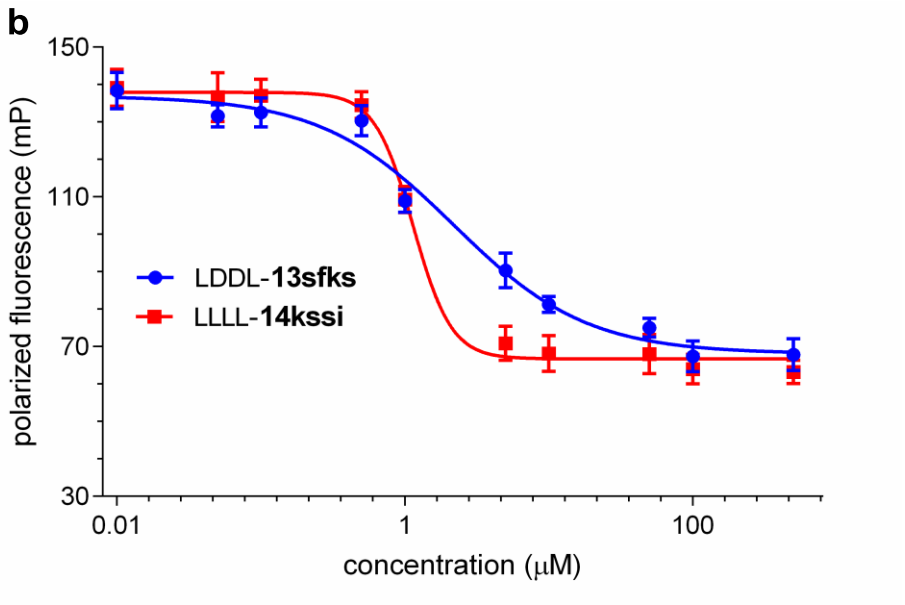

Figure 5-5. Continued.

Surface plasmon resonance (SPR) data was obtained for DDD-**10skf**, LDDL-**13sfks**, and LLLL-**14kssi**; these are given in Table 5-1 and compared with the others for our previous compound LLL-**12fsi**, and Meroueh's compounds **B**[104] and **C**.[105] Compounds DDD-**10skf**, LDDL-**13sfks**, and LLLL-**14kssi** have values in the low micromolar range. **B** and **C** have comparable K_i values with those previously mentioned, but their reported IC_{50} values were higher; K_d values could not be compared since they were not reported. Meanwhile, earlier reported data[106] of LLL-**12fsi** showed higher IC_{50} and K_i values, but it has the lowest K_d out of all the tested compounds based on recent SPR experiments. IC_{50} and K_i values of the hybrids LDDL-**13sfks**, and LLLL-**14kssi** are lower than those of DDD-**10skf** and LLL-**12fsi**, but formation of these chimeric molecules did not have a profound effect when all the data is considered together.

Table 5-1. Comparison of IC_{50}, K_i, and K_d values of compounds **10** and **12-14** against other small molecules **B**[104] and **C**.[105]

Compound	IC_{50} (μM)[a]	K_i (μM)[b]	K_d (μM)[c]
DDD-**10skf**	3.06 ± 0.04	2.75 ± 0.06	0.21 ± 0.09
LLL-**12fsi**	8.35 ± 0.05	7.5 ± 0.1	0.07 ± 0.02
LDDL-**13sfks**	2.22 ± 0.09	1.99 ± 0.09	4 ± 3
LLLL-**14kssi**	2.52 ± 0.08	2.26 ± 0.08	0.2 ± 0.1
B	18.4	0.7	N.D.
C	15.5	2.5	N.D.

Values were obtained from [a]ELISA, [b]FP, and [c]SPR. N.D.: No data was provided in the text.

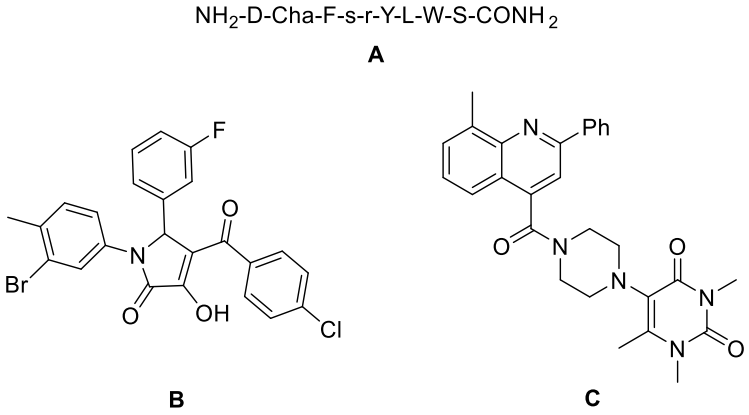

Mimics DDD-**10skf**, LDDL-**13sfks** and LLLL-**14kssi** were evaluated in wound healing, cell migration, and invasion assays using MDA-MB-231 cells throughout. Some of the compounds appear to show a trend, but the values obtained are within experimental error, while others show clear dose dependence (Figure 5-6). Of the three featured compounds, DDD-**10skf** suppress migration (Figure 5-6b) and invasion (Figure 5-6c) most effectively, while compound LDDL-**13sfks** was most effective in the wound healing assay (Figure 5-6a).

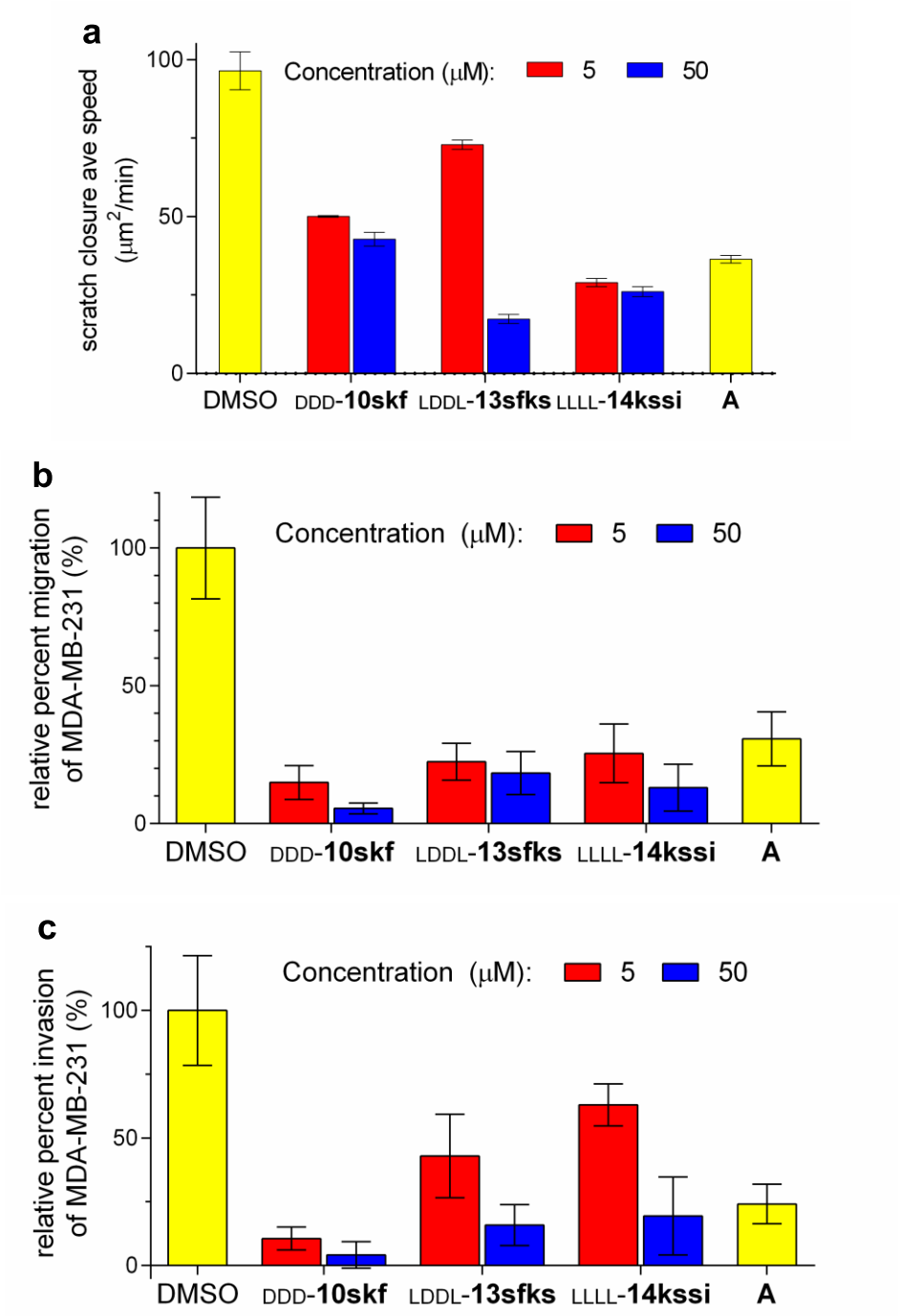

Figure 5-6. a Wound healing, **b** migration, and **c** invasion assay of compounds **10**, **13** and **14** on MDA-MB-231. The concentration of compound A in the experiments was 0.5 μM.

5.3. Conclusions

All the piptide chemotypes bound uPAR at concentrations of 50 μM or less. Select members of this series had K_d values as low as 0.2 μM and showed favorable responses in cellular assays designed to simulate wound healing, migration, and invasion; these data are comparable with the best small molecule uPA•uPAR disruptors in the literature (from conventional screening).

6. CONCLUSIONS AND FUTURE WORK

6.1. Conclusions

Piptides can be prepared expeditiously by researchers with only moderate synthesis skills; and they would become even more accessible if pip acids became commercially available.

Other work from these laboratories has demonstrated the use of EKO technique on: HIV-1 protease dimer,[32] antithrombin oligomer formation,[71] PCSK9•LDLR,[72] NEDD8•NAE,[111] and which now includes EGF•EGFR[112] and uPA•uPAR.[106] Here, and in the examples featuring PCSK9•LDLR and NEDD8•NAE, the compounds were also active in cellular assays. This validates the EKO approach for identification of chemotypes with micromolar affinities to the protein receptor.

The closest parallel to piptides in the literature is oligooxopiperazines.[113] Oligooxopiperazines have been used for disrupting PPIs,[114-116] but are harder to access, and the range of side chains so far incorporated is less. Further, the two chemotypes are simply different, thus probably suitable for complementary applications.

6.2. Future Work

It should be possible to optimize these leads using conventional docking techniques and iterative cycles of synthesis and testing to establish SAR. However, it has

been generally difficult to obtain sub-micromolar binders for these PPIs directly from the EKO technique. We conclude that this is likely because EKO is restricted to small molecule chemotypes wherein only three amino acid side chains are conformationally matched on the PPI interface. Consequently, other methods could be developed that complement EKO, but which facilitate identification molecules that can be related to larger segments of PPI interface.

A solid supported library can also be prepared via split-mix methodology, according to the method of Lam *et al.*[117] That library will include most natural amino acid side-chains (which should also contain the ones implicated by EKO), to make a one-bead-one-compound (OBOC) library. Positive hits not implied by EKO could be discovered with this strategy.

This study does not feature intracellular targets, but researchers might be interested in applying the strategy to such PPIs. Other PPIs implicated by EKO for scaffolds **10** and **12** include the biomedicinally significant intracellular targets RAS•SOS[118] and PD-L1•PD-1.[119] An attractive feature of piperazines is that they can be reversibly protonated, and this can facilitate passive diffusion through membranes. Piptides with appropriate side chains might conceivably be somewhat cell permeable. Doing a chloroalkane penetration assay (CAPA),[120] by adding a chloroalkyl group to the N-terminus, can also be used to measure and optimize cell penetration of piptides.

Piptides can also be further studied to: see if it could form other structures or if it can be synthesized and utilized as a polymer like with peptoids,[121] synthesize on different solid supports like smart polymers that might have potential to be utilized in drug delivery, or be included as linkers for PROTACs.[122]

REFERENCES

1. Gao, M.; Yu, F.; Lv, C.; Choo, J.; Chen, L., Fluorescent chemical probes for accurate tumor diagnosis and targeting therapy. *Chem. Soc. Rev.* **2017,** *46*, 2237-2271.

2. Barglow, K. T.; Cravatt, B. F., Activity-based protein profiling for the functional annotation of enzymes. *Nat. Methods* **2007,** *4*, 822-827.

3. Ursu, A.; Waldmann, H., Hide and seek: Identification and confirmation of small molecule protein targets. *Bioorg. Med. Chem. Lett.* **2015,** *25* (16), 3079-3086.

4. Meireles, L. M. C.; Mustata, G., Discovery of modulators of protein-protein interactions: current approaches and limitations. *Curr. Top. Med. Chem.* **2011,** *11* (3), 248-257.

5. Macarron, R.; Banks, M. N.; Bojanic, D.; Burns, D. J.; Cirovic, D. A.; Garyantes, T.; Green, D. V. S.; Hertzberg, R. P.; Janzen, W. P.; Paslay, J. W.; Schopfer, U.; Sittampalam, G. S., Impact of high-throughput screening in biomedical research. *Nat. Rev. Drug Discov.* **2011,** *10* (3), 188-195.

6. Gray, B. P.; Brown, K. C., Combinatorial Peptide Libraries: Mining for Cell-Binding Peptides. *Chem. Rev.* **2014,** *114* (2), 1020-1081.

7. Welsch, M. E.; Snyder, S. A.; Stockwell, B. R., Privileged scaffolds for library design and drug discovery. *Curr. Opin. Chem. Biol.* **2010,** *14* (3), 347-361.

8. Hill, T. A.; Shepherd, N. E.; Diness, F.; Fairlie, D. P., Constraining Cyclic Peptides To Mimic Protein Structure Motifs. *Angew. Chem. Int. Ed.* **2014,** *53*, 13020-13041.

9. Giudicessi, S. L.; Gurevich-Messina, J. M.; Martinez-Ceron, M. C.; Erra-Balsells, R.; Albericio, F.; Cascone, O.; Camperi, S. A., Friendly Strategy to Prepare Encoded One Bead-One Compound Cyclic Peptide Library. *ACS Comb. Sci.* **2013,** *15* (10), 525-529.

10. Weinmueller, M.; Rechenmacher, F.; Kiran Marelli, U.; Reichart, F.; Kapp, T. G.; Raeder, A. F. B.; Di Leva, F. S.; Marinelli, L.; Novellino, E.; Munoz-Felix, J. M.; Hodivala-Dilke, K.; Schumacher, A.; Fanous, J.; Gilon, C.; Hoffman, A.; Kessler, H., Overcoming the Lack of Oral Availability of Cyclic Hexapeptides: Design of a Selective and Orally Available Ligand for the Integrin αvβ3. *Angew. Chem., Int. Ed.* **2017,** *56*, 16405-16409.

11. White, T. R.; Renzelman, C. M.; Rand, A. C.; Rezai, T.; McEwen, C. M.; Gelev, V. M.; Turner, R. A.; Linington, R. G.; Leung, S. S. F.; Kalgutkar, A. S.; Bauman, J. N.; Zhang, Y.; Liras, S.; Price, D. A.; Mathiowetz, A. M.; Jacobson, M. P.; Lokey, R. S., On-resin N-methylation of cyclic peptides for discovery of orally bioavailable scaffolds. *Nat. Chem. Biol.* **2011,** *7* (11), 810-817.

12. Biron, E.; Chatterjee, J.; Ovadia, O.; Langenegger, D.; Brueggen, J.; Hoyer, D.; Schmid, H. A.; Jelnick, R.; Gilon, C.; Hoffman, A.; Kessler, H., Improving oral bioavailability of peptides by multiple N-methylation: somatostatin analogues. *Angew. Chem., Int. Ed.* **2008,** *47* (14), 2595-2599.

13. Raeder, A. F. B.; Weinmueller, M.; Reichart, F.; Schumacher-Klinger, A.; Merzbach, S.; Gilon, C.; Hoffman, A.; Kessler, H., Orally Active Peptides: Is There a Magic Bullet? *Angew. Chem., Int. Ed.* **2018,** *57*, 14414-14438.

14. Dougherty, P. G.; Sahni, A.; Pei, D., Understanding Cell Penetration of Cyclic Peptides. *Chem. Rev.* **2019,** *119* (17), 10241-10287.

15. Simon, R. J.; Kania, R. S.; Zuckermann, R. N.; Huebner, V. D.; Jewell, D. A.; Banville, S.; Ng, S.; Wang, L.; Rosenberg, S.; Marlowe, C. K.; Spellmeyer, D. C.; Tan, R.; Frankel, A. D.; Santi, D. V.; Cohen, F. E.; Bartlett, P. A., Peptoids: A Modular Approach to Drug Discovery. *Proc. Natl. Acad. Sci.* **1992,** *89*, 9367-71.

16. Zuckermann, R. N.; Kerr, J. M.; Kent, S. B. H.; Moos, W. H., Efficient Method for the Preparation of Peptoids [Oligo(N-substituted glycines)] by Submonomer Solid-Phase Synthesis. *J. Am. Chem. Soc.* **1992,** *114*, 10646-7.

17. Gangloff, N.; Ulbricht, J.; Lorson, T.; Schlaad, H.; Luxenhofer, R., Peptoids and Polypeptoids at the Frontier of Supra- and Macromolecular Engineering. *Chem. Rev.* **2016,** *116*, 1753-1802.

18. Udugamasooriya, D. G.; Dineen, S. P.; Brekken, R. A.; Kodadek, T., A Peptoid "Antibody Surrogate" That Antagonizes VEGF Receptor 2 Activity. *J. Am. Chem. Soc.* **2008,** *130*, 5744-5752.

19. Hooks, J. C.; Matharage, J. P.; Udugamasooriya, D. G., Development of homomultimers and heteromultimers of lung cancer-specific peptoids. *Biopolymers* **2011,** *96*, 567-577.

20. Gao, Y.; Kodadek, T., Synthesis and Screening of Stereochemically Diverse Combinatorial Libraries of Peptide Tertiary Amides. *Chem. Biol.* **2013,** *20*, 360-369.

21. Vendrell-Navarro, G.; Rua, F.; Bujons, J.; Brockmeyer, A.; Janning, P.; Ziegler, S.; Messeguer, A.; Waldmann, H., Positional Scanning Synthesis of a Peptoid Library Yields New Inducers of Apoptosis that Target Karyopherins and Tubulin. *ChemBioChem* **2015,** *16*, 1580-1587.

22. Nnanabu, E.; Burgess, K., Cyclic-Semipeptoids: Peptoid-Organic Hybrid Macrocycles. *Org. Lett.* **2006,** *8*, 1259-62.

23. Comegna, D.; Benincasa, M.; Gennaro, R.; Izzo, I.; De Riccardis, F., Design, synthesis and antimicrobial properties of non-hemolytic cationic alpha -cyclopeptoids. *Bioorg. Med. Chem.* **2010,** *18* (5), 2010-2018.

24. Suwal, S.; Kodadek, T., Synthesis of libraries of peptidomimetic compounds containing a 2-oxopiperazine unit in the main chain. *Org. Biomol. Chem.* **2013,** *11*, 2088-2092.

25. Shin, S. B. Y.; Yoo, B.; Todaro, L. J.; Kirshenbaum, K., Cyclic peptoids. *J. Am. Chem. Soc.* **2007,** *129*, 3218-3225.

26. Kaniraj, P. J.; Maayan, G., A Facile Strategy for the Construction of Cyclic Peptoids under Microwave Irradiation through a Simple Substitution Reaction. *Org. Lett.* **2015,** *17*, 2110-2113.

27. Fu, X.; Li, Z.; Wei, J.; Sun, J.; Li, Z., Schiff base and reductive amination reactions of α-amino acids: a facile route toward N-alkylated amino acids and peptoid synthesis. *Polym. Chem.* **2018,** *9* (37), 4617-4624.

28. Seebach, D.; Overhand, M.; Kuehnle, F. N. M.; Martinoni, B., β-Peptides. Synthesis by Arndt-Eistert homologation with concomitant peptide coupling. Structure determination by NMR and CD spectroscopy and by x-ray crystallography. Helical secondary structure of a β-hexapeptide in solution and its stability towards pepsin. *Helv. Chim. Acta* **1996,** *79*, 913-941.

29. Appella, D. H.; Christianson, L. A.; Karle, I. L.; Powell, D. R.; Gellman, S. H., beta-Peptide Foldamers: Robust Helix Formation in a New Family of b-Amino Acid Oligomers. *J. Am. Chem. Soc.* **1996,** *118*, 13071-2.

30. Gellman, S. H., Foldamers: A Manifesto. *Acc. Chem. Res.* **1998,** *31* (4), 173-180.

31. Horne, W. S.; Gellman, S. H., Foldamers with Heterogeneous Backbones. *Acc. Chem. Res.* **2008,** *41* (10), 1399-1408.

32. Ko, E.; Raghuraman, A.; Perez, L. M.; Ioerger, T. R.; Burgess, K., Exploring Key Orientations at Protein-Protein Interfaces with Small Molecule Probes. *J. Am. Chem. Soc.* **2013,** *135*, 167-173.

33. Ko, E.; Liu, J.; Burgess, K., Minimalist and Universal Peptidomimetics. *Chem. Soc. Rev.* **2011,** *40*, 4411-4421.

34. Xin, D.; Ko, E.; Perez, L. M.; Ioerger, T. R.; Burgess, K., Evaluating Minimalist Mimics by Exploring Key Orientations on Secondary Structures (EKOS). *Org. Biomol. Chem.* **2013,** *11*, 7789-7801.

35. Harfenist, M., Unsymetrically substituted piperazines. VII. *J. Am. Chem. Soc.* **1954,** *76*, 4991-3.

36. Herova, D.; Pazdera, P., Efficient solid support catalyzed mono-aza-Michael addition reactions of piperazine. *Monatsh. Chem.* **2015,** *146* (4), 653-661.

37. Gao, R.; Canney, D. J., A Versatile and Practical Microwave-Assisted Synthesis of Sterically Hindered N-Arylpiperazines. *J. Org. Chem.* **2010,** *75* (21), 7451-7453.

38. Fields, G. B.; Noble, R. L., Solid Phase Peptide Synthesis Utilizing 9-Flourenylmethoxycarbonyl Amino Acids. *Int. J. Peptide Protein Res.* **1990,** *35*, 161-214.

39. Patek, M., Multistep Deprotection for Peptide Chemistry. *Int. J. Peptide Protein Res.* **1993,** *42*, 97-117.

40. Knorr, R.; Trzeciak, A.; Bannwarth, W.; Gillessen, D., New Coupling Reagents in Peptide Chemistry. *Tetrahedron Lett.* **1989,** *30*, 1927-30.

41. Carpino, L. A.; Imazumi, H.; El-Faham, A.; Ferrer, F. J.; Zhang, C.; Lee, Y.; Foxman, B. M.; Henklein, P.; Hanay, C.; Mugge, C.; Wenschuh, H.; Klose, J.; Beyermann, M.; Bienert, M., The Uronium/Guanidinium Peptide Coupling Reagents: Finally the True Uronium Salts. *Angew. Chem. Int. Ed.* **2002,** *41*, 442-5.

42. El-Faham, A.; Albericio, F., Peptide Coupling Reagents, More than a Letter Soup. *Chem. Rev.* **2011,** *111* (11), 6557-6602.

43. Christensen, T., A qualitative test for monitoring coupling completeness in solid phase peptide synthesis using chloranil. *Acta Chem. Scand. B* **1979,** *B33*, 763-6.

44. Sarin, V. K.; Kent, S. B. H.; Tam, J. P.; Merrifield, R. B., Quantitative Monitoring of Solid-Phase Peptide Synthesis by the Ninhydrin Reaction. *Anal. Biochem.* **1981,** *117*, 147-57.

45. Joullie, M. M.; Thompson, T. R.; Nemerof, N. H., Ninhydrin and Ninhydrin Analogs. Syntheses and Applications. *Tetrahedron* **1991,** *47*, 8791-830.

46. Leggio, A.; Di Gioia, M. L.; Perri, F.; Liguori, A., N-Nosyl-alpha-amino acids in solution phase peptide synthesis. *Tetrahedron* **2007,** *63* (34), 8164-8173.

47. Jorgensen, W. L.; Duffy, E. M., Prediction of drug solubility from Monte Carlo simulations. *Bioorg. Med. Chem. Lett.* **2000,** *10* (11), 1155-1158.

48. Duffy, E. M.; Jorgensen, W. L., Prediction of Properties from Simulations: Free Energies of Solvation in Hexadecane, Octanol, and Water. *J. Am. Chem. Soc.* **2000,** *122* (12), 2878-2888.

49. Jurasek, L.; Johnson, P.; Olafson, R. W.; Smillie, L. B., An Improved fractionation system for pronase on CM-Sephadex. *Can. J. Biochem.* **1971,** *49* (11), 1195-1201.

50. Taechalertpaisarn, J.; Lyu, R.-L.; Arancillo, M.; Lin, C.-M.; Jiang, Z.; Perez, L. M.; Ioerger, T. R.; Burgess, K., Design Criteria for Minimalist Mimics of Protein-protein Interface Segments. *Org. Biomol. Chem.* **2019,** *17*, 908-915.

51. Taechalertpaisarn, J.; Lyu, R.-L.; Arancillo, M.; Lin, C.-M.; Perez, L. M.; Ioerger, T. R.; Burgess, K., Correlations between secondary structure- and protein-protein interface-mimicry. *Org. Biomol. Chem.* **2019,** *17*, 3267-3274.

52. Woodburn, J. R., The epidermal growth factor receptor and its inhibition in cancer therapy. *Pharmacol. Ther.* **1999,** *82* (2-3), 241-250.

53. Normanno, N.; Bianco, C.; Strizzi, L.; Mancino, M.; Maiello, M. R.; De Luca, A.; Caponigro, F.; Salomon, D. S., The ErbB receptors and their ligands in cancer: An overview. *Curr. Drug Targets* **2005,** *6* (3), 243-257.

54. Mitsudomi, T.; Yatabe, Y., Epidermal growth factor receptor in relation to tumor development: EGFR gene and cancer. *FEBS J.* **2010,** *277* (2), 301-308.

55. Kalyankrishna, S.; Grandis, J. R., Epidermal growth factor receptor biology in head and neck cancer. *J. Clin. Oncol.* **2006,** *24* (17), 2666-2672.

56. Normanno, N.; De Luca, A.; Bianco, C.; Strizzi, L.; Mancino, M.; Maiello, M. R.; Carotenuto, A.; De Feo, G.; Caponigro, F.; Salomon, D. S., Epidermal growth factor receptor (EGFR) signaling in cancer. *Gene* **2006,** *366* (1), 2-16.

57. Pao, W.; Miller, V. A., Epidermal growth factor receptor mutations, small-molecule kinase inhibitors, and non-small-cell lung cancer: current knowledge and future directions. *J. Clin. Oncol.* **2005,** *23* (11), 2556-2568.

58. Breuhahn, K.; Longerich, T.; Schirmacher, P., Dysregulation of growth factor signaling in human hepatocellular carcinoma. *Oncogene* **2006,** *25* (27), 3787-3800.

59. Lippitz, B. E., Cytokine patterns in patients with cancer: a systematic review. *Lancet Oncol.* **2013,** *14* (6), e218-e228.

60. Goldstein, N. I.; Prewett, M.; Zuklys, K.; Rockwell, P.; Mendelsohn, J., Biological efficacy of a chimeric antibody to the epidermal growth factor receptor in a human tumor xenograft model. *Clin. Cancer Res.* **1995,** *1*, 1311-8.

61. Hynes, N. E.; Lane, H. A., ERBB receptors and cancer: the complexity of targeted inhibitors. *Nat. Rev. Cancer* **2005,** *5* (5), 341-354.

62. Okines, A.; Cunningham, D.; Chau, I., Targeting the human EGFR family in esophagogastric cancer. *Nat. Rev. Clin. Oncol.* **2011,** *8* (8), 492-503.

63. Wheeler, D. L.; Dunn, E. F.; Harari, P. M., Understanding resistance to EGFR inhibitors-impact on future treatment strategies. *Nat. Rev. Clin. Oncol.* **2010,** *7* (9), 493-507.

64. Lurje, G.; Lenz, H.-J., EGFR Signaling and Drug Discovery. *Oncology* **2009,** *77* (6), 400-410.

65. Ciardiello, F.; Caputo, R.; Bianco, R.; Damiano, V.; Pomatico, G.; De Placido, S.; Bianco, A. R.; Tortora, G., Antitumor effect and potentiation of cytotoxic drugs activity in human cancer cells by ZD-1839 (Iressa), an epidermal growth factor receptor-selective tyrosine kinase inhibitor. *Clin. Cancer Res.* **2000,** *6* (5), 2053-63.

66. Anderson, N. G.; Ahmad, T.; Chan, K.; Dobson, R.; Bundred, N. J., ZD1839 (Iressa), a novel epidermal growth factor receptor (EGFR) tyrosine kinase inhibitor, potently inhibits the growth of EGFR-positive cancer cell lines with or without erbB2 overexpression. *Int. J. Cancer* **2001,** *94*, 774-82.

67. Garrett, T. P. J.; McKern, N. M.; Lou, M.; Elleman, T. C.; Adams, T. E.; Lovrecz, G. O.; Zhu, H.-J.; Walker, F.; Frenkel, M. J.; Hoyne, P. A.; Jorissen, R. N.; Nice, E. C.; Burgess, A. W.; Ward, C. W., Crystal structure of a truncated epidermal growth factor receptor extracellular domain bound to transforming growth factor alpha. *Cell* **2002,** *110*, 763-773.

68. Ferguson, K. M.; Berger, M. B.; Mendrola, J. M.; Cho, H.-S.; Leahy, D. J.; Lemmon, M. A., EGF activates its receptor by removing interactions that autoinhibit ectodomain dimerization. *Mol. Cell* **2003,** *11* (2), 507-517.

69. Groenen, L. C.; Nice, E. C.; Burgess, A. W., Structure-function relationships for the EGF/TGF-alpha family of mitogens. *Growth Factors* **1994,** *11* (4), 235-57.

70. Sanders, J. M.; Wampole, M. E.; Thakur, M. L.; Wickstrom, E., Molecular determinants of epidermal growth factor binding: a molecular dynamics study. *PLoS One* **2013,** *8*, e54136.

71. Xin, D.; Holzenburg, A.; Burgess, K., Small Molecule Probes that Perturb a Protein-protein Interface in Antithrombin. *Chem. Sci.* **2014,** *5*, 4914-4921.

72. Taechalertpaisarn, J.; Zhao, B.; Liang, X.; Burgess, K., Small Molecule Inhibitors of the PCSK9-LDLR Interaction. *J. Am. Chem. Soc.* **2018,** *140*, 3242-3249.

73. Rachwal, W. J.; Bongiorno, P. F.; Orringer, M. B.; Whyte, R. I.; Ethier, S. P.; Beer, D. G., Expression and activation of erbB-2 and epidermal growth factor receptor in lung adenocarcinomas. *Br. J. Cancer* **1995,** *72*, 56-64.

74. Choi, E.-J.; Ryu, Y.-K.; Kim, S.-Y.; Wu, H.-G.; Kim, J.-S.; Kim, I.-H.; Kim, I.-A., Targeting Epidermal Growth Factor Receptor-Associated Signaling Pathways in Non-Small Cell Lung Cancer Cells: Implication in Radiation Response. *Mol. Cancer Res.* **2010,** *8*, 1027-1036.

75. Mahipal, A.; Kothari, N.; Gupta, S., Epidermal growth factor receptor inhibitors: coming of age. *Cancer Control* **2014,** *21* (1), 74-79.

76. Roskoski, R., Jr., ErbB/HER protein-tyrosine kinases: Structures and small molecule inhibitors. *Pharmacol. Res.* **2014,** *87*, 42-59.

77. Dass, K.; Ahmad, A.; Azmi, A. S.; Sarkar, S. H.; Sarkar, F. H., Evolving role of uPA/uPAR system in human cancers. *Cancer Treat. Rev.* **2008,** *34*, 122-136.

78. Kriegbaum, M. C.; Persson, M.; Haldager, L.; Alpizar-Alpizar, W.; Jacobsen, B.; Gaardsvoll, H.; Kjaer, A.; Ploug, M., Rational targeting of the urokinase receptor (uPAR): development of antagonists and non-invasive imaging probes. *Curr. Drug Targets* **2011,** *12* (12), 1711-1728.

79. Tang, L.; Han, X., The urokinase plasminogen activator system in breast cancer invasion and metastasis. *Biomed. Pharmacother.* **2013,** *67* (2), 179-182.

80. Carriero, M. V.; Franco, P.; Votta, G.; Longanesi-Cattani, I.; Vento, M. T.; Masucci, M. T.; Mancini, A.; Caputi, M.; Iaccarino, I.; Stoppelli, M. P., Regulation of cell migration and invasion by specific modules of uPA: mechanistic insights and specific inhibitors. *Curr. Drug Targets* **2011,** *12* (12), 1761-1771.

81. Rosenberg, S., New developments in the urokinase-type plasminogen activator systems. *Expert Opin. Ther. Tar.* **2001,** *5*, 711-722.

82. Ngo, J. C. K.; Jiang, L.; Lin, Z.; Yuan, C.; Chen, Z.; Zhang, X.; Yu, H.; Wang, J.; Lin, L.; Huang, M., Structural basis for therapeutic intervention of uPA/uPAR system. *Curr. Drug Targets* **2011,** *12* (12), 1729-1743.

83. Mahmood, N., Multifaceted role of the urokinase-type plasminogen activator (uPA) and its receptor (uPAR): Diagnositc, prognostic, and therapeutic applications. *Front. Oncol.* **2018,** *8*, 24.1 - 24.21.

84. Bauer, T. W.; Liu, W.; Fan, F.; Camp, E. R.; Yang, A.; Somcio, R. J.; Bucana, C. D.; Callahan, J.; Parry, G. C.; Evans, D. B.; Boyd, D. D.; Mazar, A.; Ellis, L. M., Targeting of Urokinase Plasminogen Activator Receptor in Human Pancreatic Carcinoma Cells Inhibits c-Met– and Insulin-like Growth Factor-I Receptor–Mediated Migration and Invasion and Orthotopic Tumor Growth in Mice. *Cancer Res.* **2005,** *65*, 7775-7781.

85. Van Buren, G., II; Gray, M. J.; Dallas, N. A.; Xia, L.; Lim, S. J.; Fan, F.; Mazar, A. P.; Ellis, L. M., Targeting the Urokinase Plasminogen Activator Receptor With a Monoclonal Antibody Impairs the Growth of Human Colorectal Cancer in the Liver. *Cancer* **2009,** *115*, 3360-3368.

86. Rabbani, S. A.; Ateeq, B.; Arakelian, A.; Valentino, M. L.; Shaw, D. E.; Dauffenbach, L. M.; Kerfoot, C. A.; Mazar, A. P., An Anti–Urokinase Plasminogen Activator Receptor Antibody (ATN-658) Blocks Prostate Cancer Invasion, Migration, Growth, and Experimental Skeletal Metastasis In Vitro and In Vivo. *Neoplasia* **2010,** *12*, 778-788.

87. Goodson, R. J.; Doyle, M. V.; Kaufman, S. E.; Rosenberg, S., High-affinity urokinase receptor antagonists identified with bacteriophage peptide display. *Proc. Natl. Acad. Sci.* **1994,** *91* (15), 7129-7133.

88. Ploug, M.; Ostergaard, S.; Gaardsvoll, H.; Kovalski, K.; Holst-Hansen, C.; Holm, A.; Ossowski, L.; Dano, K., Peptide-Derived Antagonists of the Urokinase Receptor. Affinity Maturation by Combinatorial Chemistry, Identification of Functional Epitopes, and Inhibitory Effect on Cancer Cell Intravasation. *Biochemistry* **2001,** *40* (40), 12157-12168.

89. Burgle, M.; Koppitz, M.; Riemer, C.; Kessler, H.; Konig, B.; Weidle, U. H.; Kellermann, J.; Lottspeich, F.; Graeff, H.; Schmitt, M.; Goretzki, L.; Reuning, U.; Wilhelm, O.; Magdolen, V., Inhibition of the interaction of urokinase-type plasminogen activator (uPA) with its receptor (uPAR) by synthetic peptides. *Biol. Chem.* **1997,** *378*, 231-237.

90. Magdolen, V.; Burgle, M.; Arroyo De Prada, N.; Schmiedeberg, N.; Riemer, C.; Schroeck, F.; Kellermann, J.; Degitz, K.; Wilhelm, O. G.; Schmitt, M.; Kessler, H., Cyclo19,31[D-Cys19]-uPA19-31 is a potent competitive antagonist of the interaction of urokinase-type plasminogen activator with its receptor (CD87). *Biol. Chem.* **2001,** *382* (8), 1197-1205.

91. Sato, S.; Kopitz, C.; Schmalix, W. A.; Muehlenweg, B.; Kessler, H.; Schmitt, M.; Kruger, A.; Magdolen, V., High-affinity urokinase-derived cyclic peptides inhibiting urokinase/urokinase receptor-interaction: effects on tumor growth and spread. *FEBS Lett.* **2002,** *528* (1-3), 212-216.

92. Schmiedeberg, N.; Schmitt, M.; Roelz, C.; Truffault, V.; Sukopp, M.; Buergle, M.; Wilhelm, O. G.; Schmalix, W.; Magdolen, V.; Kessler, H., Synthesis, Solution Structure, and Biological Evaluation of Urokinase Type Plasminogen Activator (uPA)-Derived Receptor Binding Domain Mimetics. *J. Med. Chem.* **2002,** *45* (23), 4984-4994.

93. Rosenberg, S.; Spear, K. L.; Martin, E. J. Urokinase Receptor Ligands. WO 96/40747, December 19, 1996.

94. Rosenberg, S.; Spear, K. L.; Martin, E. J. Urokinase Receptor Ligands. US005747458A, May 5, 1998.

95. Kobayshi, H.; Sugino, D.; She, M. Y.; Ohi, H.; Hirashima, Y.; Shinohara, H.; Fuje, M.; Shibata, K.; Terao, T., A bifunctional hybrid molecule of the amino-terminal fragment

of urokinase and domain II of bikunin efficiently inhibits tumor cell invasion and metastasis. *Eur. J. Biochem.* **1998,** *253*, 817-826.

96. Muehlenweg, B.; Assfalg-Machleidt, I.; Parradoi, S. G.; Burgle, M.; Creutzburg, S.; Schmitt, M.; Auerswaldi, E. A.; Machleidt, W.; Magdolen, V., A Novel Type of Bifunctional Inhibitor Directed against Proteolytic Activity and Receptor/Ligand Interaction: Cystatin With a Urokinase Receptor B inding Site. *J. Biol. Chem.* **2000,** *275*, 33562-33566.

97. Quax, P. H. A.; Lamfers, M. L. M.; Lardenoye, J. H. P.; Grimbergen, J. M.; de Vries, M. R.; Slomp, J.; de Ruiter, M. C.; Kockx, M. M.; Verheijen, J. H.; van Hinsbergh, V. W. M., Adenoviral Expression of a Urokinase Receptor–Targeted Protease Inhibitor Inhibits Neointima Formation in Murine and Human Blood Vessels. *Circulation* **2001,** *103*, 562-569.

98. Konig, B.; Weidle, U.; Krell, H.; Kilpert, C.; Knipp, B. Oligothiophenes useful as antimetastatic agents, a preparation thereof and pharmaceutical compositions containing them. WO0979731645, 1997.

99. Di Domenico, R.; De Cillis, G.; Konig, B.; Zimmermann, G. Oligo-Thiophenes Useful as Antimetastatic Agents, a Preparation thereof and Pharmaceutical Compositions Containing Them. WO9906393, 1999.

100. Bauer, S.; Endele, R.; Fertig, G.; Friebe, W.-G.; Koerner, M.; Krell, H.-W. Novel Hydroxycoumarone Derivatives as Antitumor and Antimetastatic Agents with Improved Biological Activity in Cellular Assays and Improved Stability. WO 2004/076444 A2, September 10, 2004.

101. de Cillis, G.; di Domenico, R.; Koenig, B.; Oliva, A. O-Substituted Hydroxycumaronne Derivatives as Antitumor and Antimetastatic Agents. WO 99/06387, 1999.

102. Blood, C. H.; Neustadt, B. R.; Smith, E. M. Derivatives of aminobenzoic and aminobiphenylcarboxylic acids useful as anti-cancer agents. US 6,28,985 B1, May 8, 2001.

103. Khanna, M.; Wang, F.; Jo, I.; Knabe, W. E.; Wilson, S. M.; Li, L.; Bum-Erdene, K.; Li, J.; Sledge, G. W.; Khanna, R.; Meroueh, S. O., Targeting Multiple Conformations Leads to Small Molecule Inhibitors of the uPAR·uPA Protein-Protein Interaction That Block Cancer Cell Invasion. *ACS Chem. Biol.* **2011,** *6* (11), 1232-1243.

104. Liu, D.; Zhou, D.; Wang, B.; Knabe, W. E.; Meroueh, S. O., A New Class of Orthosteric uPAR•uPA Small-Molecule Antagonists Are Allosteric Inhibitors of the uPAR•Vitronectin Interaction. *ACS Chem. Biol.* **2015,** *10*, 1521-1534.

105. Xu, D.; Bum-Erdene, K.; Si, Y.; Zhou, D.; Ghozayel, M. K.; Meroueh, S. O., Mimicking Intermolecular Interactions of Tight Protein-Protein Complexes for Small-Molecule Antagonists. *ChemMedChem* **2017,** *12*, 1794-1809.

106. Lin, C.-M.; Arancillo, M.; Whisenant, J.; Burgess, K., Unconventional Secondary Structure Mimics: Ladder-rungs. *Angew. Chem., Int. Ed.* **2020,** *59*, 9398-9402.

107. D'Mello, V.; Singh, S.; Wu, Y.; Birge, R. B., The Urokinase Plasminogen Activator Receptor Promotes Efferocytosis of Apoptotic Cells. *J. Biol. Chem.* **2009,** *284* (25), 17030-17038.

108. Jorgensen, T. J. D.; Gaardsvoll, H.; Dano, K.; Roepstorff, P.; Ploug, M., Dynamics of Urokinase Receptor Interaction with Peptide Antagonists Studied by Amide Hydrogen Exchange and Mass Spectrometry. *Biochemistry* **2004,** *43* (47), 15044-15057.

109. Kolb, H. C.; Finn, M. G.; Sharpless, K. B., Click Chemistry: Diverse Chemical Function from a Few Good Reactions. *Angew. Chem. Int. Ed.* **2001,** *40*, 2004-21.

110. Limal, D.; Semetey, V.; Dalbon, P.; Jolivet, M.; Briand, J.-P., Solid-phase Synthesis of N,N'-Unsymmetrically Substituted Ureas: Application to the Synthesis of Carbaza Peptides. *Tetrahedron Lett.* **1999,** *40*, 2749-2752.

111. Lin, C.-M.; Jiang, Z.; Gao, Z.; Arancillo, M.; Burgess, K., Small Molecules Targeting The NEDD8 NAE Protein-Protein Interaction. *Chem. Sci.* **2021**, *12*, 1535-1543.

112. Arancillo, M.; Taechalertpaisarn, J.; Liang, X.; Burgess, K., Piptides: New, Easily Accessible Chemotypes For Interactions With Biomolecules. *Angew. Chem. Int. Ed.* **2020**, accepted.

113. Tosovska, P.; Arora, P. S., Oligooxopiperazines as nonpeptidic alpha-helix mimetics. *Org. Lett.* **2010,** *12* (7), 1588-1591.

114. Lao, B. B.; Drew, K.; Guarracino, D. A.; Brewer, T. F.; Heindel, D. W.; Bonneau, R.; Arora, P. S., Rational Design of Topographical Helix Mimics as Potent Inhibitors of Protein-Protein Interactions. *J. Am. Chem. Soc.* **2014,** *136* (22), 7877-7888.

115. Drew, K.; Renfrew, P. D.; Craven, T. W.; Butterfoss, G. L.; Chou, F.-C.; Lyskov, S.; Bullock, B. N.; Watkins, A.; Labonte, J. W.; Pacella, M.; Kilambi, K. P.; Leaver-Fay, A.; Kuhlman, B.; Gray, J. J.; Bradley, P.; Kirshenbaum, K.; Arora, P. S.; Das, R.; Bonneau, R., Adding diverse noncanonical backbones to ROSETTA: enabling peptidomimetic design. *PLoS One* **2013,** *8* (7), e67051.

116. Arora, P. S.; Olenyuk, B.; Bullock, B.; Grishagin, I. Preparation of nonpeptidic α-helix mimetic oligooxopiperazines and their use for controlling hypoxia-inducible gene expression. US267222013123511, 2013.

117. Lam, K. S.; Lebl, M.; Krchňák, V., The "One-Bead-One-Compound" Combinatorial Library Method. *Chem. Rev.* **1997,** *97* (2), 411-448.

118. Lu, S.; Jang, H.; Zhang, J.; Nussinov, R., Inhibitors of Ras-SOS Interactions. *ChemMedChem* **2016,** *11*, 814-821.

119. Zhan, M.-M.; Hu, X.-Q.; Liu, X.-X.; Ruan, B.-F.; Xu, J.; Liao, C., From monoclonal antibodies to small molecules: the development of inhibitors targeting the PD-1/PD-L1 pathway. *Drug Discov. Today* **2016,** *21*, 1027-1036.

120. Peraro, L.; Deprey, K. L.; Moser, M. K.; Zou, Z.; Ball, H. L.; Levine, B.; Kritzer, J. A., Cell Penetration Profiling Using the Chloroalkane Penetration Assay. *J. Am. Chem. Soc.* **2018,** *140*, 11360-11369.

121. Goodman, C. M.; Choi, S.; Shandler, S.; DeGrado, W. F., Foldamers as versatile frameworks for the design and evolution of function. *Nat. Chem. Biol.* **2007,** *3* (5), 252-262.

122. Toure, M.; Crews, C. M., Small-Molecule PROTACS: New Approaches to Protein Degradation. *Angew. Chem., Int. Ed.* **2016,** *55*, 1966-1973.

123. Kan, T.; Fukuyama, T., Ns strategies: a highly versatile synthetic method for amines. *Chem. Commun.* **2004**, 353-59.

124. Ko, E.; Liu, J.; Perez, L. M.; Lu, G.; Schaefer, A.; Burgess, K., Universal Peptidomimetics. *J. Am. Chem. Soc.* **2011,** *133*, 462-477.

125. Eftink, M. R.; Ghiron, C. A., Fluorescence quenching studies with proteins. *Anal. Biochem.* **1981,** *114* (2), 199-227.

126. Wound Healing ACAS Image Analysis. https://ibidi.com/software-and-image-analysis/187-wound-healing-acas-image-analysis.html (accessed 02/12/2020).

127. Mani, T.; Wang, F.; Knabe, W. E.; Sinn, A. L.; Khanna, M.; Jo, I.; Sandusky, G. E.; Sledge, G. W.; Jones, D. R.; Khanna, R.; Pollok, K. E.; Meroueh, S. O., Small-molecule inhibition of the uPAR·uPA interaction: Synthesis, biochemical, cellular, in vivo pharmacokinetics and efficacy studies in breast cancer metastasis. *Bioorg. Med. Chem.* **2013,** *21* (7), 2145-2155.

128. Mani, T.; Liu, D.; Zhou, D.; Li, L.; Knabe, W. E.; Wang, F.; Oh, K.; Meroueh, S. O., Probing Binding and Cellular Activity of Pyrrolidinone and Piperidinone Small Molecules Targeting the Urokinase Receptor. *ChemMedChem* **2013,** *8* (12), 1963-1977.

129. Wang, F.; Knabe, W. E.; Li, L.; Jo, I.; Mani, T.; Roehm, H.; Oh, K.; Li, J.; Khanna, M.; Meroueh, S. O., Design, synthesis, biochemical studies, cellular characterization, and structure-based computational studies of small molecules targeting the urokinase receptor. *Bioorg. Med. Chem.* **2012,** *20* (15), 4760-4773.

130. Wang, F.; Li, J.; Sinn, A. L.; Knabe, W. E.; Khanna, M.; Jo, I.; Silver, J. M.; Oh, K.; Li, L.; Sandusky, G. E.; Sledge, G. W., Jr.; Nakshatri, H.; Jones, D. R.; Pollok, K. E.; Meroueh, S. O., Virtual Screening Targeting the Urokinase Receptor, Biochemical and Cell-Based Studies, Synthesis, Pharmacokinetic Characterization, and Effect on Breast Tumor Metastasis. *J. Med. Chem.* **2011,** *54* (20), 7193-7205.

131. Antonyak, H.; Babych, N.; Solohub, L.; Snitynski, V.; Binder, B., Regulation of expression of the components of plasminogen activation system in leukemic cells. *Eksp. Onkol.* **2001,** *23* (4), 253-259.

132. Qi, J.; Oppenheimer, M.; Sobrado, P., Fluorescence polarization binding assay for Aspergillus fumigatus virulence factor UDP-galactopyranose mutase. *Enzyme Res.* **2011**, 513905, 9 pp.

133. Rossi, A. M.; Taylor, C. W., Analysis of protein-ligand interactions by fluorescence polarization. *Nat. Protoc.* **2011,** *6* (3), 365-387.

134. Feng, B. Y.; Shoichet, B. K., A detergent-based assay for the detection of promiscuous inhibitors. *Nat. Protoc.* **2006,** *1* (2), 550-553.

APPENDIX A*

SUPPORTING INFORMATION FOR CHAPTERS 2-4

General Experimental Procedures

All reactions were carried out under an inert atmosphere (nitrogen, or argon where stated) with dry solvents under anhydrous conditions. Glassware for anhydrous reactions was dried in an oven at 140 ºC for minimum 6 h prior to use. Dry solvents were obtained by passing the previously degassed solvents through activated alumina columns. Reagents were purchased at a high commercial quality (typically 97 % or higher) and used without further purification. Analytical thin layer chromatography (TLC) was carried out on Merck silica gel plates with QF 254 indicator and visualized by UV, ceric ammonium molybdate, ninhydrin, para-methoxybenzaldehyde and/or potassium permanganate stains. Flash chromatography was performed using silica gel (230-600 mesh). Microwave irradiation for solid-phase syntheses was done using CEM MARS 5® system. LC-MS analyses were collected from Agilent 1260 Infinity Quaternary LC and Agilent 6120 Quadrupole LC-MS modules using Poroshell 120 EC-C18 2.7 μM (4.6 x 50 mm) column in 10-90% MeCN/water gradient with 0.1% formic acid over 10 minutes. Agilent 1260

---

* Reprinted with permission from "Piptides: New, Easily Accessible Chemotypes For Interactions With Biomolecules" by Maritess Arancillo, Jaru Taechalertpaisarn, Xiaowen Liang, and Kevin Burgess, 2020. *Angew. Chem., Int. Ed.*, DOI: 10.1002/anie.202015203, Copyright 2020 by Wiley-VCH Verlag GmbH & Co. KGaA, Weinheim.

Infinity II LC together with the Agilent 1290 Evaporative Light Scattering Detector was used with Poroshell 120 EC-C18 2.7 μM (4.6 x 100 mm) column in 10-90% MeCN/water gradient with 0.1% TFA over 25 minutes. Well plates for bioassays were analyzed using Biotek Synergy H4 Microplate Reader. Circular Dichroism spectrums were recorded on a CD spectrometer using a 2 mm quartz cuvette at 200 μM in acetonitrile. High field NMR spectra were recorded with Bruker Avance III at 400 MHz for ^{1}H, and 100 MHz for ^{13}C and were calibrated using residual deuterated solvent as an internal reference ($CDCl_3$: ^{1}H NMR = 7.24, ^{13}C NMR = 77.0, MeOD: ^{1}H NMR = 3.30, ^{13}C NMR = 49.0, DMSO-d_6: ^{1}H NMR = 2.50, ^{13}C NMR = 39.5). The following abbreviations were used to explain the multiplicities: s = singlet, d = doublet, t = triplet, q = quartet, quint = quintet, dd = double doublet, dt = double triplet, dq = double quartet, m = multiplet, br = broad. Electrospray ionization mass spectrometry (ESI+MS) data were collected on triple-stage quadrupole instrument in a positive mode.

All statistical analyses were carried out by Graphpad Prism version 6.0 (Graphpad Software). Student's t-test was used to determine significant differences between compounds and negative control. Results are represented as means ± SD.

Syntheses of Pip Acids 5

Generalized Procedure

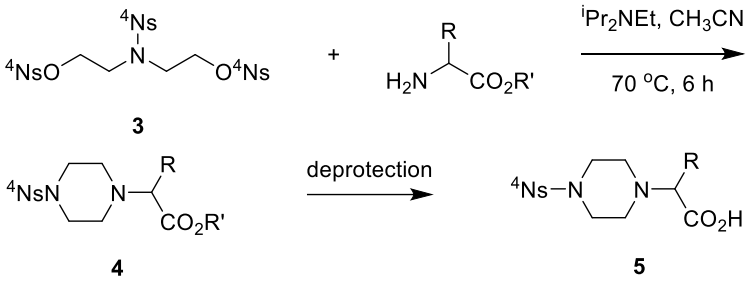

Tri(4-nitrobenzene sulfonate) {tri-nosyl or tri-^{4}Ns} **3** had been reacted with primary arylamines under microwave conditions to give N-aryl,N-^{4}Ns-piperazines. Following this lead, we explored reactions of **3**, and its tri(2-nitrobenzene sulfonate) {tri-^{2}Ns} analog, with amino acid esters. Studies of the ^{2}Ns-compounds were abandoned because more impurities were generated in the formation of pip acids, and removal of ^{2}Ns[123] required harsher conditions, presumably due to steric effects.

The ^{4}Ns -protected diethanolamine, **3**, was prepared as previously described.[37] Compound **3** (1 eq), the (acid-labile) side-chain and appropriate *C*-terminus-protected amino acids (1.2 eq), and $^{i}Pr_2NEt_2$ (4.0 eq), were mixed in acetonitrile (1 M) and stirred for 6 h at 70 ^{o}C. Solvent was completely removed *in vacuo*, re-dissolved in 10 mL CH_2Cl_2,

then extracted with 10 mL each of 10% aq. citric acid, saturated $NaHCO_3$, and brine. The organic phase was dried over $MgSO_4$ and concentrated *in vacuo* to afford the crude product. This crude product was purified by flash column chromatography (50-90% hexane/EtOAc or 0-15% CH_2Cl_2/MeOH) to give compound **4**. Deprotection of the ester gave the product **5**.

Deprotection of t-butyl esters

Compound **4** was dissolved in 5 mL 75% TFA/DCM and stirred for 2 h at 25°C. Solvent was removed and product was re-dissolved in 5 mL 1M HCl in MeOH for another 30 min at 25°C. Solvent was again removed *in vacuo*.

Deprotection of methyl esters

Compound **4** (1 eq) was dissolved in 5 mL anhydrous ethyl acetate under argon. Lithium iodide (12 eq) was added, and reaction was refluxed for 48 h under argon. The reaction mixture was diluted with 5 mL water and adjusted to pH 3 with 10% aq. citric acid and then washed with 15 mL CH_2Cl_2. The organic phase was dried over $MgSO_4$ and removed *in vacuo*.

L-**5d'**

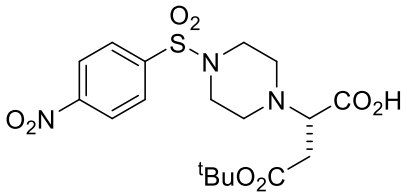

(S)-4-(Tert-butoxy)-2-(4-((4-nitrophenyl)sulfonyl)piperazin-1-yl)-4-oxobutanoic acid, 55%, white solid

^{1}H NMR (400 MHz, MeOD) δ 8.45 (d, J = 8.3 Hz, 2H), 8.01 (d, J = 8.3 Hz, 2H), 3.51 (t, J = 7.4 Hz, 1H), 2.93 (m, 4H), 2.71 (d, J = 4.5 Hz, 2H), 2.55 (m, 3H), 2.35 (dd, J = 15.3, 7.1 Hz, 1H), 1.28 (s, 9H).

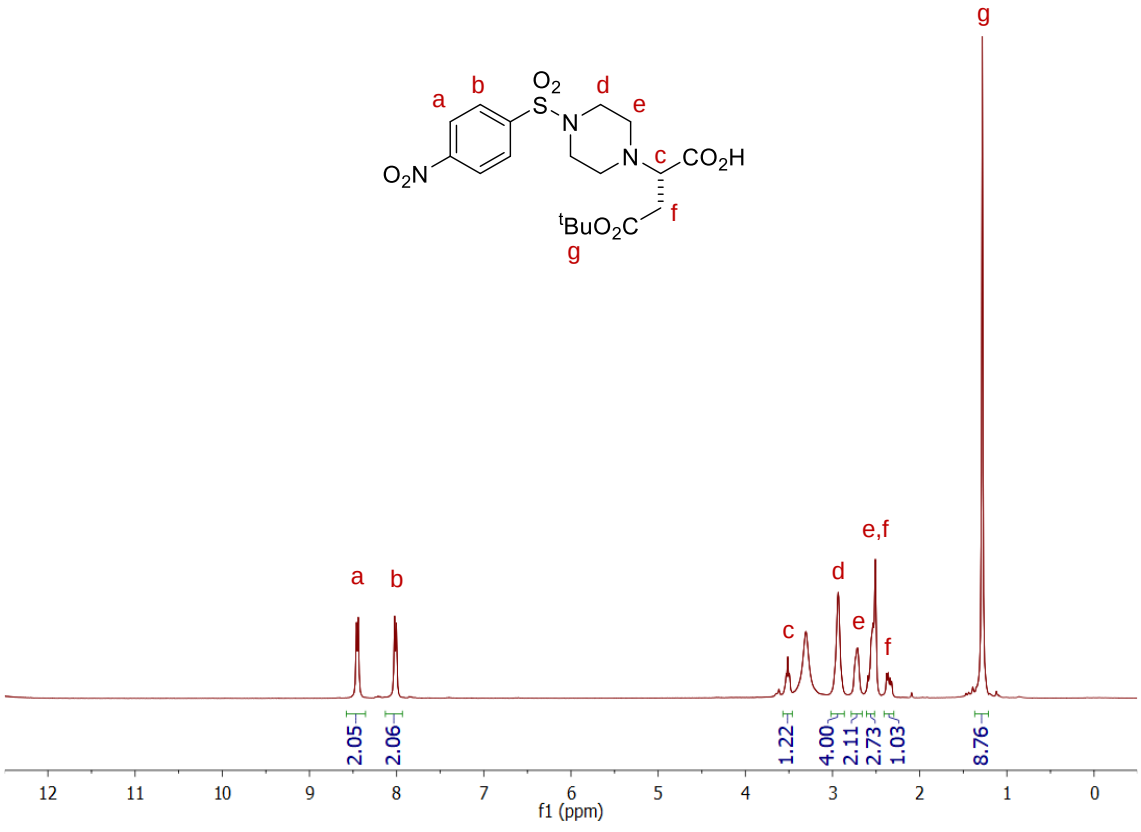

^{13}C NMR (100 MHz, DMSO-d_6) δ 171.8, 170.4, 150.6, 141.1, 129.6, 125.1, 80.30, 63.49, 48.45, 46.85, 35.44, 28.06.

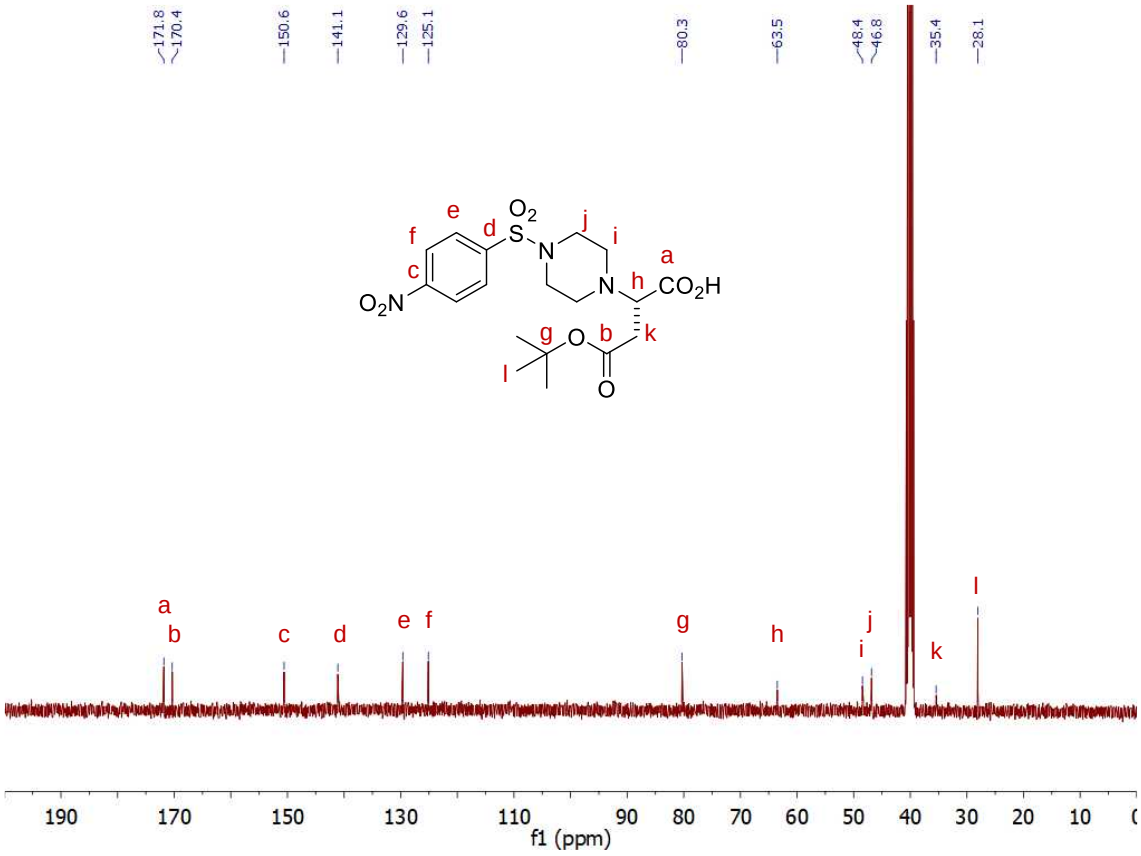

HRMS (ESI) m/z calc'd for $C_{18}H_{26}N_3O_8S^+$ 444.1362; found 444.1365.

L-**5e'**

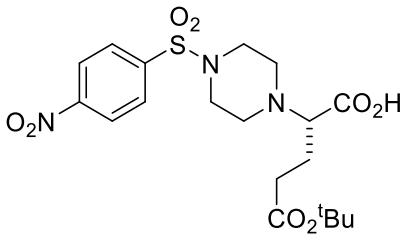

(S)-5-(Tert-butoxy)-2-(4-((4-nitrophenyl)sulfonyl)piperazin-1-yl)-5-oxopentanoic acid, 35%, white solid

^{1}H NMR (400 MHz, acetone-d_6) δ 8.59 – 8.44 (m, 2H), 8.19 – 8.00 (m, 2H), 3.21 – 3.14 (m, 1H), 3.09 (dt, J = 16.3, 5.8 Hz, 4H), 2.91 – 2.84 (m, 2H), 2.70 – 2.60 (m, 2H), 2.21 (m, 2H), 1.88 – 1.78 (m, 2H), 1.36 (s, 9H).

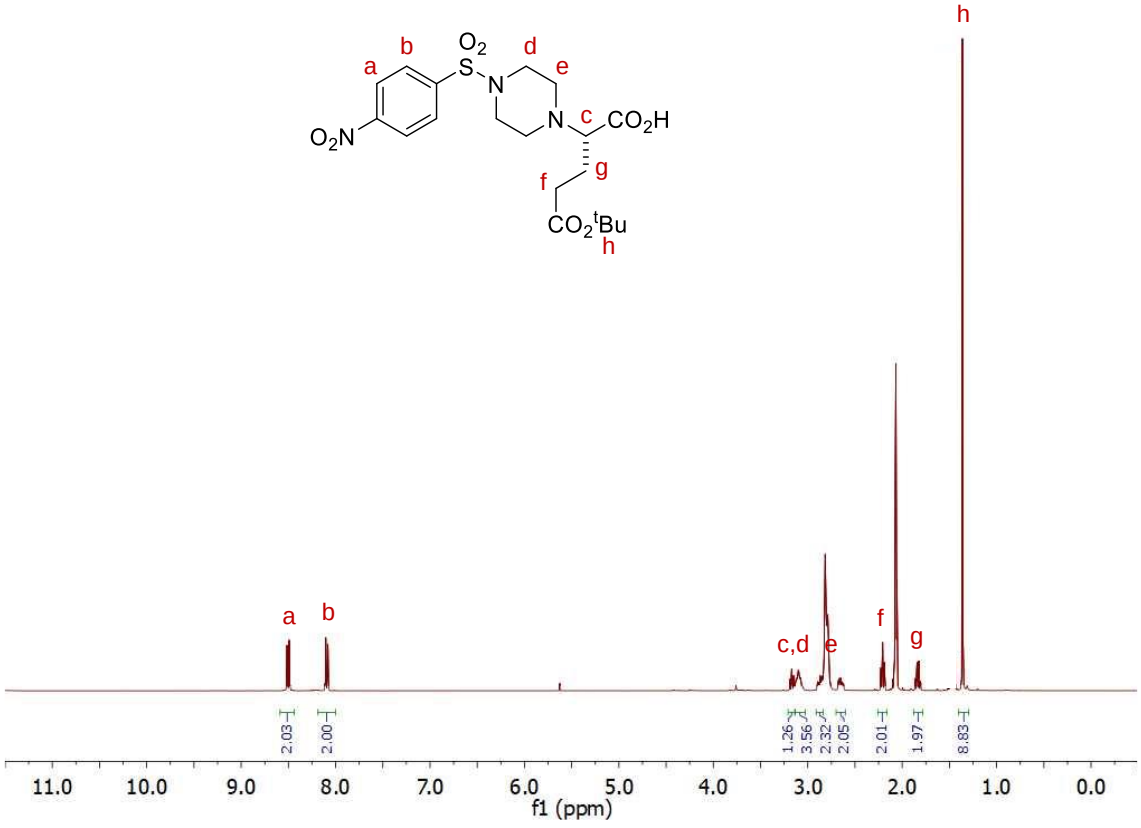

^{13}C NMR (100 MHz, MeOD) δ 174.17, 171.07, 150.47, 141.75, 128.89, 124.11, 63.31, 60.17, 53.38, 50.54, 34.43, 19.46, 13.05.

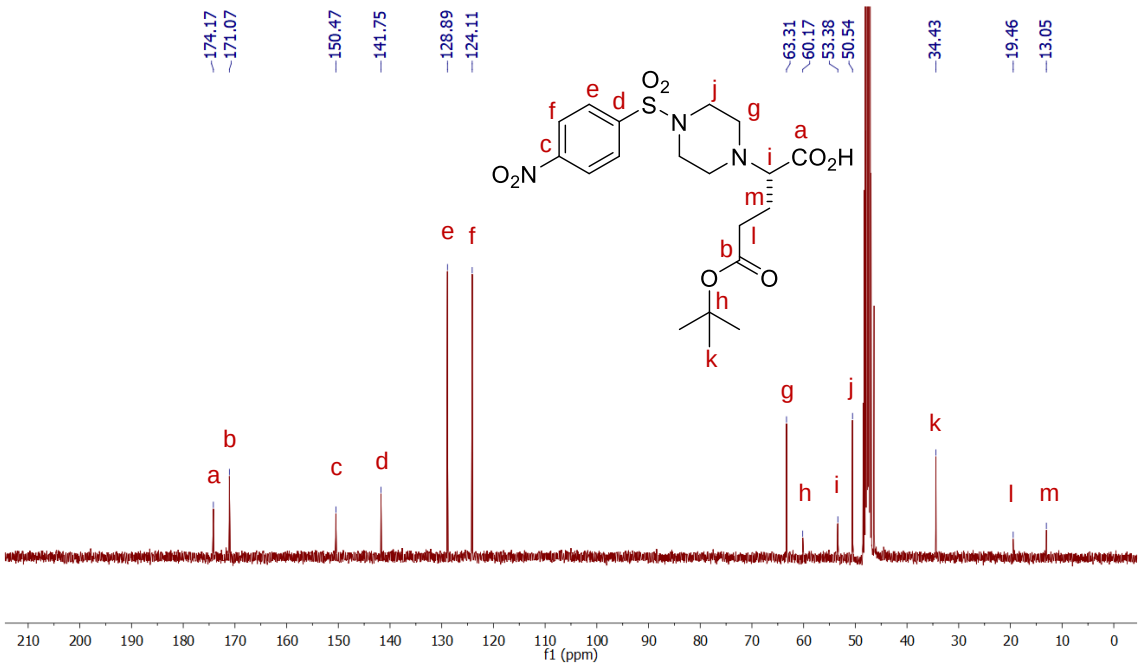

HRMS (ESI) m/z calc'd for $C_{19}H_{28}N_3O_8S^+$ 458.1519; found 458.1515.

L-**5f**

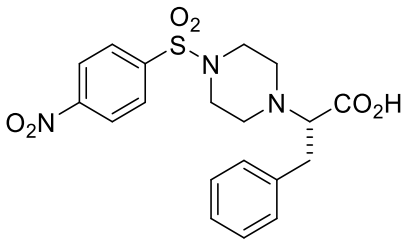

(S)-2-(4-((4-Nitrophenyl)sulfonyl)piperazin-1-yl)-3-phenylpropanoic acid, 98%, light yellow solid

^{1}H NMR (400 MHz, $CDCl_3$) δ 8.40 (d, J = 8.8 Hz, 2H), 7.96 (d, J = 8.8 Hz, 2H), 7.27 – 7.11 (m, 5H), 3.34 (dd, J = 9.3, 6.0 Hz, 1H), 3.18 – 2.96 (m, 5H), 2.91 – 2.69 (m, 5H).

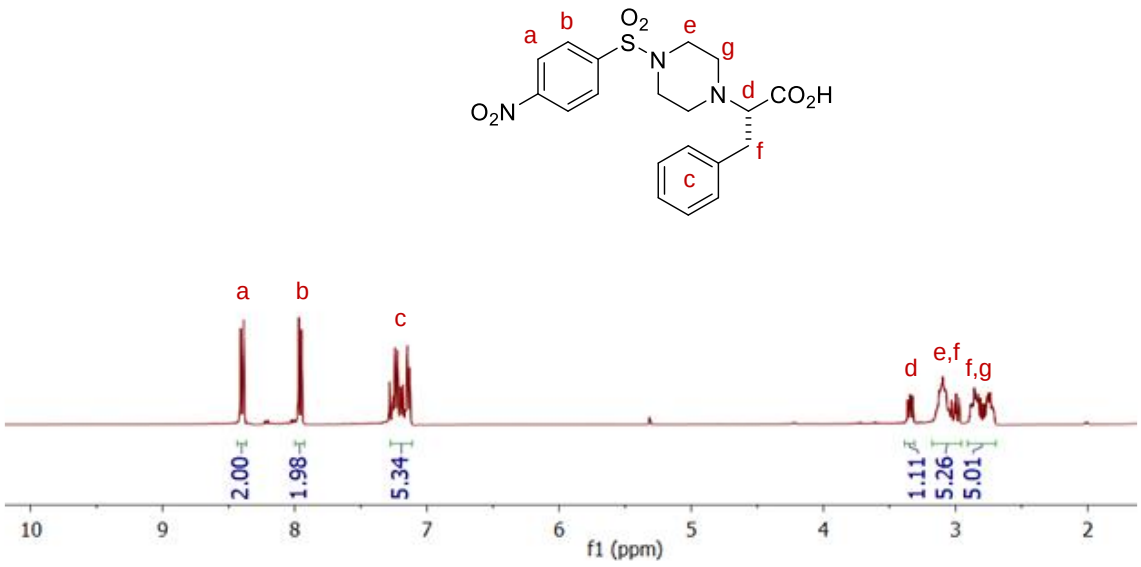

^{13}C NMR (100 MHz, DMSO-d_6) δ 150.78, 141.11, 129.96, 129.71, 129.62, 129.00, 128.85, 127.33, 125.31, 100.00, 49.05, 48.99, 33.66.

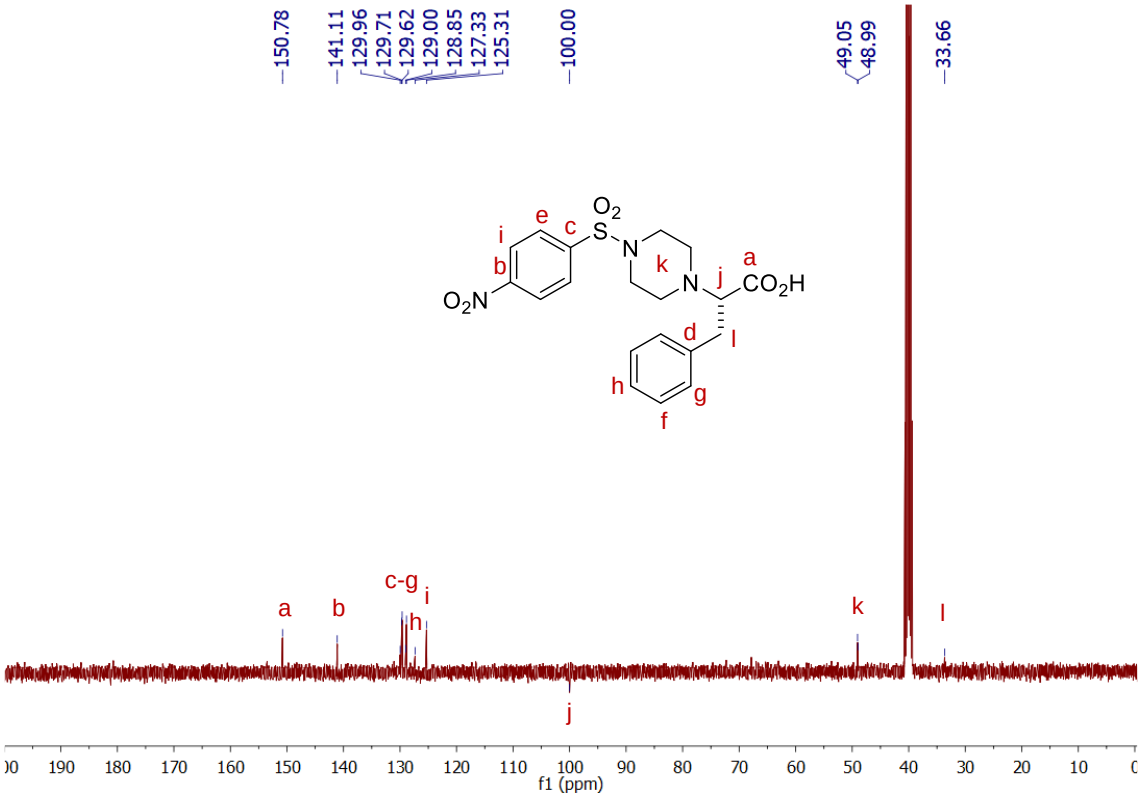

HRMS (ESI) m/z calc'd for $C_{19}H_{22}N_3O_6S^+$ 420.1151; found 420.1150.

L-**5h'**

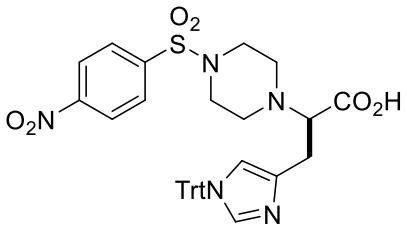

(R)-2-(4-((4-Nitrophenyl)sulfonyl)piperazin-1-yl)-3-(1-trityl-1H-imidazol-4-yl)propanoic acid, 35%, white solid

^{1}H NMR (400 MHz, DMSO-d_6) δ 8.43 (m, 2H), 8.19 – 7.88 (m, 2H), 7.54 – 7.29 (m, 10H), 7.02 (m, 6H), 6.64 (s, 1H), 3.46 (t, J = 7.4 Hz, 1H), 2.88 (s, 4H), 2.82 – 2.64 (m, 4H), 2.54 (dd, J = 10.6, 4.9 Hz, 2H).

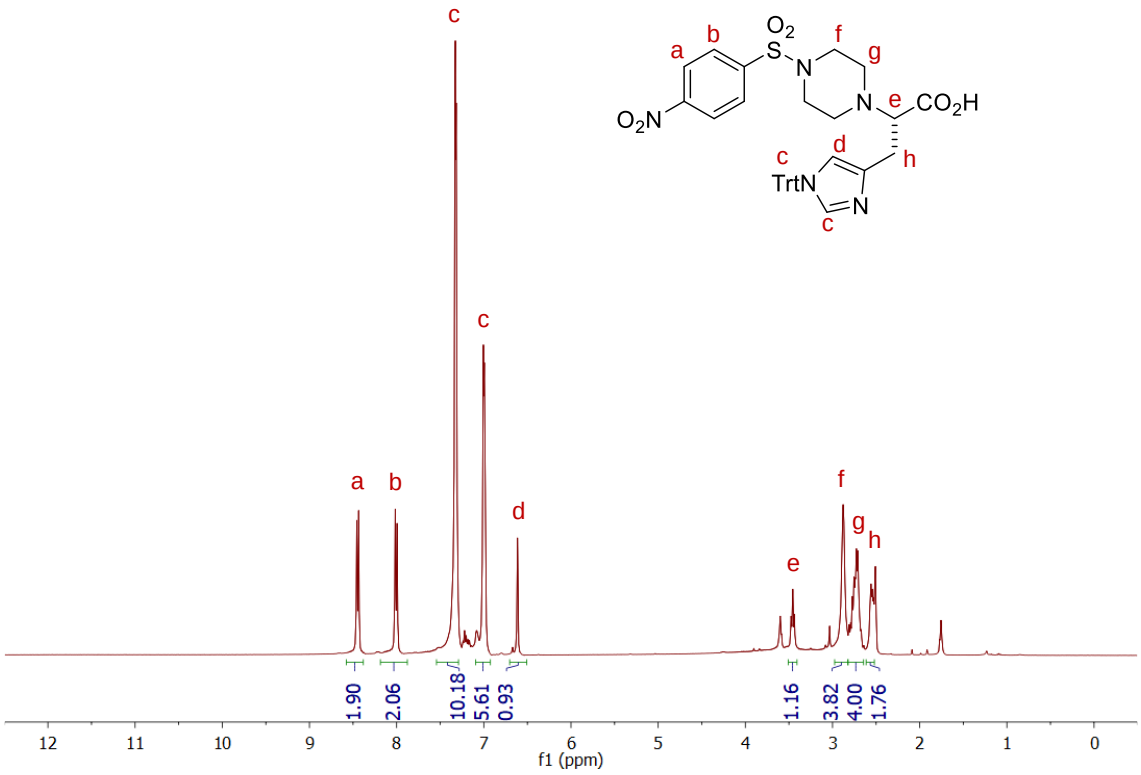

^{13}C NMR (100 MHz, DMSO-d_6) δ 172.65, 150.45, 142.56, 141.54, 137.54, 137.37, 129.60, 128.56, 125.18, 119.48, 75.04, 67.49, 66.44, 48.31, 46.85, 25.59.

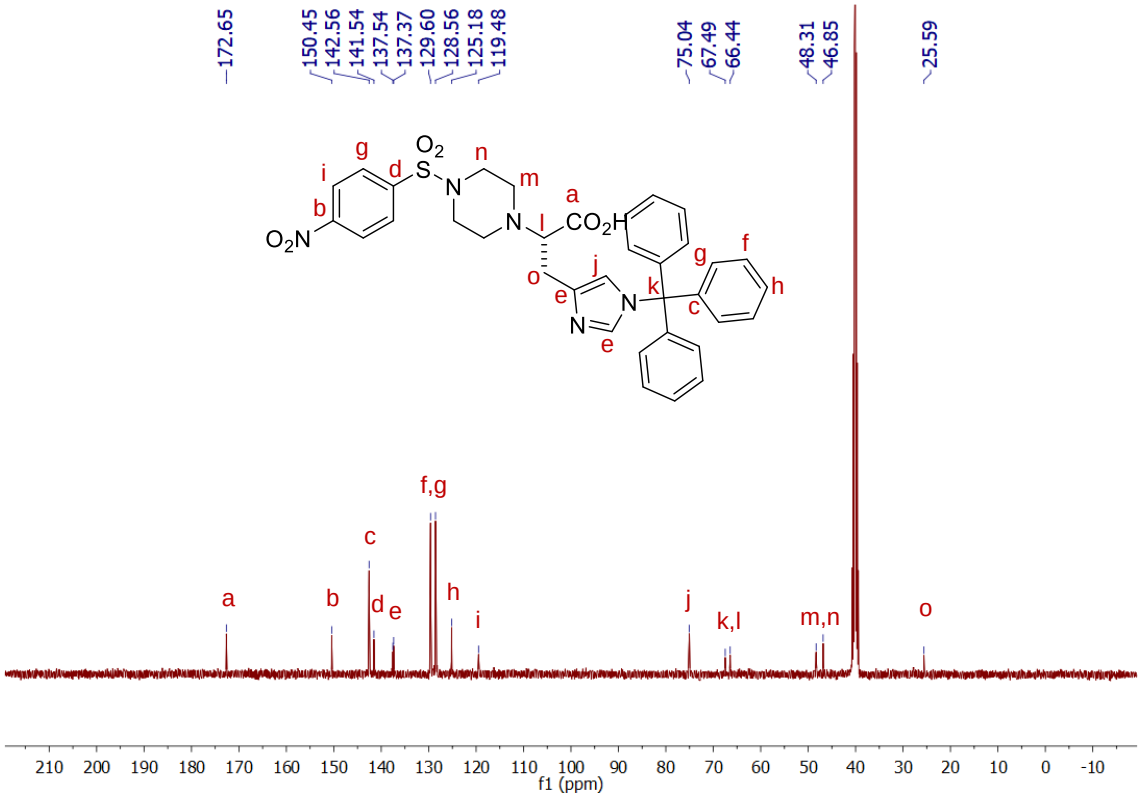

HRMS (ESI) m/z calc'd for $C_{35}H_{34}N_5O_6S^+$ 652.2152; found 652.2153.

L-**5i**

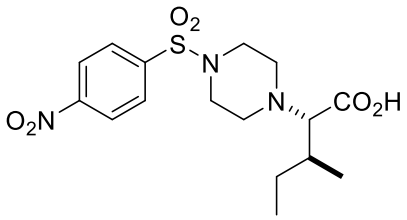

(2S,3S)-3-Methyl-2-(4-((4-nitrophenyl)sulfonyl)piperazin-1-yl)pentanoic acid, 60%, white solid

^{1}H NMR (400 MHz, DMSO-d_6) δ 12.40 (s, 1H), 8.45 (d, J = 8.8 Hz, 2H), 8.01 (d, J = 8.8 Hz, 2H), 3.47 – 3.34 (m, 1H), 2.98 (s, 4H), 2.78 – 2.53 (m, 4H), 1.79 – 1.42 (m, 2H), 0.97 (m, 1H), 0.86 – 0.70 (m, 6H).

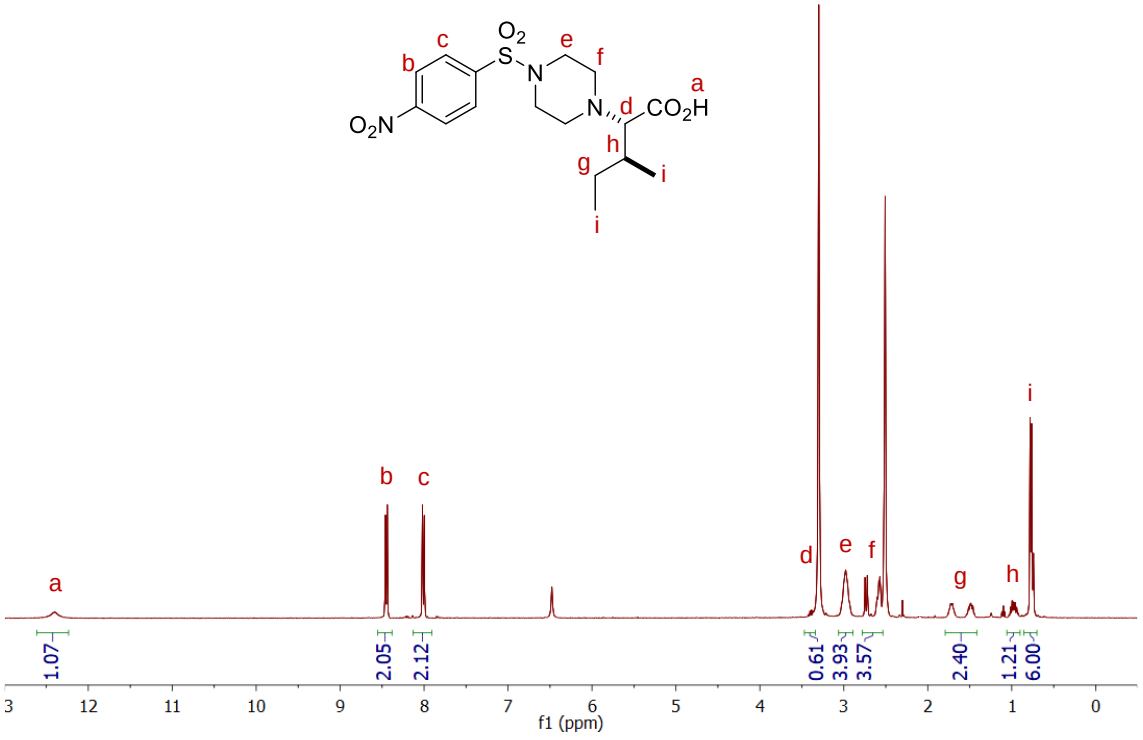

^{13}C NMR (100 MHz, DMSO-d_6) δ 172.11, 150.59, 141.48, 129.52, 125.21, 100.00, 46.85, 46.74, 32.03, 26.42, 11.50, 10.60.

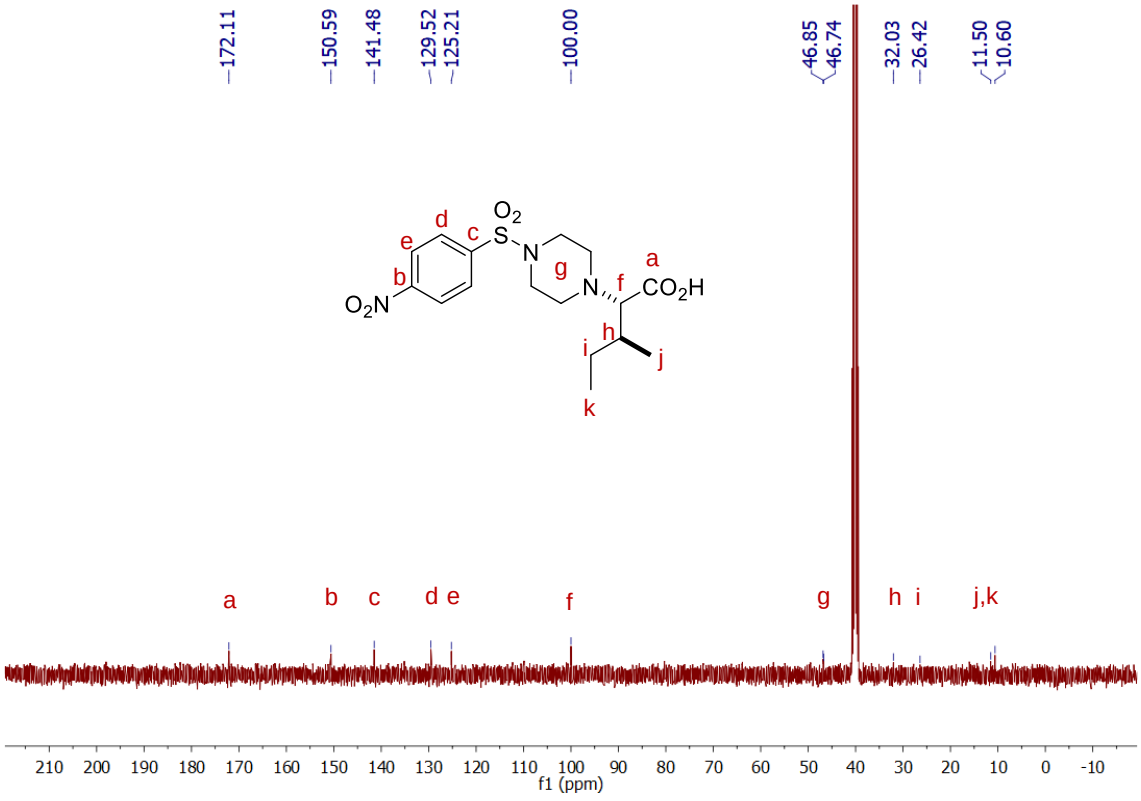

HRMS (ESI+) m/z calc'd for $C_{16}H_{24}N_3O_6S^+$ 386.1308; found 386.1311.

L-**5k'**

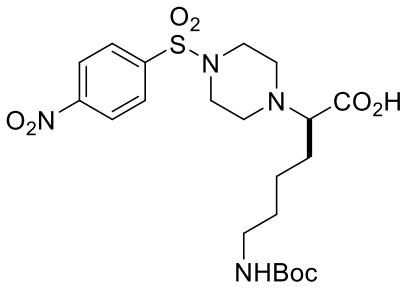

(R)-6-((Tert-butoxycarbonyl)amino)-2-(4-((4-nitrophenyl)sulfonyl)piperazin-1-yl)hexanoic acid, 69%, white solid

^{1}H NMR (400 MHz, DMSO-d_6) δ 8.47 (d, J = 11.1 Hz, 2H), 8.05 (dd, J = 27.5, 8.7 Hz, 2H), 6.68 (s, 1H), 3.11 (s, 1H), 2.99 (s, 4H), 2.85 (m, 2H), 2.66 (m, 4H), 2.51 (s, 1H), 1.54 (m, 2H), 1.39 – 1.28 (m, 11H), 1.18 (m, 2H).

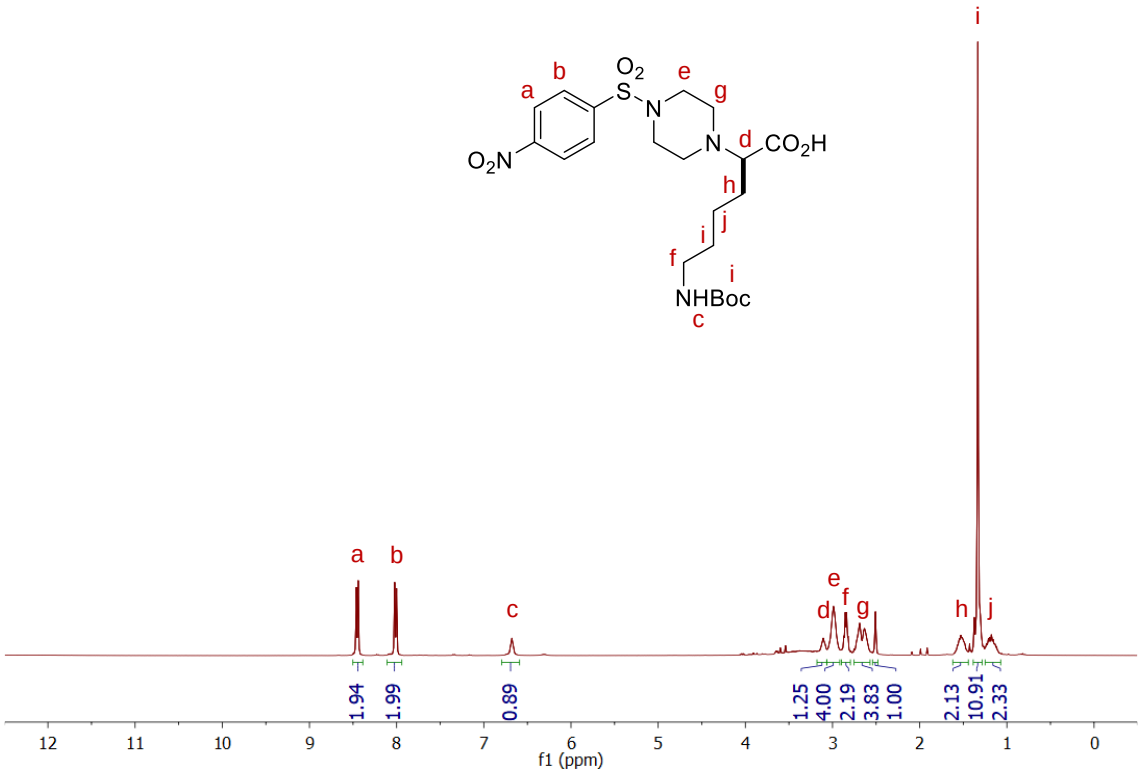

^{13}C NMR (100 MHz, DMSO-d_6) δ 173.13, 156.01, 150.58, 141.45, 129.54, 125.18, 77.72, 66.51, 48.27, 46.65, 29.91, 29.69, 28.70, 28.39, 23.31.

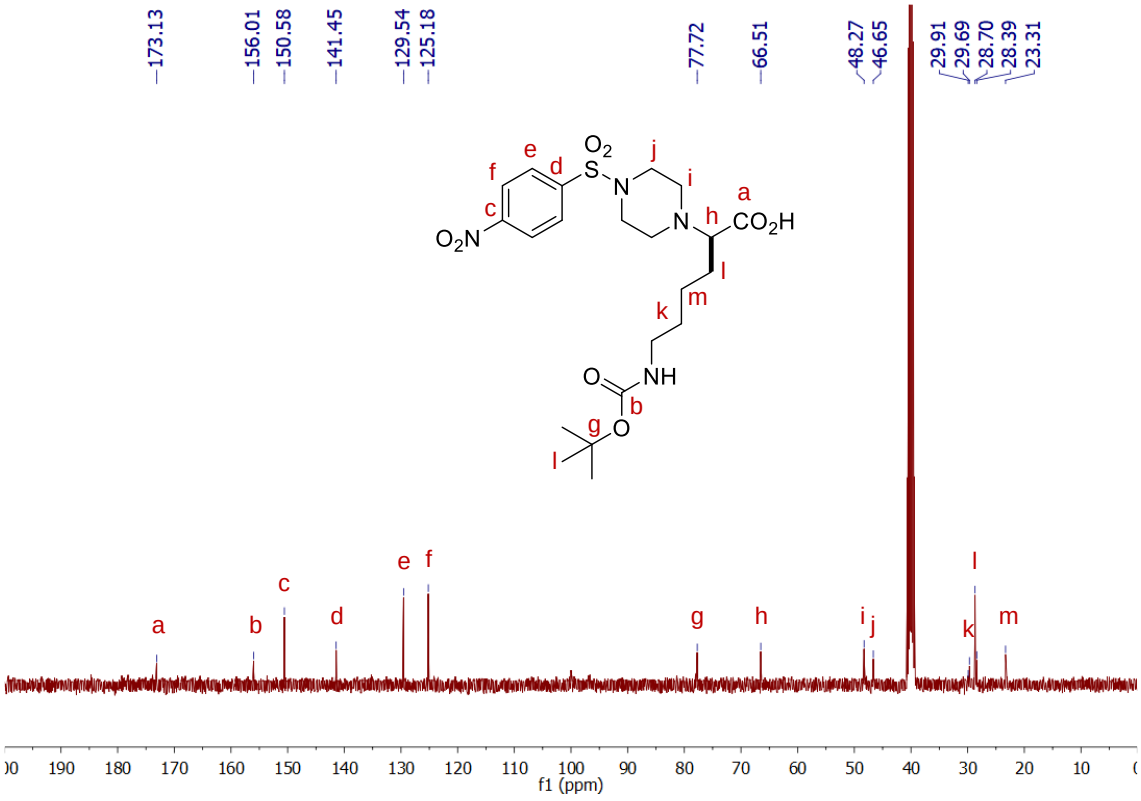

HRMS (ESI+) m/z calc'd for $C_{21}H_{33}N_4O_8S^+$ 501.1941, found 501.1940.

L-**5l**

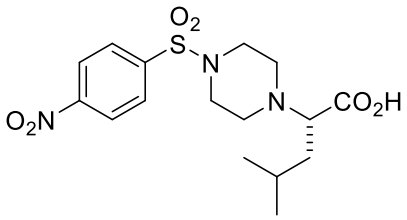

(S)-4-Methyl-2-(4-((4-nitrophenyl)sulfonyl)piperazin-1-yl)pentanoic acid, 80%, white solid

^{1}H NMR (400 MHz, MeOD) δ 8.48 (dd, J = 9.1, 2.1 Hz, 2H), 8.11 – 8.06 (m, 2H), 3.98 (dd, J = 9.7, 4.0 Hz, 1H), 3.67 – 3.34 (m, 8H), 1.89 – 1.68 (m, 3H), 1.04 – 0.92 (m, 6H).

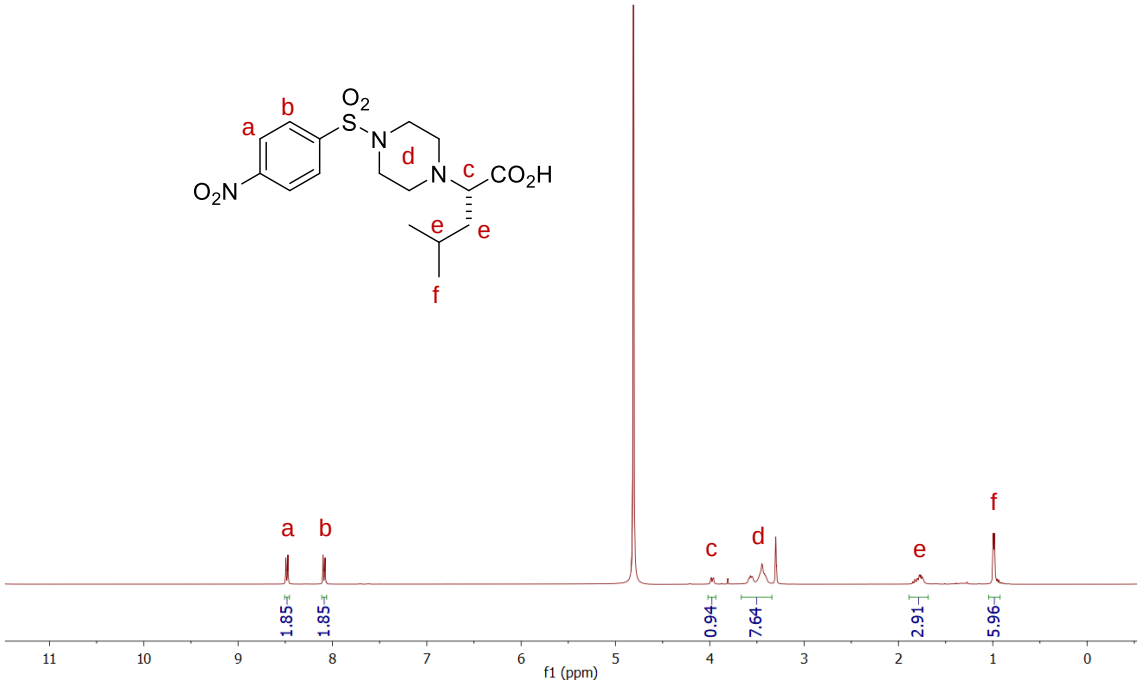

^{13}C NMR (100 MHz, MeOD) δ 170.64, 152.22, 142.50, 130.45, 125.84, 67.54, 50.77, 44.66, 37.29, 26.59, 23.58, 21.46.

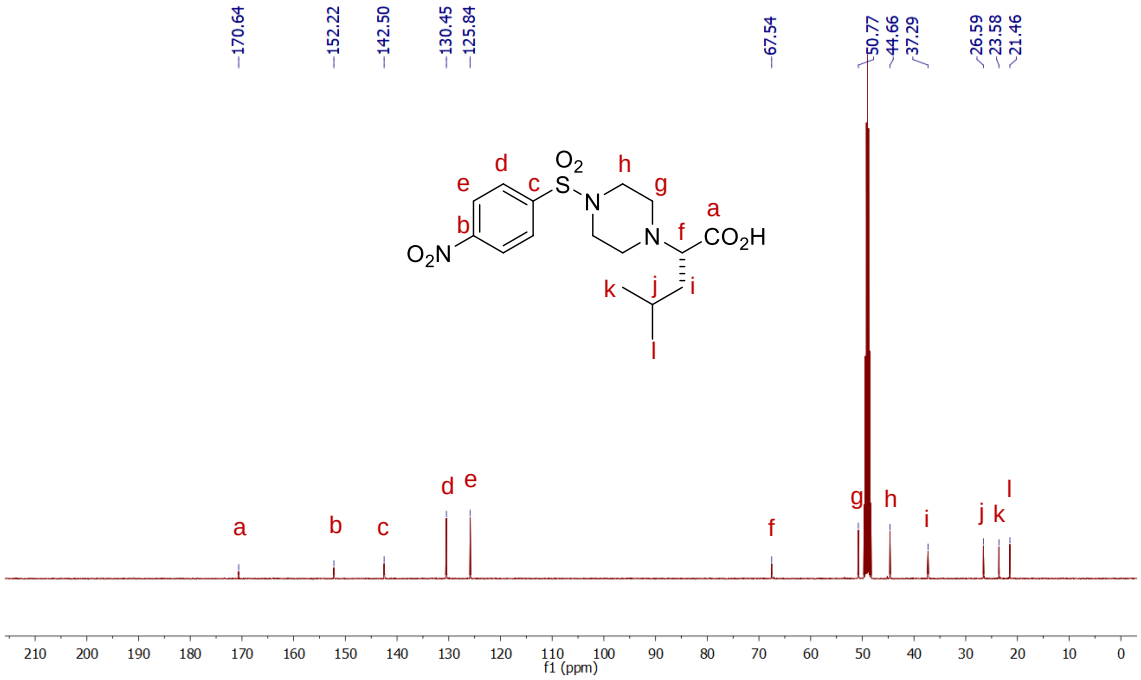

HRMS (ESI+) m/z calc'd for $C_{16}H_{24}N_3O_6S^+$ 386.1308, found 386.1309.

L-**5q'**

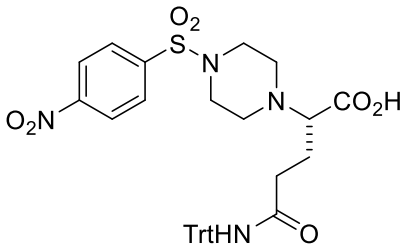

(S)-2-(4-((4-nitrophenyl)sulfonyl)piperazin-1-yl)-5-oxo-5-(tritylamino)pentanoic acid,

55%, yellow solid

^{1}H NMR (400 MHz, DMSO-d_6) δ 8.64 (s, 1H), 8.44 (d, J = 8.8 Hz, 2H), 8.05 (d, J = 8.7 Hz, 2H), 7.11 (m, 15H), 3.62 (m, 1H), 2.96 (m, 4H), 2.95 – 2.85 (m, 2H), 2.70 (dd, J = 14.7, 10.4 Hz, 1H), 2.65 – 2.55 (m, 2H), 2.41 (dd, J = 14.8, 4.9 Hz, 1H), 1.84 – 1.70 (m, 2H).

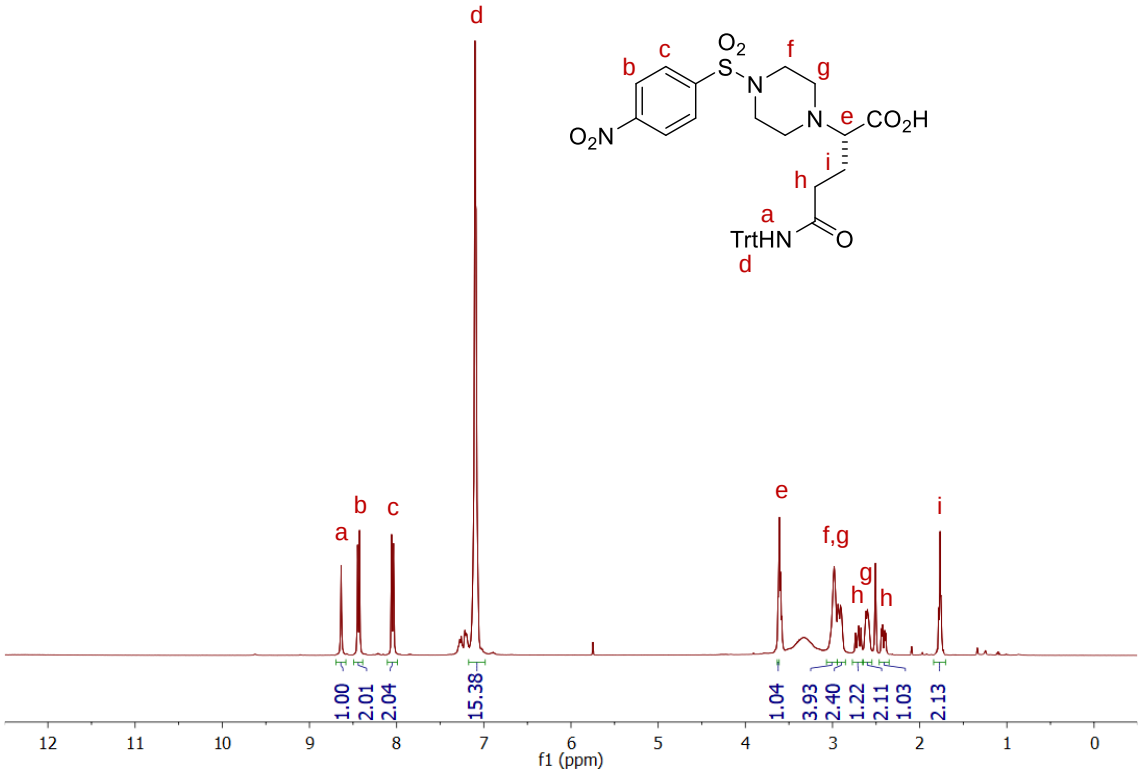

^{13}C NMR (100 MHz, DMSO-d_6) δ 172.39, 169.65, 150.47, 145.15, 140.99, 129.68, 128.96, 127.71, 126.58, 125.21, 69.66, 67.49, 48.30, 46.88, 25.60.

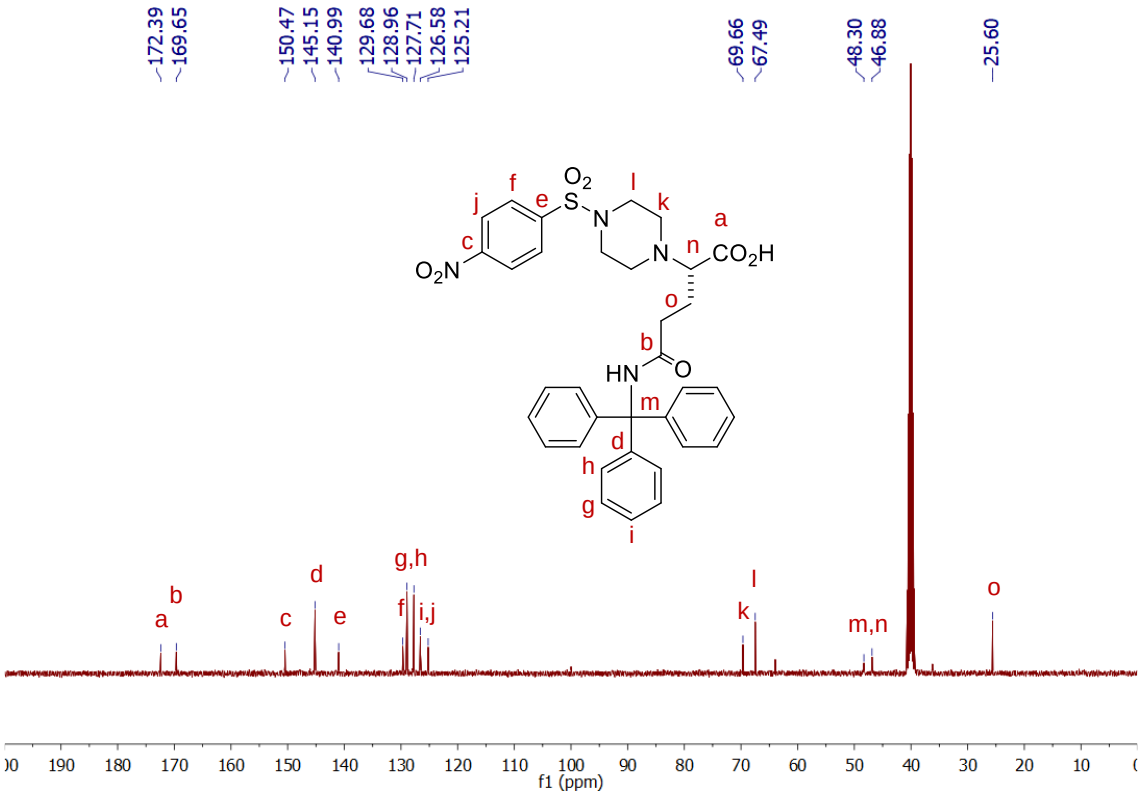

HRMS (ESI+) m/z calc'd for $C_{33}H_{33}N_4O_7S^+$ 629.1992, found 629.1990.

L-**5s'**

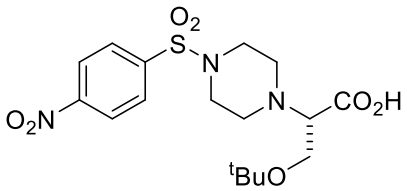

(S)-3-(Tert-butoxy)-2-(4-((4-nitrophenyl)sulfonyl)piperazin-1-yl)propanoic acid, 80%, white solid

^{1}H NMR (400 MHz, $CDCl_3$) δ 8.38 (d, J = 8.8 Hz, 2H), 7.93 (d, J = 8.8 Hz, 2H), 3.70 – 3.64 (m, 1H), 3.05 (s, 4H), 2.85 – 2.76 (m, 2H), 2.70 (dd, J = 15.7, 8.2 Hz, 1H), 2.65 – 2.57 (m, 2H), 2.43 (dd, J = 15.7, 7.0 Hz, 1H), 1.35 (s, 9H).

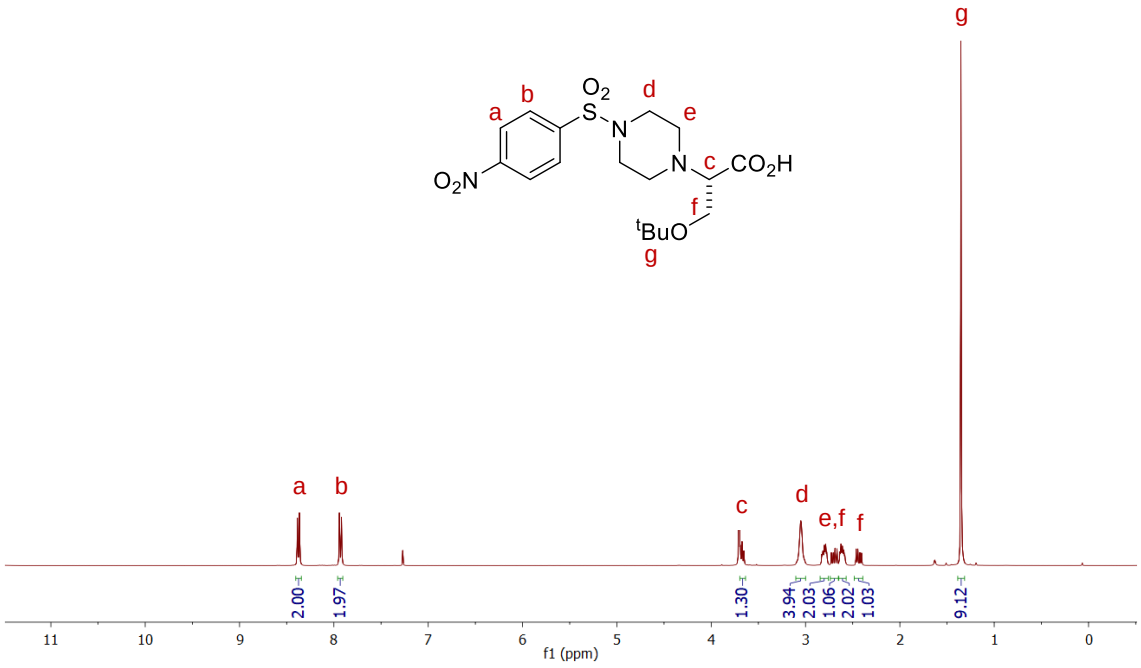

^{13}C NMR (100 MHz, $CDCl_3$) δ 175.7, 151.3, 146.0, 128.4, 128.4, 124.9, 124.7, 82.3, 71.2, 62.7, 51.3, 51.2, 49.2, 49.1, 28.9, 28.7

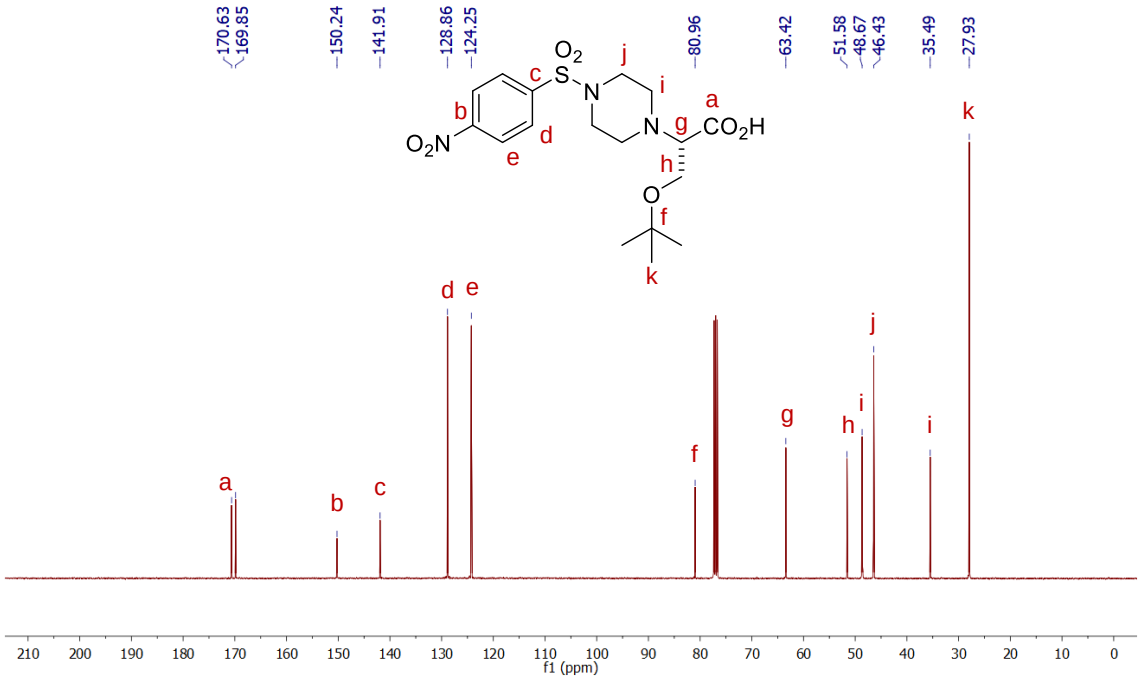

HRMS (ESI+) m/z calc'd for $C_{17}H_{26}N_3O_7S^+$ 416.1413; found 416.1412.

L-**5t'**

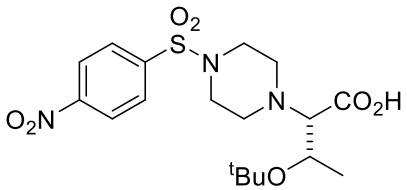

(2S,3S)-3-(Tert-butoxy)-2-(4-((4-nitrophenyl)sulfonyl)piperazin-1-yl)butanoic acid, 95%, light yellow solid

^{1}H NMR (400 MHz, DMSO-d_6) δ 8.45 (d, J = 8.8 Hz, 2H), 8.01 (d, J = 8.8 Hz, 2H), 4.03 (p, J = 6.1 Hz, 1H), 3.17 (d, J = 5.4 Hz, 1H), 2.95 (m, 4H), 2.87 – 2.67 (m, 4H), 2.54 – 2.47 (m, 3H), 1.06 (s, 9H).

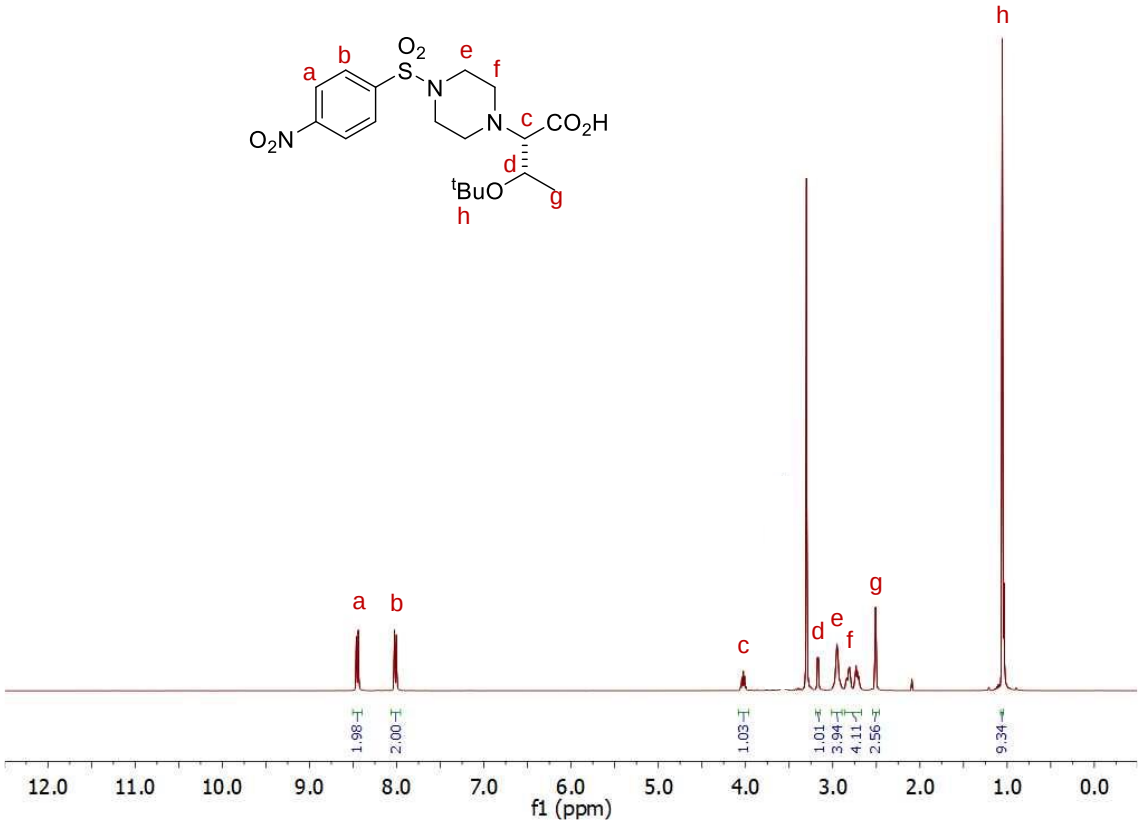

^{13}C NMR (100 MHz, DMSO-d_6) δ 171.17, 150.57, 141.37, 129.57, 125.16, 73.77, 72.21, 67.49, 51.22, 49.54, 46.81, 28.75, 20.30.

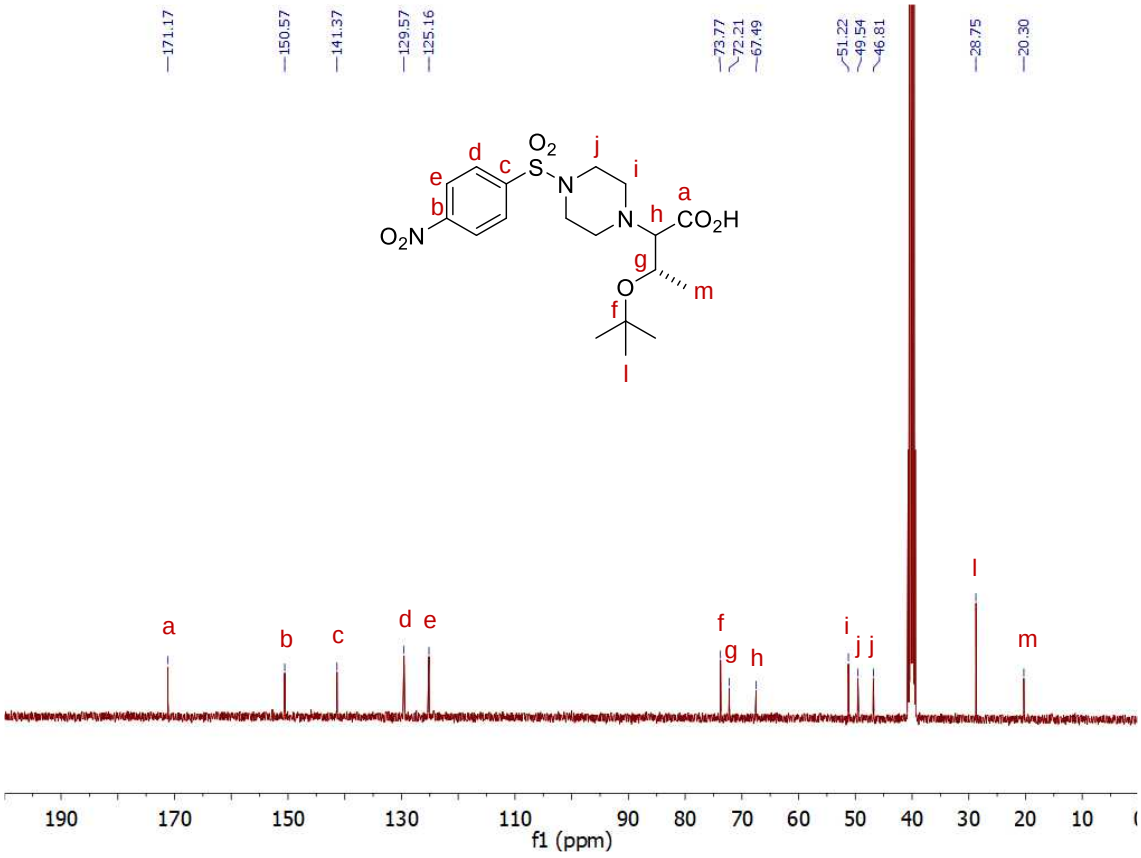

HRMS (ESI+) m/z calc'd for $C_{18}H_{28}N_3O_7S^+$ 430.1570; found 430.1575.

L-**5v**

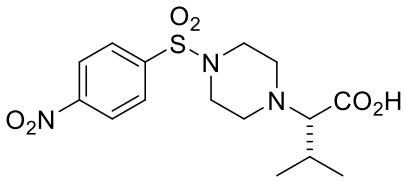

(S)-3-Methyl-2-(4-((4-nitrophenyl)sulfonyl)piperazin-1-yl)butanoic acid, 77%, brown solid

^{1}H NMR (400 MHz, $CDCl_3$) δ 8.43 – 8.38 (m, 2H), 7.99 – 7.93 (m, 2H), 3.09 (dd, J = 15.1, 11.6 Hz, 4H), 2.78 – 2.61 (m, 4H), 2.59 (d, J = 10.7 Hz, 1H), 2.01 – 1.89 (m, 1H), 0.84 (m, 6H).

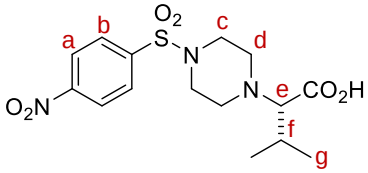

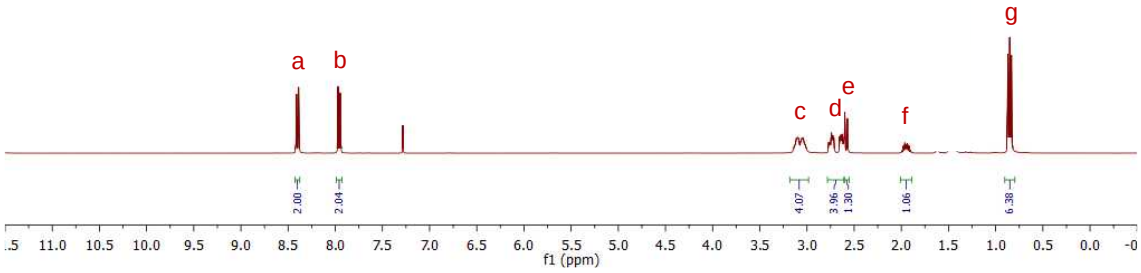

^{13}C NMR (100 MHz, $CDCl_3$) δ 170.31, 150.24, 142.20, 128.86, 124.31, 81.32, 74.93, 48.48, 46.64, 28.35, 26.63, 19.46, 19.15.

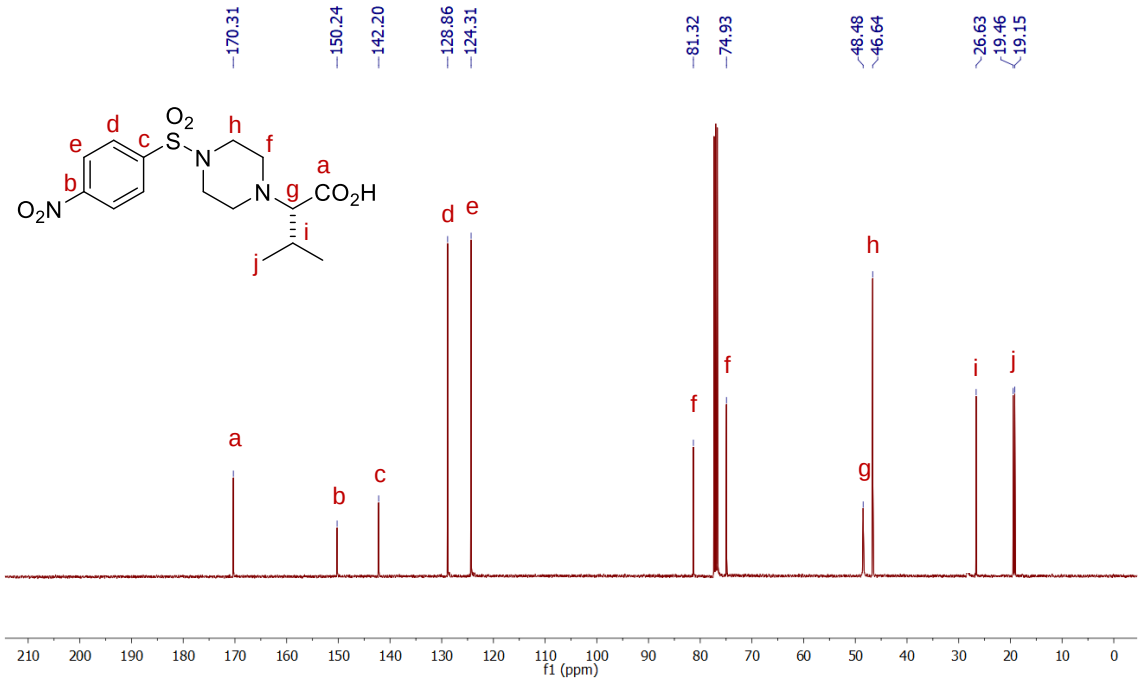

HRMS (ESI+) m/z calc'd for $C_{15}H_{22}N_3O_6S^+$ 372.1151; found 372.1153.

L-**5w**

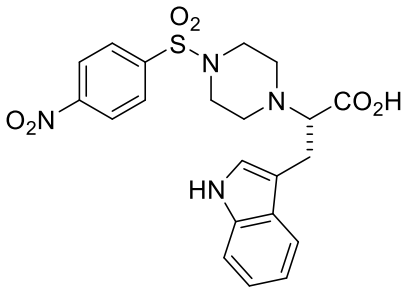

(S)-3-(1H-Indol-3-yl)-2-(4-((4-nitrophenyl)sulfonyl)piperazin-1-yl)propanoic acid, 48%, white solid

^{1}H NMR (400 MHz, DMSO-d_6) δ 10.74 (s, 1H), 8.45 (d, J = 8.7 Hz, 2H), 8.01 (d, J = 8.7 Hz, 2H), 7.45 (d, J = 7.8 Hz, 1H), 7.30 (d, J = 8.1 Hz, 1H), 7.12 – 6.98 (m, 2H), 6.93 (t, J = 7.4 Hz, 1H), 3.46 (m, 1H), 3.13 – 3.03 (m, 1H), 2.98 (s, 4H), 2.90 – 2.82 (m, 1H), 2.72 (m, 4H).

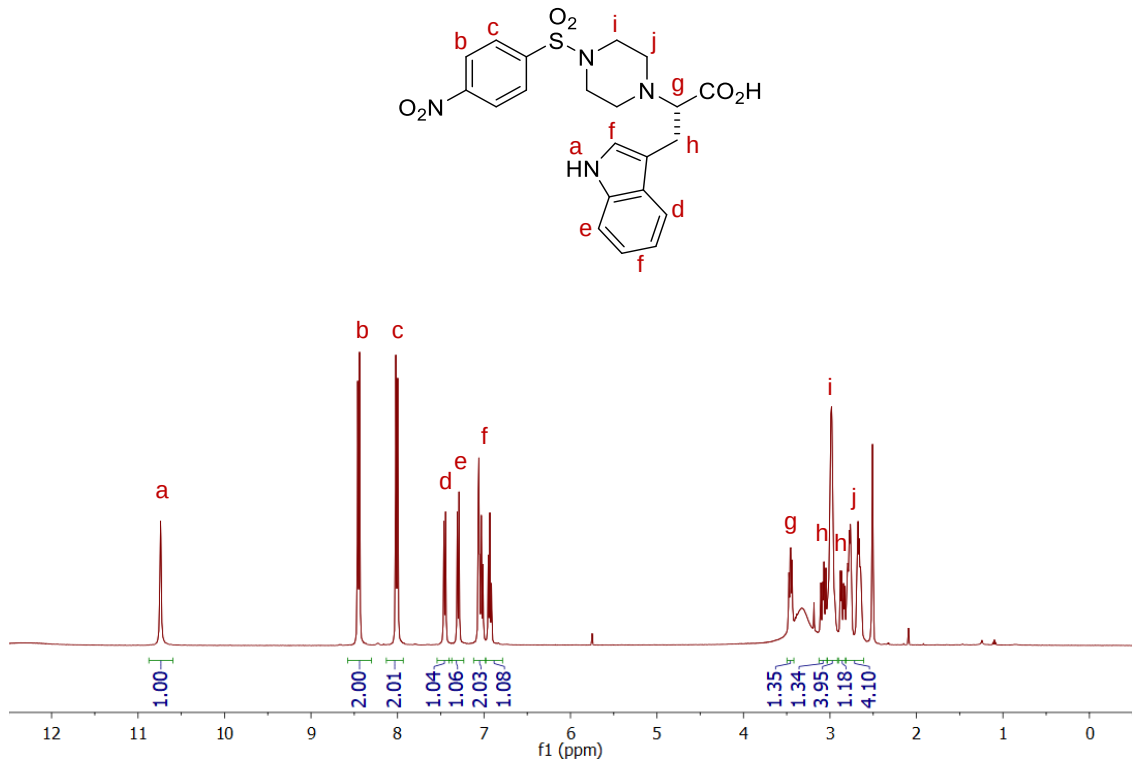

^{13}C NMR (100 MHz, DMSO-d_6) δ 172.61, 150.58, 141.31, 136.48, 129.55, 127.64, 125.16, 123.69, 121.28, 118.69, 118.60, 111.79, 110.82, 67.88, 48.61, 46.84, 24.86.

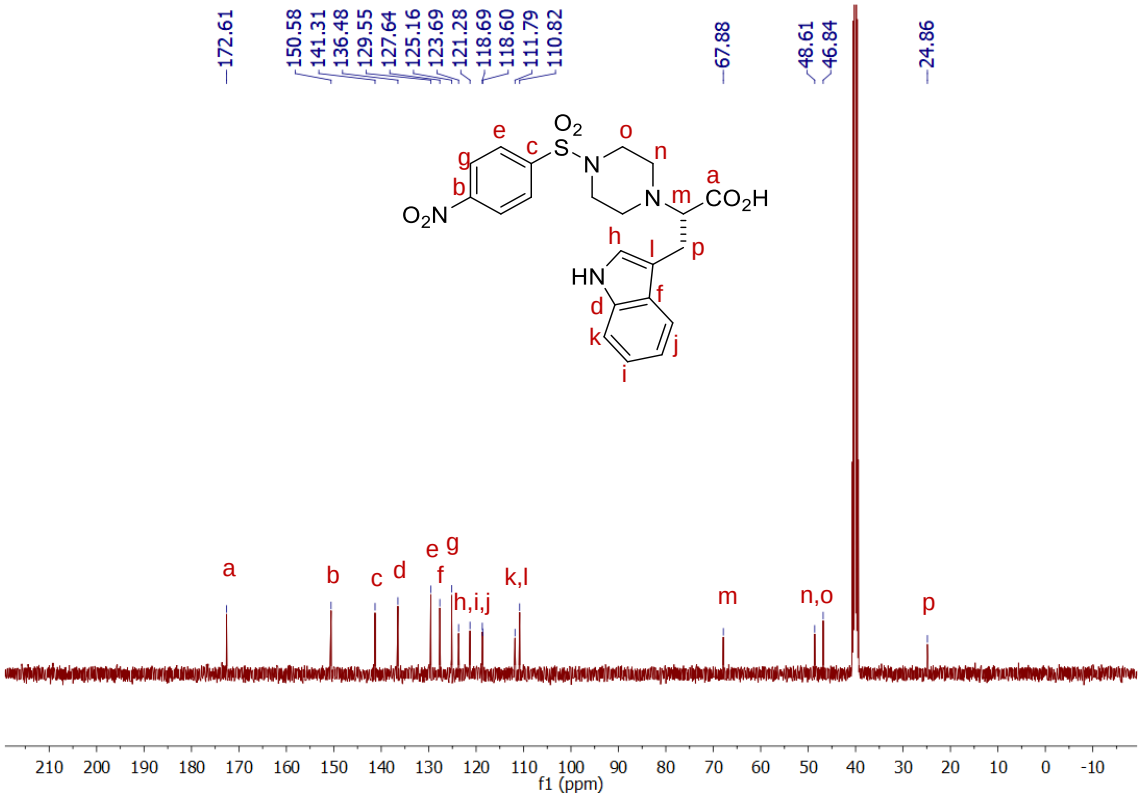

HRMS (ESI+) m/z calc'd for $C_{21}H_{23}N_4O_6S^+$ 459.1260; found 459.1263.

L-**5y'**

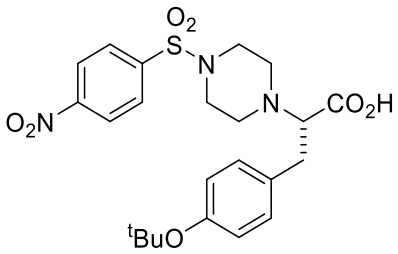

(S)-3-(4-(Tert-butoxy)phenyl)-2-(4-((4-nitrophenyl)sulfonyl)piperazin-1-yl)propanoic acid, 88%, light yellow solid

^{1}H NMR (400 MHz, DMSO-d$_6$) δ 8.44 (d, J = 8.7 Hz, 2H), 7.99 (d, J = 8.7 Hz, 2H), 7.05 (d, J = 8.3 Hz, 2H), 6.79 (d, J = 8.3 Hz, 2H), 3.41 – 3.35 (m, 1H), 2.92 (s, 4H), 2.88 – 2.82 (m, 1H), 2.78 – 2.67 (m, 3H), 2.64 – 2.54 (m, 2H), 1.21 (s, 9H).

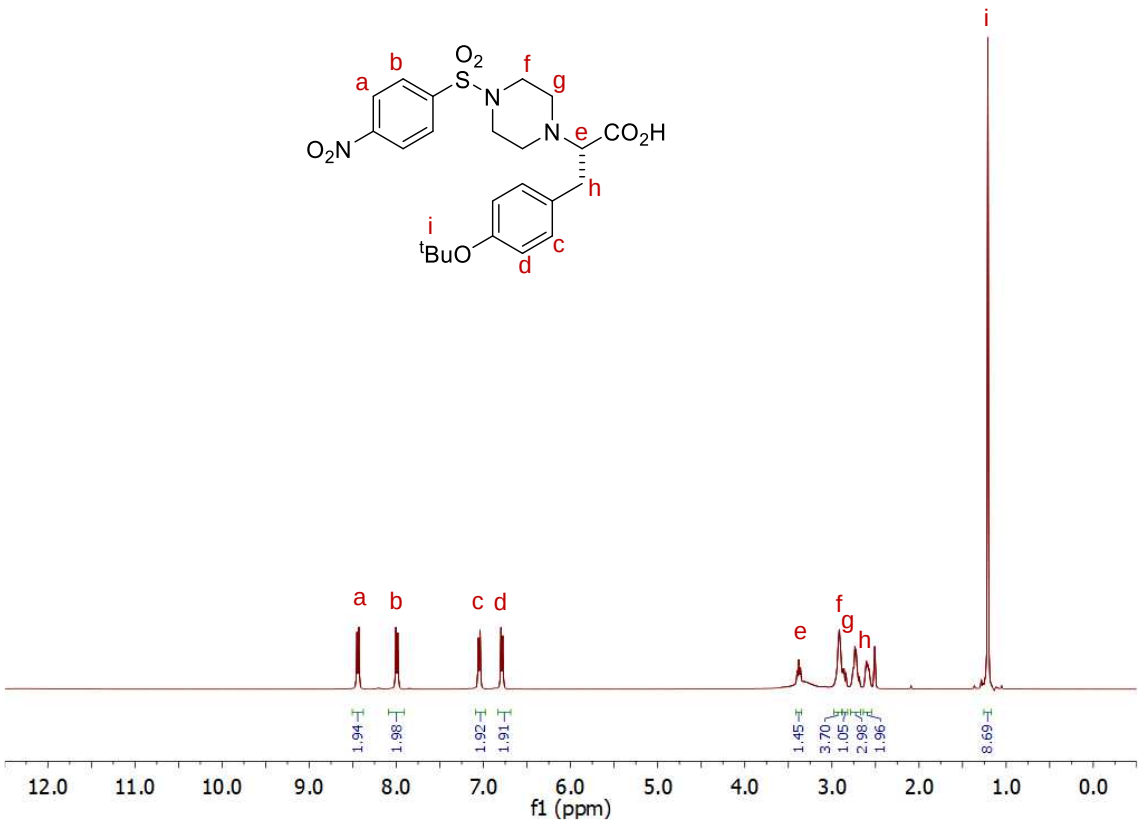

^{13}C NMR (100 MHz, DMSO-d_6) δ 172.35, 153.69, 150.54, 141.28, 133.37, 129.93, 129.54, 125.12, 123.76, 77.96, 68.38, 48.50, 46.81, 34.19, 28.96.

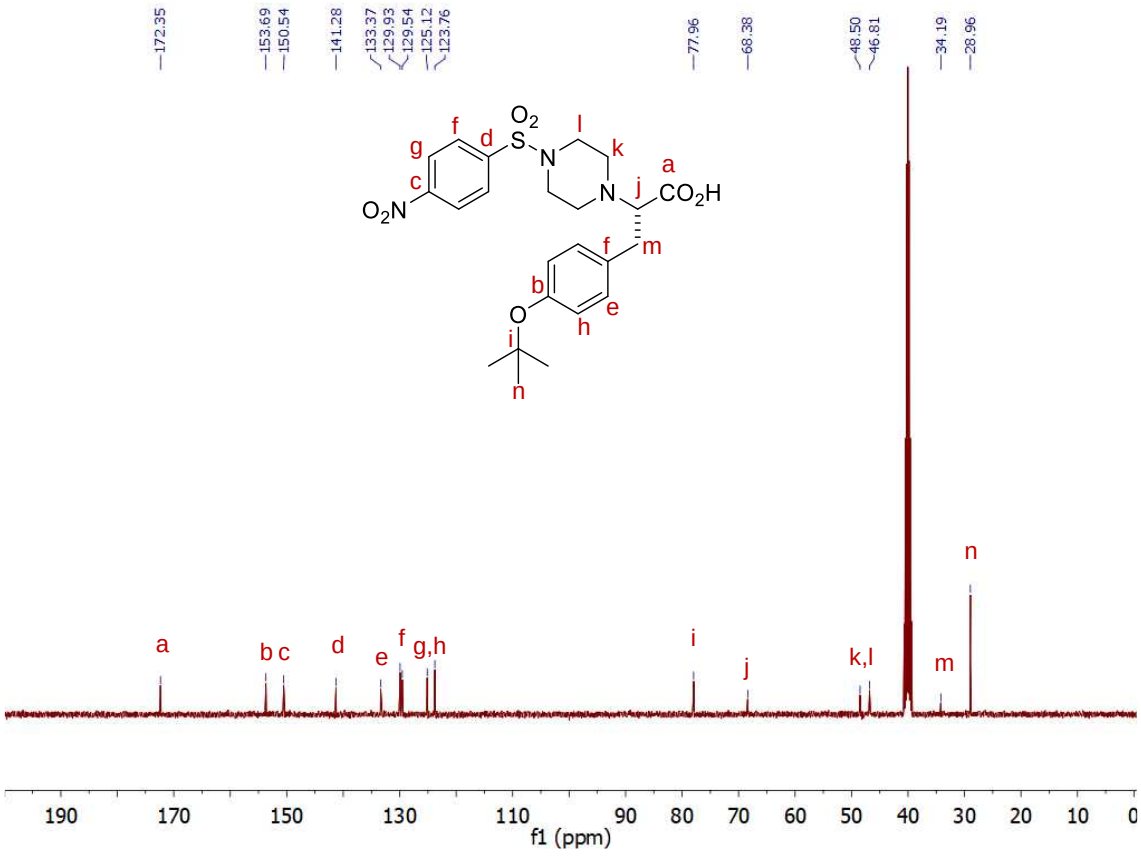

HRMS (ESI+) m/z calc'd for $C_{23}H_{30}N_3O_7S^+$ 492.1726; found 492.1730.

L-**5a**

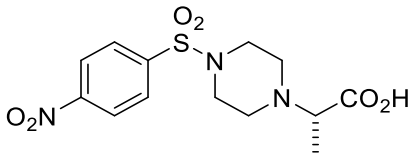

(S)-2-(4-((4-Nitrophenyl)sulfonyl)piperazin-1-yl)propanoic acid, 95 %, white solid

^{1}H NMR (400 MHz, DMSO-d_6) δ 8.51 (d, J = 8.8 Hz, 2H), 8.13 (d, J = 8.9 Hz, 2H), 4.27 (q, J = 7.2 Hz, 1H), 3.79 – 3.72 (m, 2H), 3.62 (t, J = 6.6 Hz, 2H), 3.33 (dt, J = 3.2, 1.6 Hz, 4H), 1.66 (d, J = 7.3 Hz, 3H).

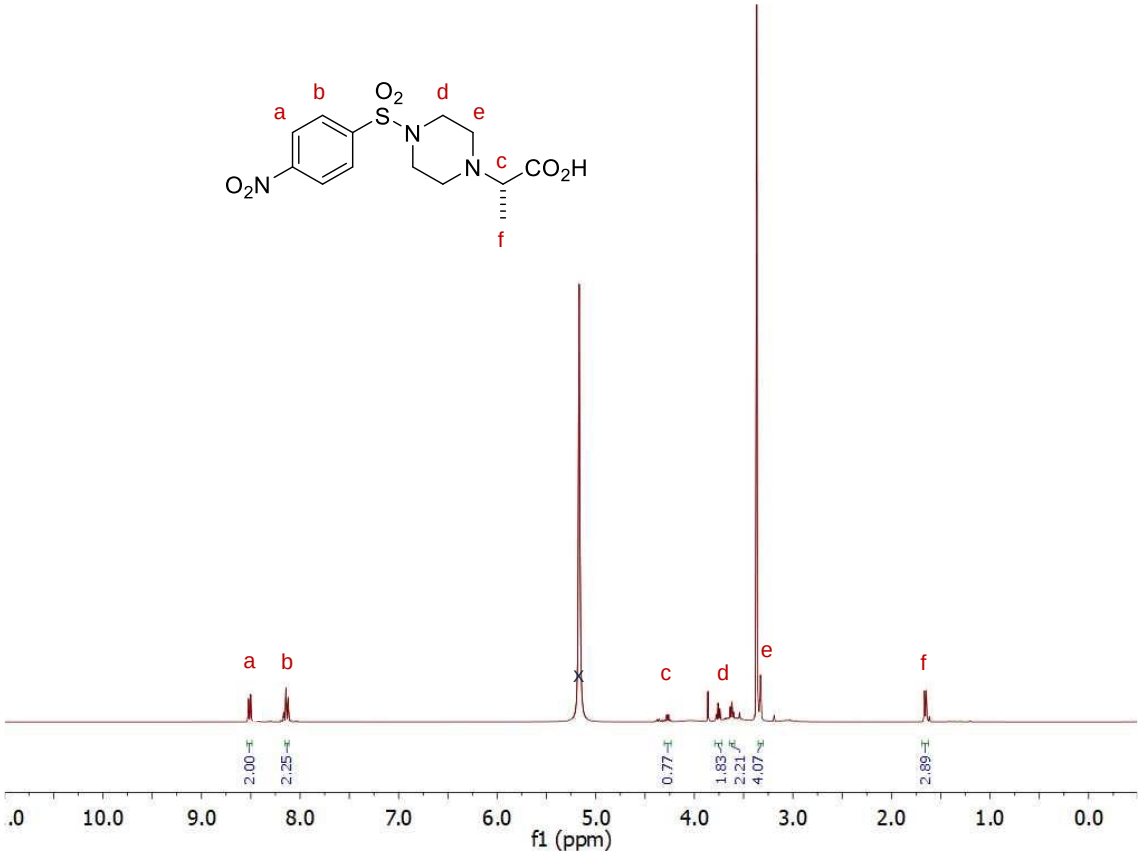

^{13}C NMR (100 MHz, MeOD) δ 169.24, 150.83, 141.08, 129.12, 128.53, 124.50, 124.25, 62.57, 52.72, 50.74, 43.03, 41.52, 11.67.

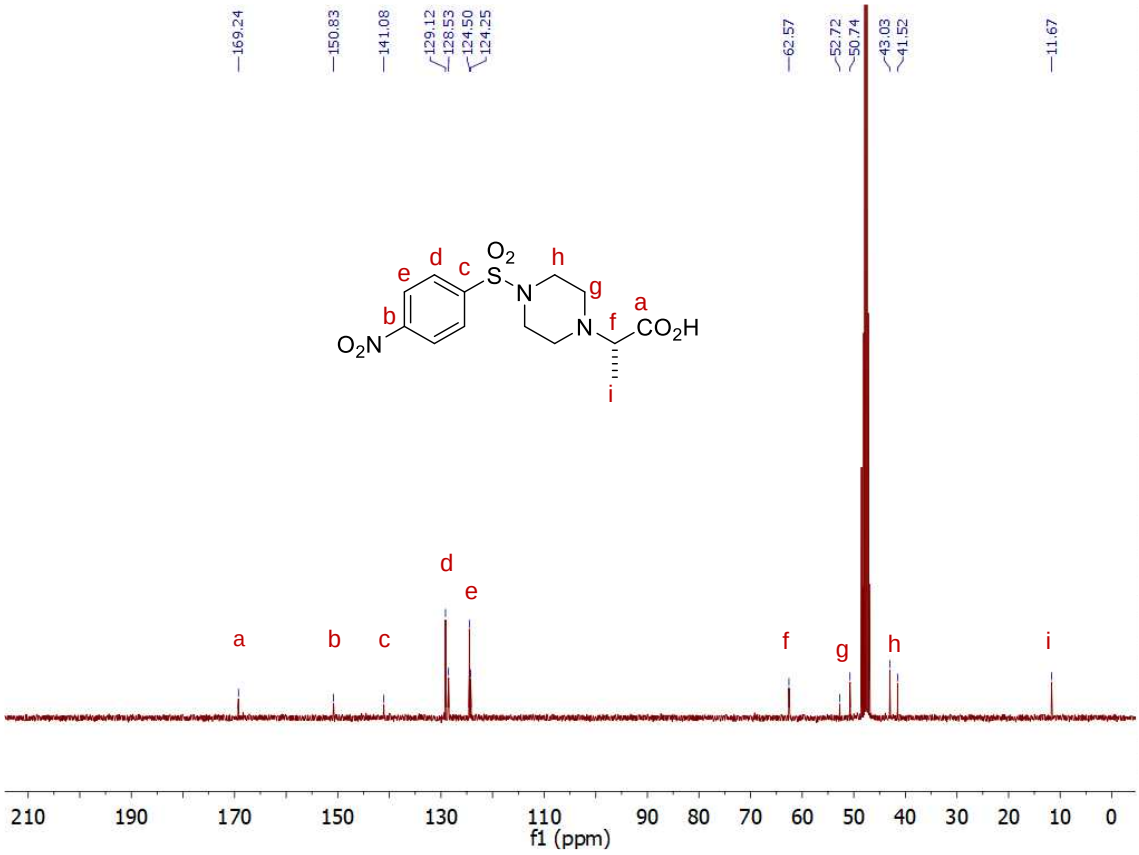

HRMS (ESI) m/z calc'd for $C_{13}H_{18}N_3O_6S^+$ 344.0838; found 344.0840.

L-**5c'**

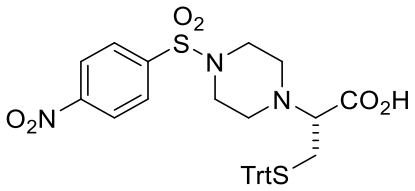

(R)-2-(4-((4-Nitrophenyl)sulfonyl)piperazin-1-yl)-3-(tritylthio)propanoic acid, 60%, yellow solid

^{1}H NMR (400 MHz, MeOD) δ 8.43 – 8.39 (m, 2H), 8.01 – 7.95 (m, 2H), 7.35 (m, 6H), 7.26 (m, 4H), 7.09 – 7.03 (m, 5H), 3.55 (dd, J = 16.2, 8.2 Hz, 1H), 3.13 – 2.81 (m, 8H), 2.63 (dd, J = 17.0, 11.1 Hz, 2H).

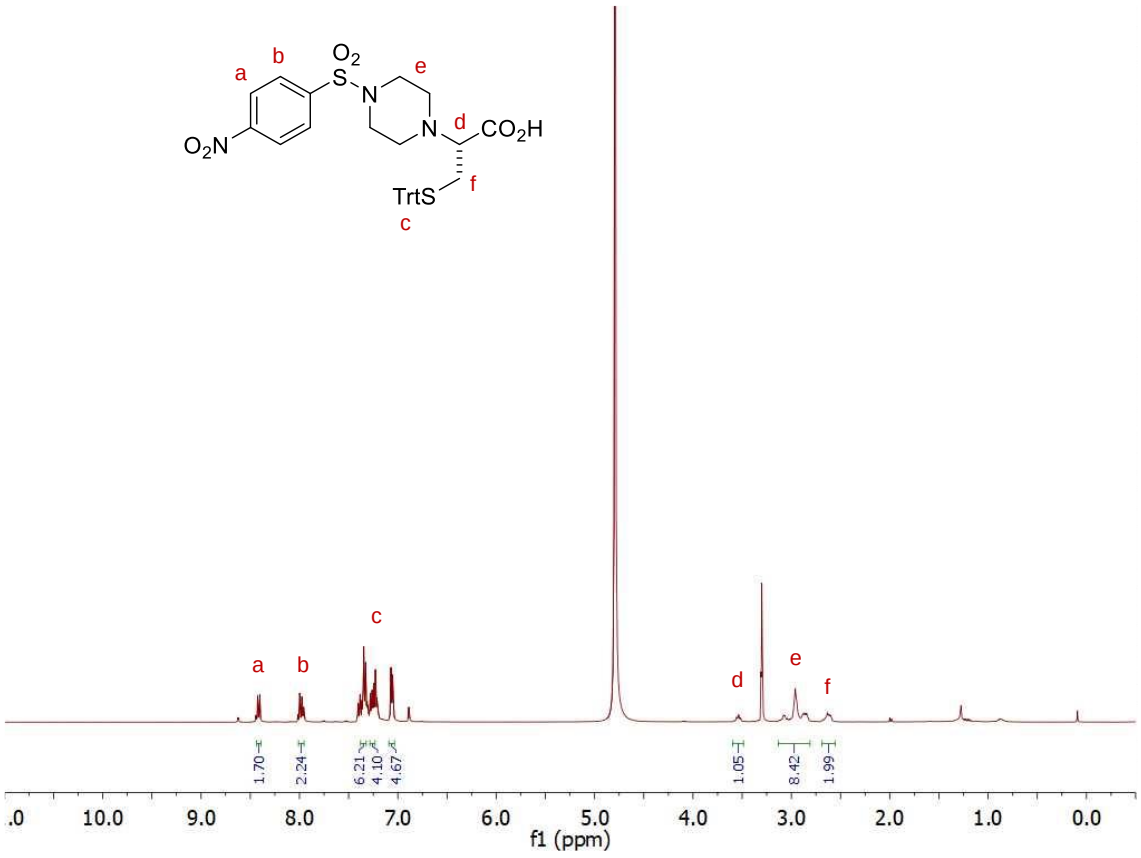

^{13}C NMR (100 MHz, MeOD) δ 173.08, 169.55, 152.21, 142.52, 130.46, 129.90, 125.82, 125.62, 64.86, 52.11, 51.43, 44.66, 42.86, 32.89.

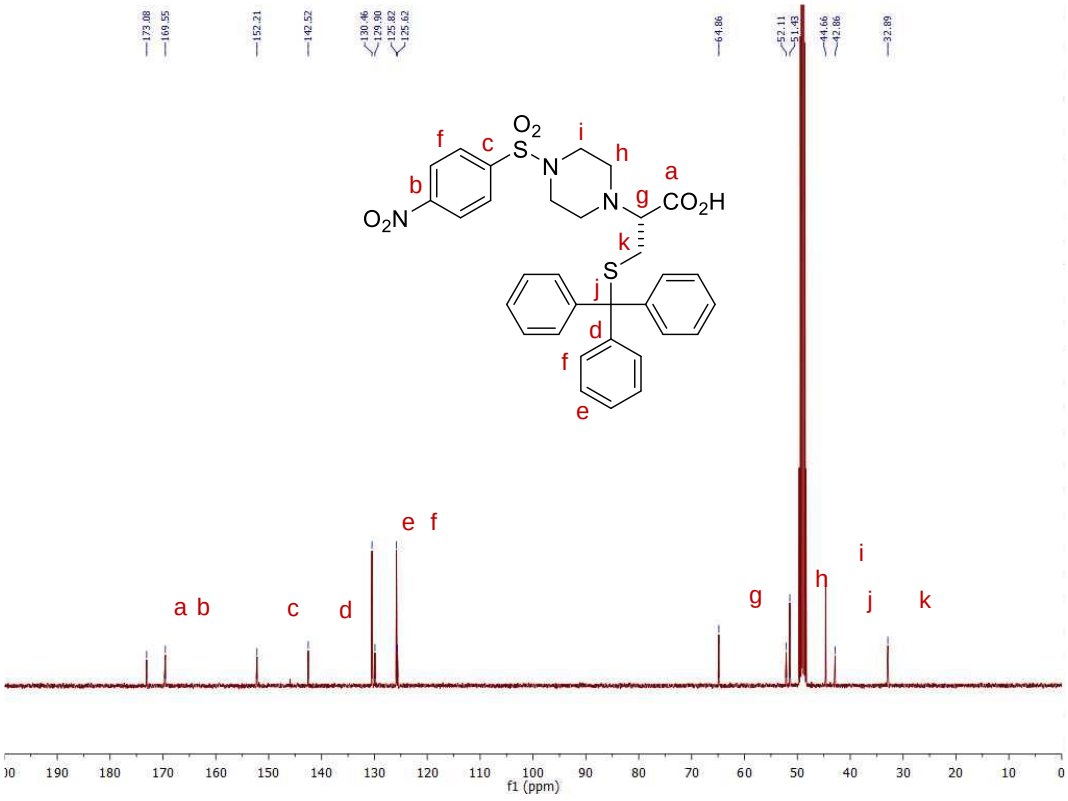

HRMS (ESI) m/z calc'd for $C_{32}H_{32}N_3O_6S_2^+$ 618.1654; found 618.1657.

Epimerization Study

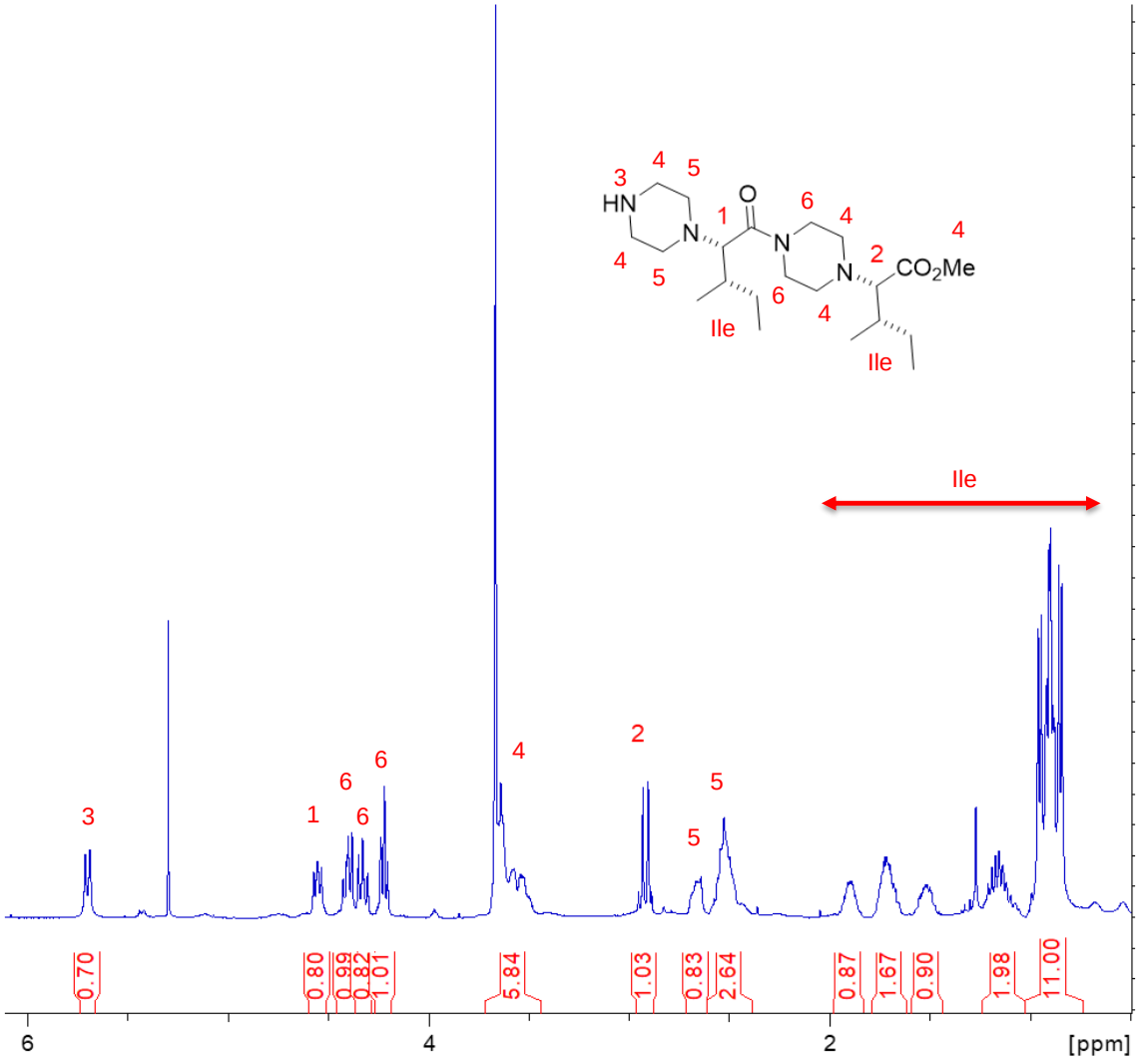

Analytical HPLC

Diode Array

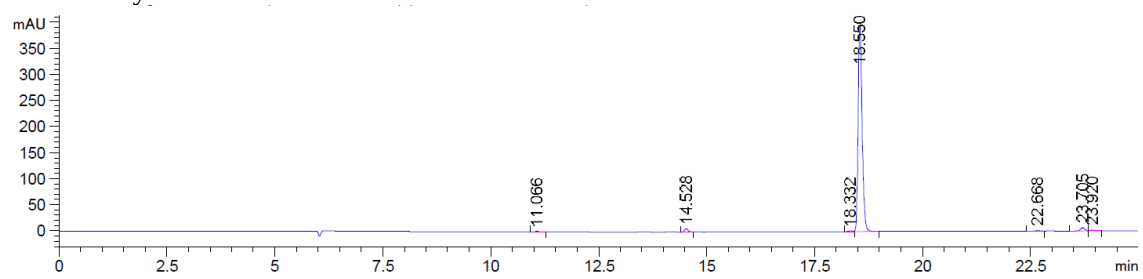

ELSD

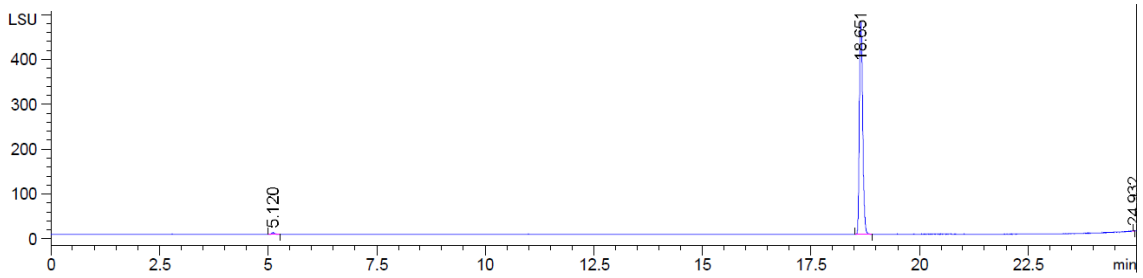

Solid-Phase Synthesis of Piptide Analogues 10

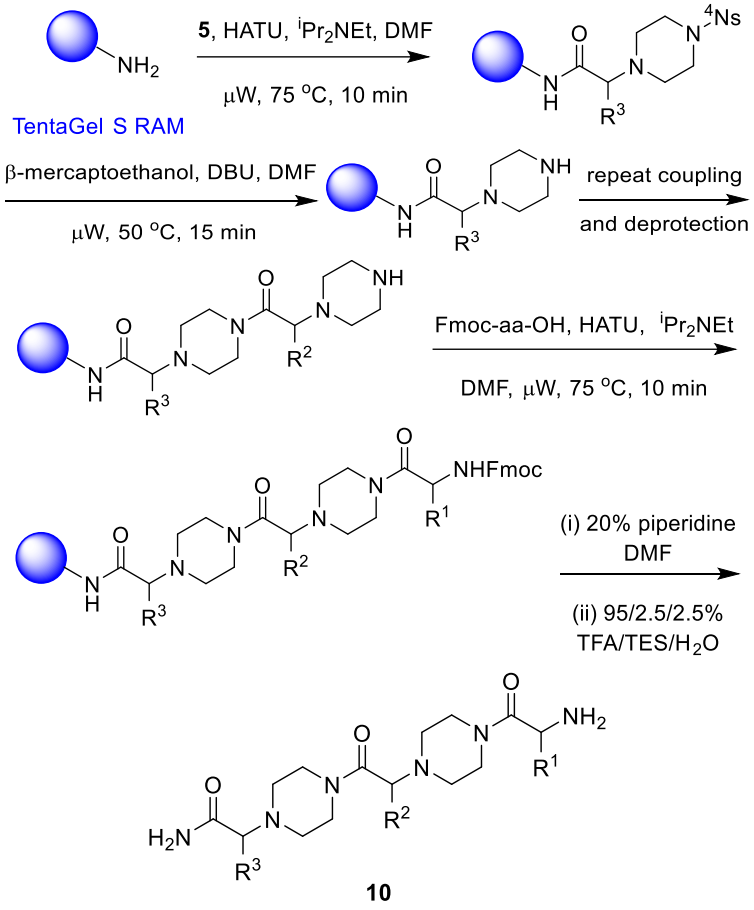

TentaGel S RAM (100 mg, 0.26 meq/g) beads were swelled in DMF for 1 h. Deprotection of Fmoc was performed by adding 20% piperidine in DMF to the beads and were heated under microwave irradiation (160 W, 75 °C, 3 min). Solution was drained, and beads were washed with DMF several times. The first pip acid was loaded through the coupling step detailed below. The beads were then capped by adding 25% acetic anhydride/DMF and made to shake at 25 °C. After 5 min, 1.5 eq of $^{i}Pr_2NEt_2$ was added to

the solution before shaking for an additional 30 min. The nosyl of the first pip acid was removed before coupling with the next pip acid (details of both coupling and deprotection outlined below). The nosyl group was deprotected again before coupling with the Fmoc-amino acid. Fmoc deprotection was done before the compound was cleaved off the bead by the addition of 95/2.5/2.5% TFA/triethylsilane/H_2O. The beads were shaken for 3 h at 25 ^oC before the solution was collected. Side chain protecting groups were also removed by the cleavage solution. The collected solution was dried under N_2 stream and purified by preparative reversed-phase HPLC (10% - 90% MeCN/water with 0.05% TFA) and lyophilized to obtain the product **10**.

Coupling on solid phase

The pip acid or amino acid (4 eq) was activated with HATU (4 eq) and $^iPr_2NEt_2$ (8 eq) in DMF (0.2 M). This solution was added to the beads and subjected to microwave irradiation (100 W, 75 ^oC, 10 min). Solution was drained, and beads were washed with DMF several times.

Deprotection of nosyl group on solid phase

2-Mercaptoethanol (3 eq) and 1,8-diazabicyclo[5.4.0]undec-7-ene (DBU, 5 eq) in DMF (1 M) were added to the beads and subjected to microwave irradiation (100 W, 50 ^oC, 15 min). Solution was drained, and beads were washed with DMF several times.

Analytical HPLC – ELSD and HRMS

HRMS (ESI) m/z calc'd for $C_{21}H_{39}N_6O_5^+$ 454.2977

LLL-**10aev**

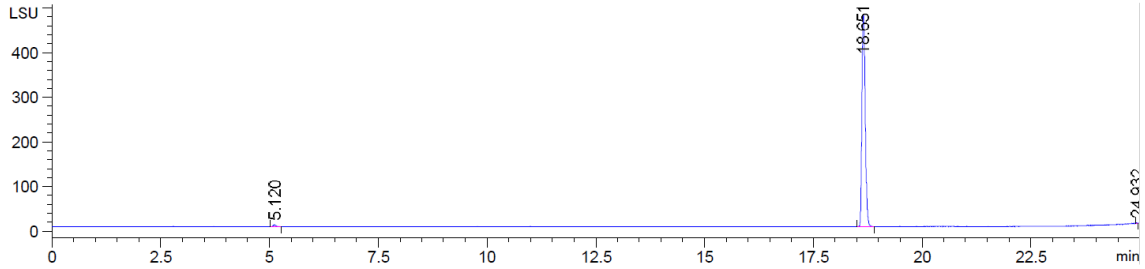

found $(M+H)^+$ 454.2975

LDL-**10eav**

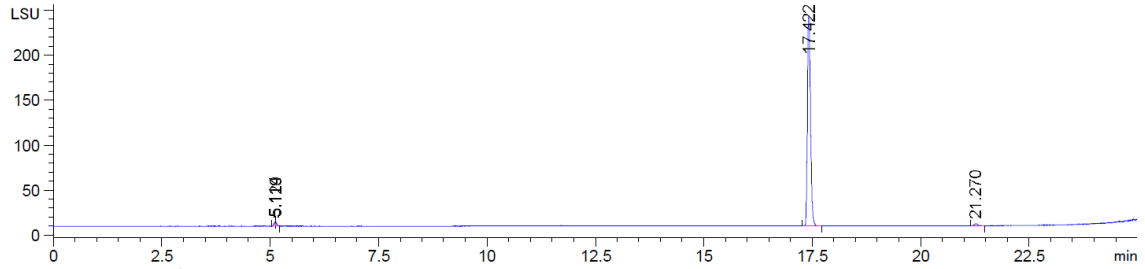

found $(M+H)^+$ 454.2980

LDL-**10vae**

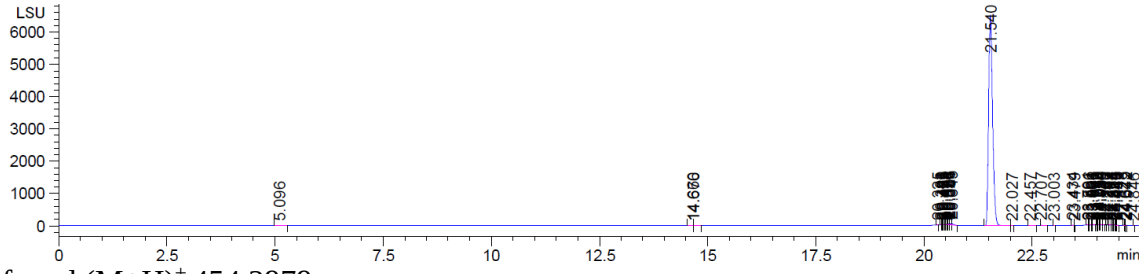

found $(M+H)^+$ 454.2979

9-mer Piptide Solid Phase Synthesis

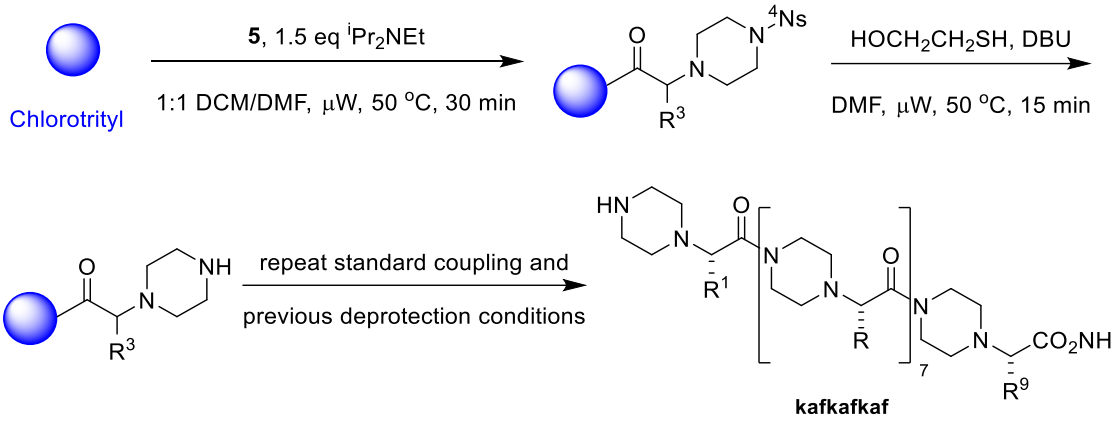

Scheme A-1. Synthesis scheme of a long piptide chain. Reprinted with permission from ref 112. Copyright 2020 Wiley-VCH Verlag GmbH & Co. KGaA, Weinheim.

ELSD Traces

After coupling of each pip acid in the long piptide chain synthesis, the resulting product was analyzed using the ELSD to check the yield each time. Internal standard (IS) is used, in this case bromobenzoic acid, to compare the ratio of the products (number beside the peak of the product, e.g. 1:164 for the first trace) relative to each other.

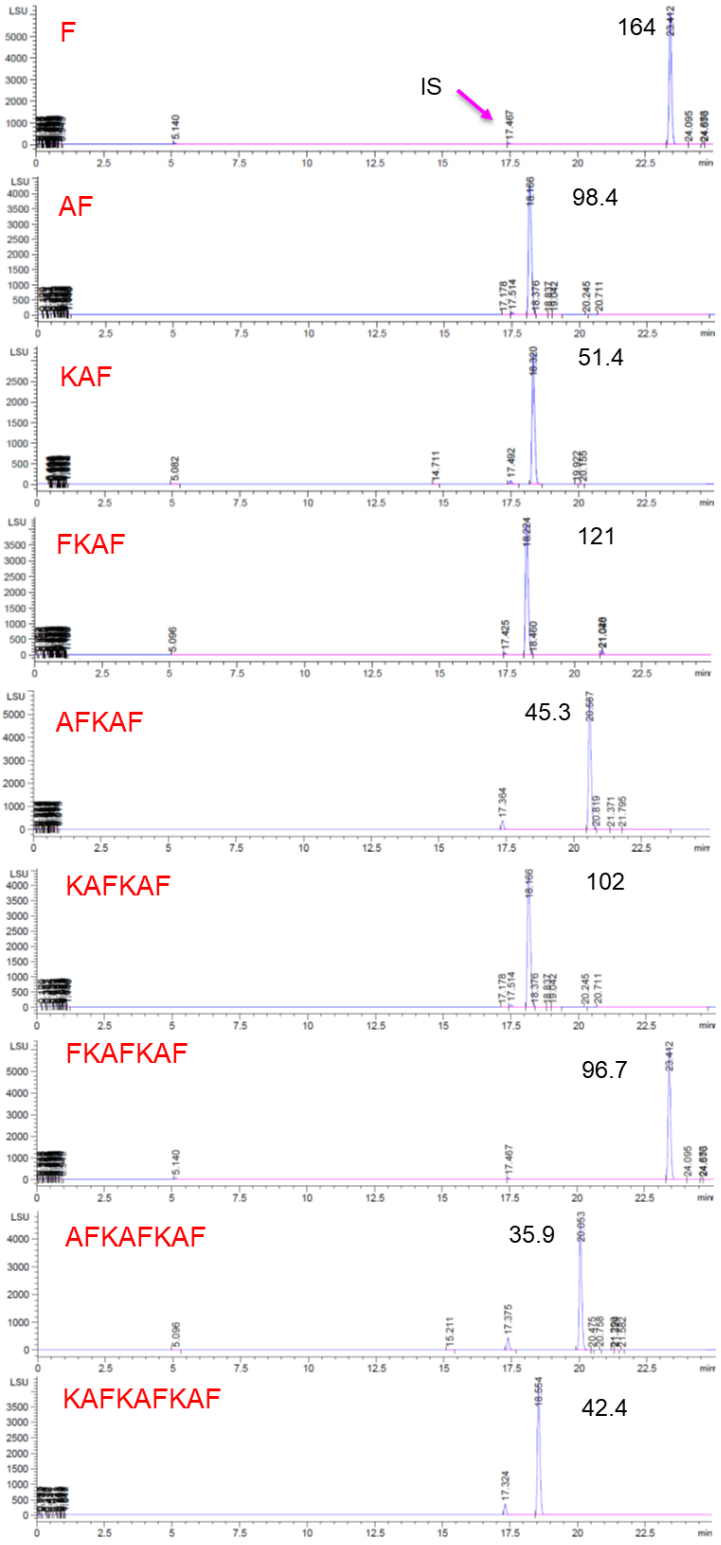
F
164
IS
AF
98.4
KAF
51.4
FKAF
121
AFKAF
45.3
KAFKAF
102
FKAFKAF
96.7
AFKAFKAF
35.9
KAFKAFKAF
42.4

pH Stability Assay

A stock solution of LLL-**10tff** (50 mM) in DMSO was prepared and stored at 25 °C. 9 μL of the DMSO stock solution was dissolved in aqueous solutions with different pH (pH 7.4, PBS buffer; pH 12, 10 mM NaOH; pH 2, 10 mM HCl) to give a 400 μM working solution. The solution was filtered through a 0.2 μm membrane filter and analyzed by reversed-phase HPLC (see general methods) at intervals. The peak areas of LLL-10tff from rp-HPLC were measured and plotted against incubation time.

Protease Stability Assay

A stock solution of LLL-**10fff** (50 mM) in DMSO was prepared and stored at 25 °C. A similar stock solution containing 50 mM linear LLL-**11fff** peptide was prepared in DMSO as a control. A 0.2 unit / mL stock solution of Pronase from Streptomyces griseus was prepared in PBS buffer and further diluted to 0.4 unit / μL with PBS buffer containing 20 % MeOH. 4.5 μL of 10 or 11 stock solution was added to 1.5 mL Pronase solution and then filtered through a 0.2 μm membrane filter and the resulting solution was analyzed by rp-HPLC at intervals. The peak areas of LLL-**10fff** or LLL-**11fff** from rp-HPLC were measured and plotted against incubation time. Under the experimental condition, no decomposition of LLL-**10fff** was observed even after 12 h, while for the control linear peptide LLL-**11fff** the half-life of decomposition was about 3 h.

Circular Dichroism Spectra of 10

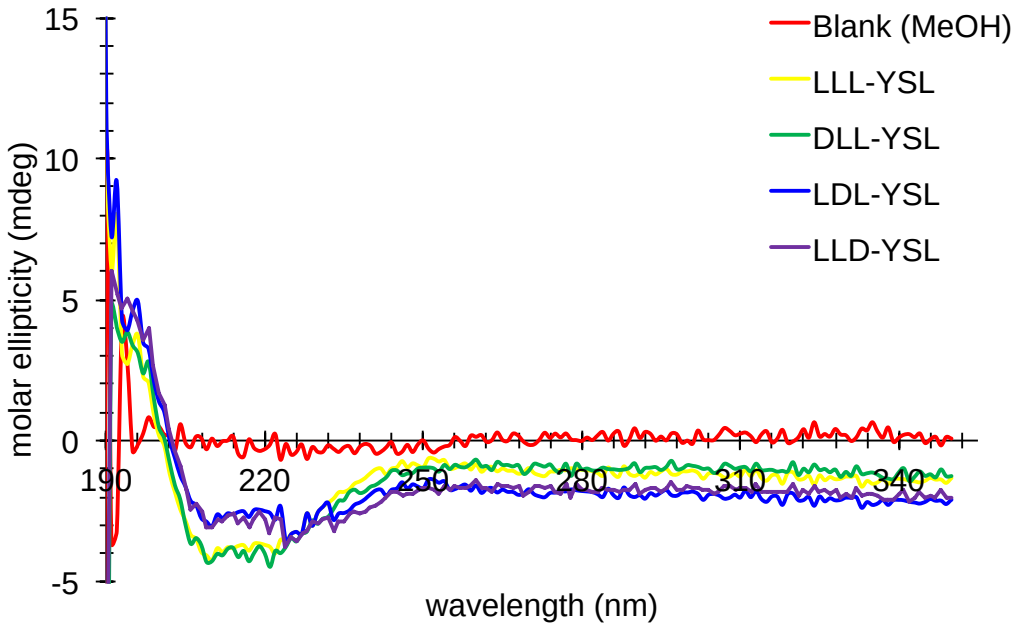

Figure A-1. CD Spectra of different configurations of **10** with the same side chains. Reprinted with permission from ref 112. Copyright 2020 Wiley-VCH Verlag GmbH & Co. KGaA, Weinheim.

QMD, EKO, EKOS and Ramachandran Plots

Quenched molecular dynamics (QMD) was used to generate simulated conformations of all diastereomers of **10aaa**. The procedures had been reported previously.[124] Approximately 1500 conformers of each diastereomer within 3.0 kcal/mol of the global minimum were matched on TGFα-EGFR protein-protein interaction (PDB ID: 1mox) using the Exploring Key Orientations (EKO) analyses.[32] The *C*α-

*C*β coordinates from the side chains of peptidomimetics were systematically overlaid on *C*α-*C*β coordinates of the TGFα side chains at the protein-protein interface using an in-house algorithm. The goodness of fit was reported as root mean square deviation (RMSD). Lower RMSDs mean the *C*α-*C*β orientations between chemotypes and protein side chains are similar, thus chemotypes can *mimic* the protein side chains. Conformers within RMSD ≤ 0.50 Å were considered as "potential hits" which were summarized in Table A-1. Only the ones in red were synthesized, since less (or none of the) starting materials were available for the others. Those with Cys residues were avoided for the meantime as well.

Table A-1. Potential TGF-α mimics (**10**) from EKO analyses within RMSD ≤ 0.50 Å. Reprinted with permission from ref 112. Copyright 2020 Wiley-VCH Verlag GmbH & Co. KGaA, Weinheim.

Configuration	R^3	R^2	R^1	*RMSD (*Å)
DDD	His	Cys	Ala	0.50
	Ala	Glu	Val	0.42
	Leu	Ala	Glu	0.47
	Thr	Phe	Phe	0.37
DDL	Thr	Phe	Phe	0.36
	Ala	Glu	Val	0.50
	Val	Ala	Glu	0.47
	Phe	Phe	Thr	0.47
	Ala	Cys	His	0.43
DLD	His	Cys	Ala	0.50
	Val	Glu	Ala	0.47
	Phe	Phe	Thr	0.21
	Glu	Val	Ala	0.41
	Val	Glu	Arg	0.50
DLL	His	Cys	Ala	0.46
	Glu	Val	Ala	0.41
	Val	Glu	Arg	0.48

Table A-1. Continued.

Configuration	R^3	R^2	R^1	RMSD (Å)
DLL	Val	Glu	Ala	0.48
	Phe	Phe	Thr	0.45
	Val	Glu	Ala	0.41
	Ala	Cys	His	0.33
LDD	Cys	Cys	Arg	0.50
	Ala	Cys	His	0.43
	Phe	Phe	Thr	0.38
	Thr	Phe	Phe	0.50
	Val	Ala	Glu	0.49
	Glu	Ala	Val	0.43
LDL	Val	Ala	Glu	0.48
	Cys	Ala	Cys	0.48
	His	Cys	Ala	0.47
	Thr	Phe	Phe	0.43
	Phe	Phe	Thr	0.39
	Glu	Val	Ala	0.50
	Ala	Cys	His	0.46
LLD	Phe	Phe	Thr	0.50
	Glu	Val	Ala	0.49
	Ala	Glu	Val	0.45
	Ala	Val	Glu	0.40
LLL	His	Cys	Ala	0.48
	Glu	Val	Ala	0.42
	Ala	Val	Glu	0.42
	Phe	Phe	Thr	0.42
	Ala	Glu	Val	0.48
	Val	Glu	Ala	0.48
	Cys	Ala	Cys	0.47

Exploring Key Orientations on Secondary Structures (EKOS) matches chemotypes to ideal secondary structures.[34] Compound **10aaa** was found to overlay better

on sheets and sheet-turn-sheets (Table A-2). No values provided means the RMSD values were too high; **10** does not overlay well on strands.

Table A-2. EKOS for compound **10**. Reprinted with permission from ref 112. Copyright 2020 Wiley-VCH Verlag GmbH & Co. KGaA, Weinheim.

	3_{10}-helix	α-helix	π-helix	γ-turn	inverse γ-turn	STS[a]	β-strand	p-sheet[b]	anti-p-sheet[c]
LLL	0.81	0.71	0.51	-	-	0.38	-	0.44	0.56
DLL	0.78	0.69	0.44	-	-	0.50	-	0.42	0.41
LDL	0.87	0.70	0.60	-	-	0.47	-	0.33	0.53
LLD	0.82	0.60	0.49	-	-	0.37	-	0.38	0.58
LDD	0.83	0.69	0.55	-	-	0.50	-	0.48	0.66
DLD	0.83	0.60	0.58	-	-	0.44	-	0.45	0.50
DDL	0.88	0.67	0.51	-	-	0.48	-	0.41	0.45
DDD	0.84	0.55	0.46	-	-	0.37	-	0.33	0.47

[a]STS: strand-turn-strand, [b]p-sheet: parallel β-sheet, [c]anti-p-sheet: anti-parallel β-sheet
red: ≤ 0.35 Å, blue: 0.35 < RMSD ≤ 0.5 Å

Ramachandran plot was also obtained for the same compound, **10aaa**, and was found to be in a different region (different conformations) than most favored and additional allowed regions of ordinary peptides (Figure A-2).

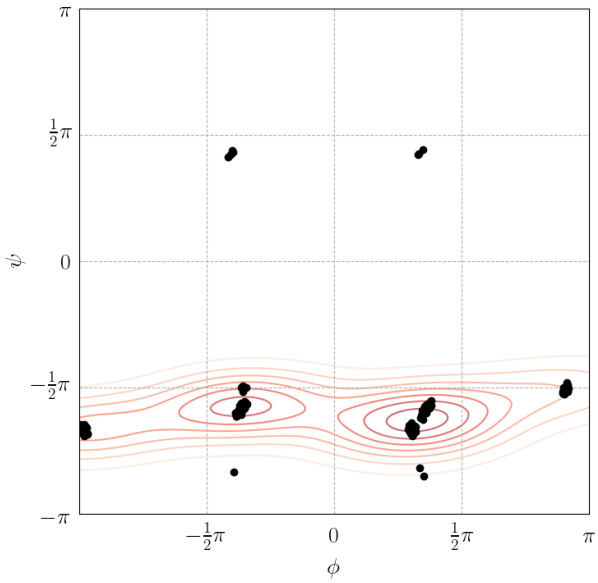

Figure A-2. Ramachandran plot of 10aaa. π is 180 degrees. Reprinted with permission from ref 112. Copyright 2020 Wiley-VCH Verlag GmbH & Co. KGaA, Weinheim.

ELISA

96-well plates were incubated overnight at 4 °C with 100 µL of 2 µg/mL Human EGFR (Sino Biological) in PBS for immobilization. The plate was washed with 0.05% Tween-20 in PBS buffer between each step. A 1:1 mixture of Superblock buffer in PBS (ThermoFisher) with 0.04 M NaH_2PO_4 and 0.3 M NaCl buffer was used for blocking at room temperature for 1 h. Various concentrations of compound 10 were added and incubated at room temperature for 2 h. Compounds were screened initially at 50 µM. For concentration-dependent studies, a range of compound concentrations from 5 µM to 100 µM in PBS was used. After washing, 5 nM EGF-biotin (ThermoFisher) in PBS was then added and incubated for 1 h. After incubation with streptavidin-HRP (ThermoFisher) for 1 h, TMB (ThermoFisher) was added and incubated for an additional 30 min. Sulfuric acid

is then incubated for 15 min acting as a stop solution. The signal was detected at 450 nm using a microplate reader.

Protein Fluorescence Quenching Experiment

Static quenching of intrinsic tryptophan fluorescence in EGFR by the compounds was conducted using spectrofluorometer LS50B (Perkin-Elmer). Five titrations of small amount of compound (0.5 µl of 5 mM, 10 mM, 20 mM, and twice of 1 µl of 20 mM) was added to 500 µl of protein solution. Fluorescence spectra were measured with excitation wavelength of 280 nm. Each fluorescence spectrum was the average of three measurements, with a scan speed of 600 nm/min. The slit widths were 10 nm for both excitation and emission monochromators. In all cases, fluorescence measurements were taken after the solutions had reached an equilibrium value. Stern–Volmer curves, where F_0 and F are the peak fluorescence intensities in the absence and presence of compound, respectively, exhibit linearity, suggesting that the quenching process arises from binding between the tryptophan fluorophore and the quencher compound. The linearity of the modified Stern–Volmer plots indicates static quenching (or binding) in the presence of an inaccessible population of fluorophores (Figure A-3a). Plots allow calculation of K_D (slope/intercept).[125]

Surface Plasmon Resonance

Direct binding of each compound to EGFR was measured by SPR using a Biacore T200 optical biosensor (GE Healthcare) at 25˚C. High density (8000-9000 RU) and low

density of EGFR (2000-2500 RU) surfaces were created using CM5 and CM4 sensor chips (GE Healthcare) respectively using standard amine coupling chemistry. The mixture of equal volume of 0.1 M N-hydroxysuccinimide and 0.4 M 1-ethyl-3-(3-dimethylaminopropyl)-carbodiimide was injected for 8 min at 5 µl/min to activate the flow cell surface. EGFR stock (0.25 mg/ml) was diluted to 10 or 50 µg/ml in 10 mM sodium acetate (pH 5.5) and injected to the activated surface and immediately followed by a 5-min injection of 1 M ethanolamine (pH 9) to deactivate the surface. Phosphate buffered saline (50 mM sodium phosphate pH 7.4, 150 mM NaCl) containing 0.01% (v/v) Tween 20 (PBST) was used for immobilization. A reference flow cell was prepared with activation and deactivation steps, but no protein coupled. All binding experiments were performed in PBST containing 2% (v/v) DMSO at a flow rate of 30 µl/min. Compound was dissolved in 100% DMSO to 20 mM and then diluted 50-fold in PBST to 400 µM concentration as working stock for further dilution in running buffer. To regenerate the sensor surface, bound molecule was removed by flowing 10 mM sodium acetate (pH 5.0) over receptor surface for 15 second. The SPR sensorgrams were reference and buffer subtracted and evaluated using the Biacore T200 Evaluation Software (version 3.1).

SPR screening showed that freshly immobilized EGFR is more reactive to the compounds. Small molecule binding to the immobilized EGFR followed by treatment of the chip at low pH to remove the compound caused binding activity of the receptor to decline. To minimize effects of that degeneration, a single cycle kinetic strategy was adopted (*i.e.* no extensive washing and retesting, instead adding the compound in progressively higher concentrations; Figure A-3b).

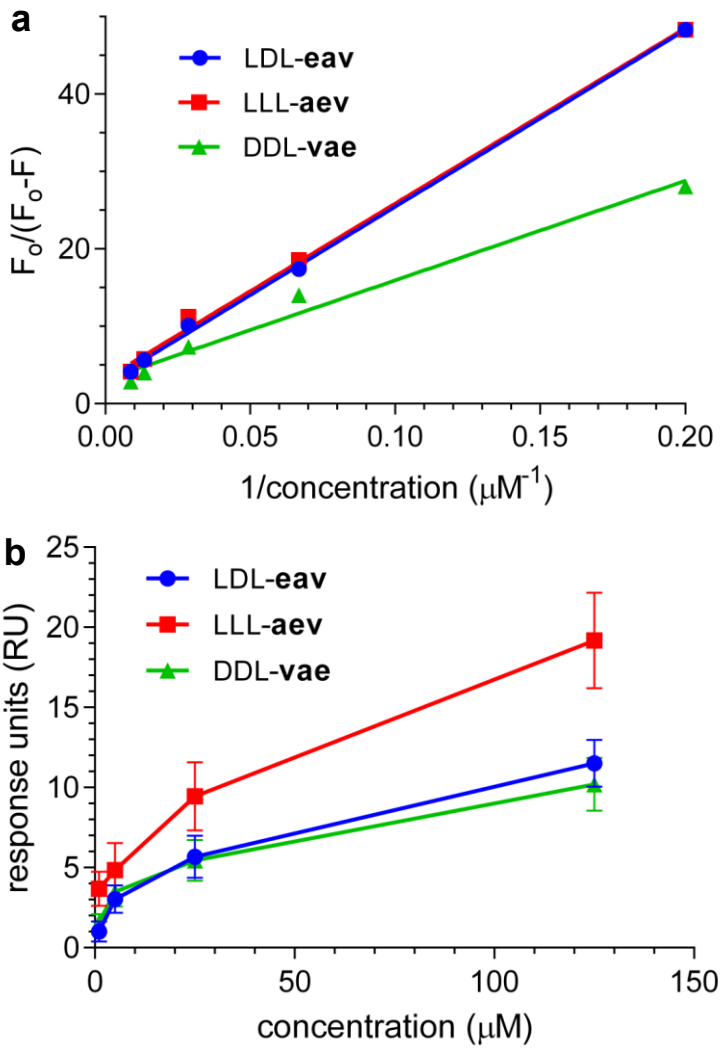

Figure A-3. Binding experiments for compounds **10** via: **a** modified Stern-Volmer plots from fluorescence quenching experiments; **b** direct binding of compounds to EGFR immobilized on Biacore sensor chip surface (SPR); and **c** competition assays with TGFα•EGFR or EGF•EGFR. Reprinted with permission from ref 112. Copyright 2020 Wiley-VCH Verlag GmbH & Co. KGaA, Weinheim.

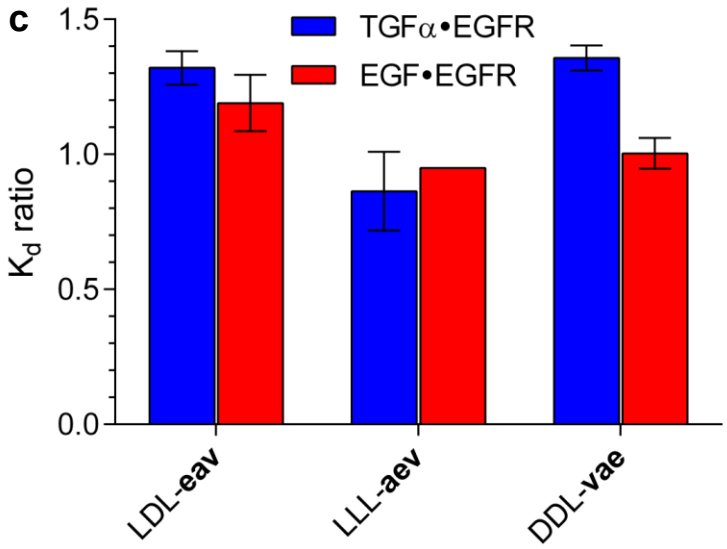

Figure A-3. Continued.

Cell Viability Assay

A549 cells (EGFR +) were seeded at 5000 cells/well (50 µL) on 96-well plates and incubated at 37ºC overnight. Various concentrations of 10 were prepared in protein-free hybridoma medium (PFHM II) and added to cells to make final concentrations from 3 µM to 500 µM. After 48 h, 10 µL of AlamarBlue reagent (Invitrogen) was added and incubated for an additional 2 h. Fluorescence intensity (Ex/Em 495/519 nm) was measured on a microplate reader. The same was done with HEK293 cells (EGFR -; Figure A-4).

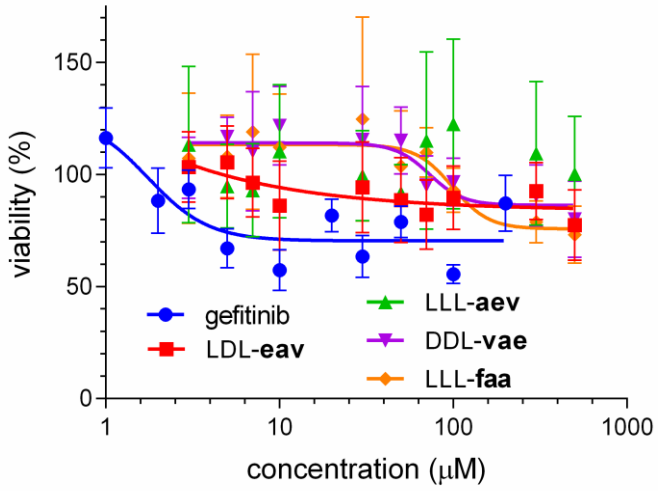

Figure A-4. HEK293 cell viabilities of **10** as monitored using alamarBlue, where gefitinib is the positive control and LLL-**10faa** is the partial negative control. Reprinted with permission from ref 112. Copyright 2020 Wiley-VCH Verlag GmbH & Co. KGaA, Weinheim.

Apoptosis/Necrosis Assay

Flow Cytometry for apoptosis/necrosis assay of compound 10 and gefitinib was determined on A549 cells using FITC annexin V/PI apoptosis detection kit. Briefly, $1x10^5$ cells were seeded in each well of 24-well plates and incubated for 24 h. Cells were detached using cell free dissociation buffer (enzyme free), washed with ice-cold PBS buffer twice, and suspended in 100 µL 1X binding buffer, followed by the addition of 5 µL FITC annexin V staining solution and 1 µL PI 1X staining solution. The cell samples were incubated for 15 min at room temperature in the dark and followed by addition of another 400 µL 1×binding buffer. The cell samples were analyzed using BD FACS Aria II.

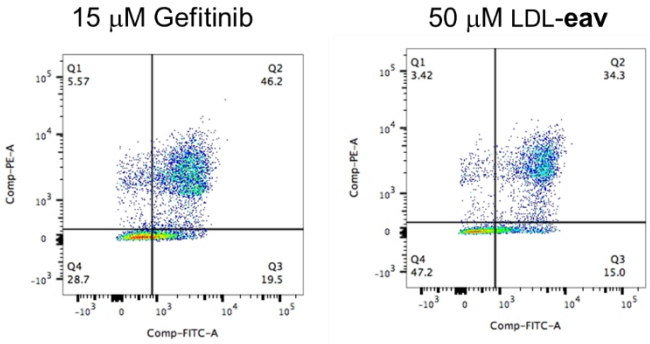

Figure A-5. Apoptosis/necrosis assay with gefitinib and LDL-**10eav**. Reprinted with permission from ref 112. Copyright 2020 Wiley-VCH Verlag GmbH & Co. KGaA, Weinheim.

Phospo-EGFR Assay

A549 cells were seeded in a 24-well plate (1 x10^5 cells/well) in RPMI-1640 medium containing 10% fetal bovine serum and were allowed to adhere overnight. Medium was replaced with Gibco® Protein Free Hybridoma Medium II (PFHM-II) containing 10% FBS premixed with different concentration of compounds (max. DMSO = 0.1%) and incubated for 1 h. 500 ng/mL EGF was then added and incubate for 15 min. For the positive control, 50 ng/mL EGF was added into the well instead. For the blank, no EGF nor compounds were added. Cells were washed twice with cold PBS and lysed by RIPA buffer (Pierce) according to manufacturer's instructions to obtain the cell lysate. The total protein concentration of all lysate samples was calibrated by BCA protein assay (Pierce). SDS-buffer was added to samples and heated at 100 °C for 10 min. SDS-PAGE was performed using a handcast 10% polyacrylamide gel (50 μg total protein loaded). The gel was washed with distilled water twice and were transferred to PVDF membrane by

Pierce Power Station according to manufacturer's instructions. The membranes were blocked with SuperBlock T20 (Thermo Fisher) for 2 h at room temperature, incubated with anti-p-EGFR pTyr1068 (Thermo Fisher, 1:1000) at 4 ℃ overnight, washed with TBST (TBS + 0.05% Tween 20) twice, incubated with HRP-conjugated anti-rabbit IgG (H+L) (Thermo Fisher, 1:2000) for 1 h at room temperature and washed again with TBST 3-5 times. Afterwards, blots were treated with ECL Western Blotting Substrate (Pierce) and scanned by ChemiDoc XRS (BioRad) imaging system.

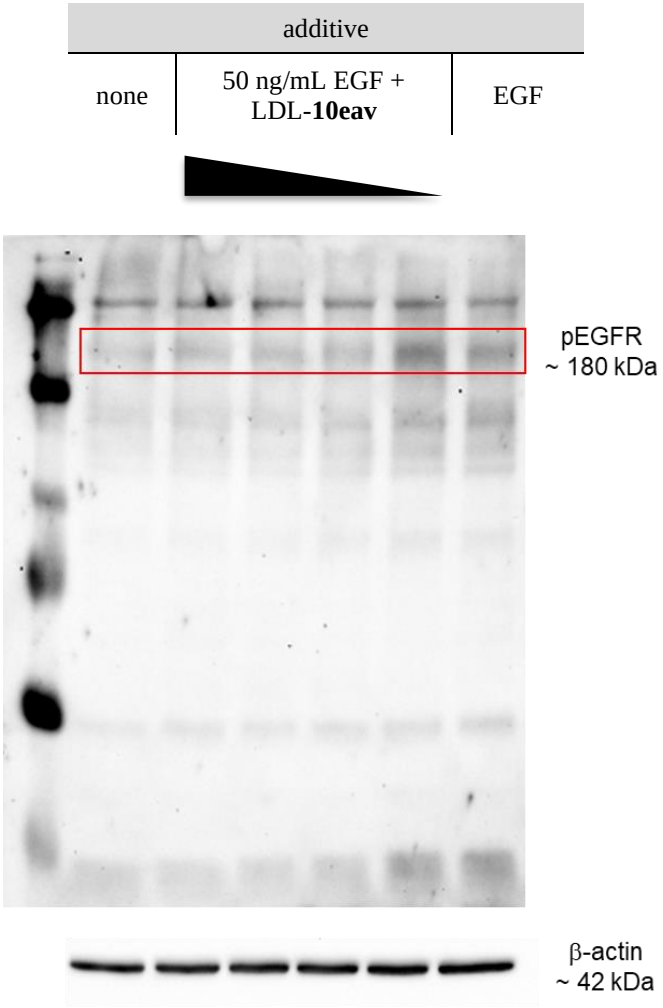

Figure A-6. Complete Western blot image of the EGFR pTyr inhibition for LDL-**10eav** at concentrations (μM) decreasing from 112.5, 75, 50, 25, 12.5 in competition with EGF (uniformly used at 50 ng/mL). Reprinted with permission from ref 112. Copyright 2020 Wiley-VCH Verlag GmbH & Co. KGaA, Weinheim.

APPENDIX B

SUPPORTING INFORMATION FOR CHAPTER 5

General Experimental Procedure

All reactions were carried out under an inert atmosphere (nitrogen, or argon where stated) with dry solvents under anhydrous conditions. Glassware for anhydrous reactions was dried in an oven at 140 ºC for minimum 6 h prior to use. Dry solvents were obtained by passing the previously degassed solvents through activated alumina columns. Reagents were purchased at a high commercial quality (typically 97 % or higher) and used without further purification. Analytical thin layer chromatography (TLC) was carried out on Merck silica gel plates with QF 254 indicator and visualized by UV, ceric ammonium molybdate, ninhydrin, para-methoxybenzaldehyde and/or potassium permanganate stains. Flash chromatography was performed using silica gel (230-600 mesh). Microwave irradiation for solid-phase syntheses was done using CEM MARS 5® system. LC-MS analyses were collected from Agilent 1260 Infinity Quaternary LC and Agilent 6120 Quadrupole LC-MS modules using Poroshell 120 EC-C18 2.7 μM (4.6 x 50 mm) column in 10-90% MeCN/water gradient with 0.1% formic acid over 10 minutes. Agilent 1260 Infinity II LC together with the Agilent 1290 Evaporative Light Scattering Detector was used in 10-90% MeCN/water gradient with 0.1% TFA over 25 minutes. A reversed phase column on Agilent PrepStar SD-1 preparative HPLC was used to purify final compounds in 10−90% MeCN/water gradient with 0.1% TFA over 20 min. The purity of the compounds was confirmed by Agilent 1260 Infinity II LC together with the Agilent 1290

Evaporative Light Scattering Detector column in 10-90% MeCN/water gradient with 0.1% TFA over 25 minutes. All the compounds had ≥95% purity.

Well plates for bioassays were analyzed using Biotek Synergy H4 Microplate Reader. High field NMR spectra were recorded with Bruker Avance III at 400 MHz for ^{1}H, and 100 MHz for ^{13}C and were calibrated using residual deuterated solvent as an internal reference ($CDCl_3$: ^{1}H NMR = 7.24, ^{13}C NMR = 77.0, MeOD: ^{1}H NMR = 3.30, ^{13}C NMR = 49.0, DMSO-d_6: ^{1}H NMR = 2.50, ^{13}C NMR = 39.5). The following abbreviations were used to explain the multiplicities: s = singlet, d = doublet, t = triplet, q = quartet, quint = quintet, dd = double doublet, dt = double triplet, dq = double quartet, m = multiplet, br = broad. Electrospray ionization mass spectrometry (ESI+ MS) data were collected on triple-stage quadrupole instrument in a positive mode.

All statistical analyses were carried out by GraphPad Prism version 6.0 (Graphpad Software). Student's t-test was used to determine significant differences between compounds and negative control. Results are represented as means ± SD.

Quenched molecular dynamics (QMD) and Exploring Key Orientations (EKO)

Quenched molecular dynamics (QMD) was used to generate simulated conformations of all diasteromers of **10aaa**. The procedures had been reported previously.[124] Approximately 1500 conformers of each diastereomer within 3.0 kcal/mol of the global minimum were matched on uPA•uPAR protein-protein interaction (PDB ID: 3bt1) using the EKO analyses.[32] The *C*α-*C*β coordinates from the side chains of peptidomimetics were systematically overlaid on *C*α-*C*β coordinates of the uPA side chains at the protein-protein

interface using an in-house algorithm. The goodness of fit was reported as root mean square deviation (RMSD). Lower RMSDs mean the *C*α-*C*β orientations between chemotypes and protein side chains are similar, thus chemotypes can *mimic* the protein side chains. Conformers within RMSD ≤ 0.50 Å were considered as "potential hits" which were summarized in Table B-1.

Table B-1. Potential uPA mimics (**10**) from EKO analyses within RMSD ≤ 0.50 Å

.

Configuration	R^1	R^2	R^3
LLL	Phe	Lys	Ser
DLL	Ser	Lys	Ser
DDL	Ser	Lys	Ser
LLD	Ser	Lys	Ser
LDD	Asn	Tyr	Ser
DDD	Ser	Lys	Ser
DDD	Phe	Asn	Ser
DDL	Ser	Lys	Phe
DDD	Ser	Lys	Phe
DLL	Lys	Ser	Ile
DDL	Tyr	Ser	Ile
LLL	Ser	Tyr	Asn
DLL	Ser	Tyr	Asn
LLD	Ser	Tyr	Asn
DLD	Ser	Tyr	Asn
DLD	Lys	Ser	Trp
DDL	Phe	Asn	His
DDD	Ile	Ser	Tyr

Solid Phase General Syntheses of 13 and 14

Syntheses of the piptides **10** used in these studies have already been reported.[112] Urea linkage was based off of a previously published procedure.[110]

Fmoc deprotection on solid phase

Deprotection of Fmoc was performed by adding 20% piperidine in DMF to the beads and were heated under microwave irradiation (160 W, 75 ºC, 3 min). Solution was drained, and beads were washed with DMF several times.

Coupling on solid phase

Acid (4 eq) was activated with HATU (4 eq) and $^{i}Pr_2NEt$ (8 eq) in DMF (0.2 M). This solution was added to the beads and subjected to microwave irradiation (100 W, 75 ºC, 10 min). Solution was drained, and beads were washed with DMF several times. The temperature was lowered to 50 ºC when working with chlorotrityl resins.

Deprotection of nosyl group on solid phase

Similar to deprotection on solution phase with 2-meraptoethanol (3 eq) and DBU (5 eq) in DMF (1 M) were added to the beads and subjected to microwave irradiation (100 W, 50 ºC, 15 min). Solution was drained, and beads were washed with DMF several times.

Click Reaction

Fmoc-amino alkyne (2 eq), $^{i}Pr_2NEt$ (4 eq), sodium ascorbate (0.2 eq), and $CuSO_4 \cdot 5H_2O$ (0.1 eq) were dissolved in DMF (2.5 mL) which were added into the resin containing azide. The beads were shaken in the dark at 25 ^{o}C for 16 h, and the beads were washed with 3 mL of 0.05 M EDTA (aq)/DMF (1:1) solution till all copper ions are removed (disappearance of green color of the bead). The beads were washed with DMF (4 mL x 5) to remove water.

Hydantoin cyclization

After the Fmoc deprotection at the R^1 position, beads were washed with CH_3CN (2 mL x 3), drained, and treated twice with *p*-nitrophenyl chloroformate (3 eq) and $^{i}Pr_2NEt$ (6 eq) in CH_3CN at ~ 0.05 M concentration. Beads were shaken at 25 ^{o}C for 15 min each. Beads were washed with CH_3CN (4 mL x 3), CH_2Cl_2 (4 mL x 3) and NMP (4 mL x 3) and shaken 5 times with 5 mL of 5 % $^{i}Pr_2NEt$ /NMP (v/v) solution for 1 h each to remove any yellowish by-products. Beads were further washed with NMP (4 mL x 5), CH_2Cl_2 (4 mL x 5) and CH_3OH (4 mL x 5).

Cleavage from the resin

For chlorotrityl resins, beads were treated with 20% HFIP/CH_2Cl_2 at 25 ^{o}C for 1 hr. Solution was collected and beads were treated with fresh 20% HFIP/CH_2Cl_2 for another 30 min. For TentaGel S Ram resins, compounds were cleaved off from the beads by treating with TFA/Et_3SiH/water (95:2.5:2.5 v/v) cocktail for 4 h at 25 ^{o}C. Collected

solutions were dried under N_2 stream and purified by preparative reversed-phase HPLC (10% - 90% MeCN/H_2O with 0.05% TFA) and lyophilized to obtain white to yellowish powders.

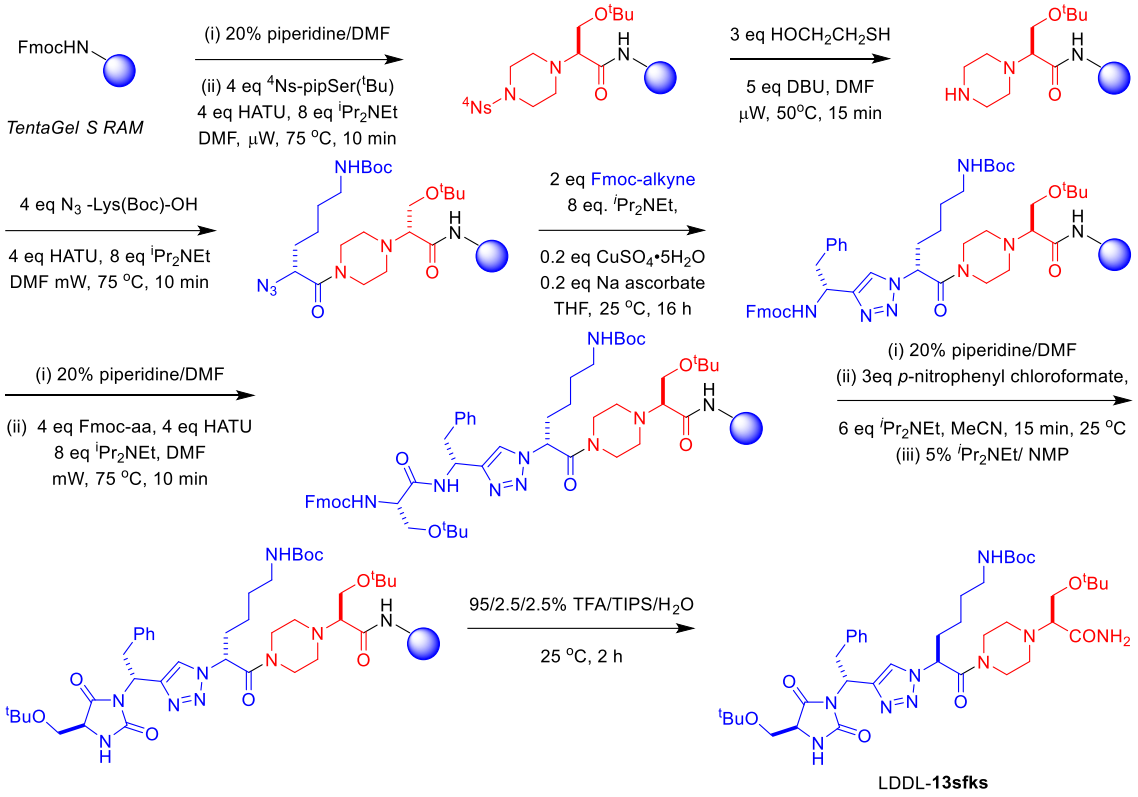

Scheme B-1. Synthesis of LDDL-**13sfks**.

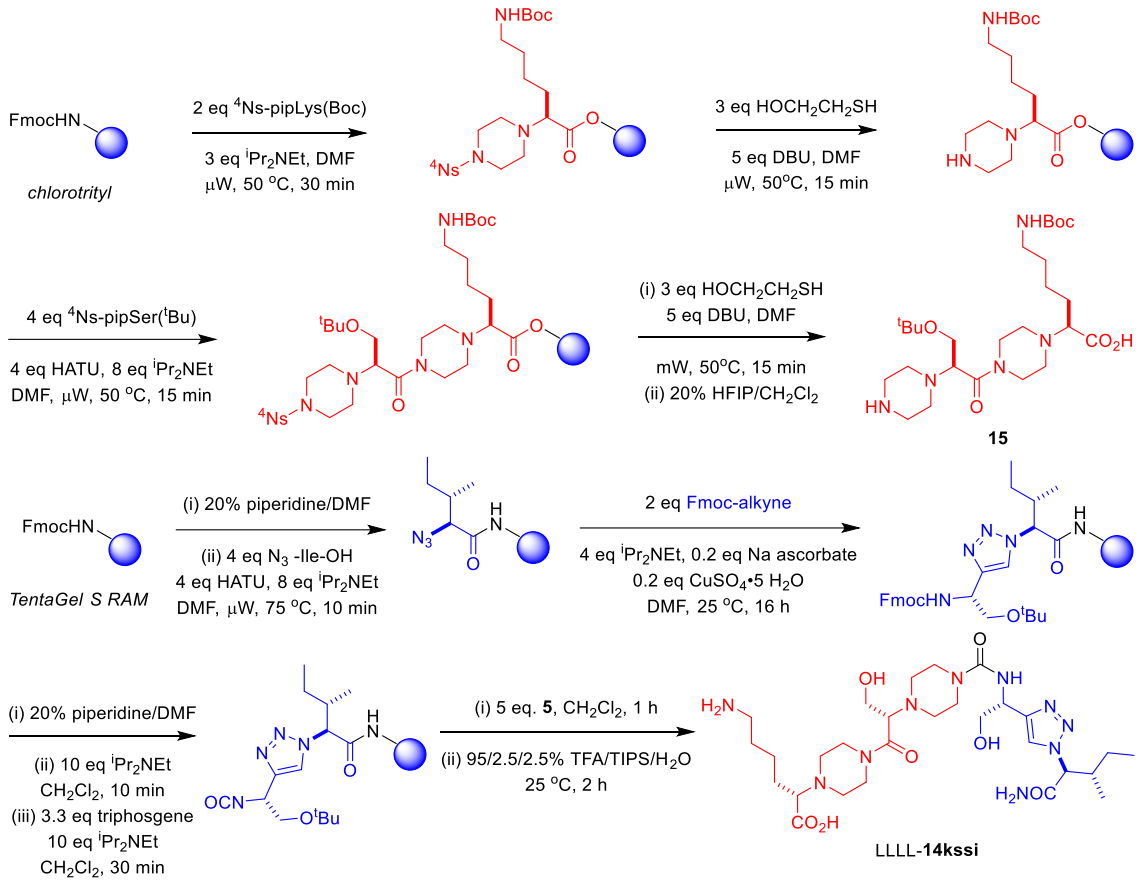

Scheme B-2. Synthesis of LLLL-**14kssi**.

Compound Characterization

*(R)-2-(4-((R)-2-(4-(D-seryl)piperazin-1-yl)-6-aminohexanoyl)piperazin-1-yl)-3-phenylpropanamide (DDD-**10skf**)*, 2.8 mg, 45% yield, white solid. ^{1}H NMR (400 MHz, DMSO-d_6) δ 9.01 (s, 2H), 7.49−7.14 (m, 7H), 5.05 (s, 1H), 4.34-3.87 (m, 3H), 3.60 (t, J = 7.5 Hz, 1H), 3.48 (t, J = 7.0 Hz, 1H), 3.34−3.19 (m, 8H), 3.08−2.66 (m, 10H), 2.55 (t, J = 7.1 Hz, 2H), 1.72-1.46 (m, 6H), 1.31-1.19 (m, 2H). ^{13}C NMR (101 MHz, DMSO-d_6) δ 177.51, 168.85, 168.43, 140.18, 129.54, 127.92, 126.03, 76.15, 70.34, 62.19, 55.32, 52.22,

50.46, 43.62, 36.03, 30.88, 28.90, 23.17. Calculated $C_{26}H_{44}N_7O_4^+$ (*m/z*): 518.3377; found $(M+H)^+$: 518.3380.

*(S)-2-(4-((R)-6-amino-2-(4-((R)-1-((S)-4-(hydroxymethyl)-2,5-dioxoimidazolidin-1-yl)-2-phenylethyl)-1H-1,2,3-triazol-1-yl)hexanoyl)piperazin-1-yl)-3-hydroxypropanamide (LDDL-**13sfks**)*, 4.8 mg, 38% yield, light yellow solid. ^{1}H NMR (400 MHz, DMSO-d_6) δ 11.08 (s, 1H), 7.64 (s, 1H), 7.25-7.13 (m, 7H), 5.26 (t, J = 7.1 Hz, 1H), 5.09 (s, 2H), 4.72-4.43 (m, 2H), 4.25-3.64 (m, 4H), 3.69 (t, J = 7.5 Hz, 1H), 3.35−3.10 (m, 5H), 3.01−2.76 (m, 5H), 2.68 (t, J = 7.0 Hz, 2H), 2.07-1.84 (m, 2H), 1.64-1.42 (m, 4H), 1.31 (m, 2H). ^{13}C NMR (101 MHz, DMSO-d_6) δ 178.31, 173.32, 172.71, 156.94, 139.52, 131.69, 128.61, 127.52, 125.47, 123.06, 78.05, 71.14, 63.45, 61.83, 60.65, 59.92, 52.60, 49.80, 42.38, 39.83, 32.51, 27.54, 28.49, 21.42. Calculated $C_{27}H_{40}N_9O_6^+$ (*m/z*): 586.3023; found $(M+H)^+$: 586.3018.

*(S)-6-amino-2-(4-((S)-2-(4-(((R)-1-(1-((2S,3S)-1-amino-3-methyl-1-oxopentan-2-yl)-1H-1,2,3-triazol-4-yl)-2-hydroxyethyl)carbamoyl)piperazin-1-yl)-3-hydroxypropanoyl)piperazin-1-yl)hexanoic acid (LLLL-**14kssi**)*, 4.1 mg, 31% yield, white solid. ^{1}H NMR (400 MHz, DMSO-d_6) δ 12.09 (s, 1H), 7.65 (s, 1H), 7.24 (s, 2H), 6.55 (s, 1H), 5.09−4.73 (m, 2H), 4.54 (d, J = 7.2 Hz, 1H), 4.29−3.70 (m, 3H), 3.67-3.37 (m, 4H), 3.32-3.21 (m, 8H), 2.91-2.75 (m, 8H), 2.70 (t, J = 7.4 Hz, 2H), 2.27 (m, 1H), 1.64-1.46 (m, 8H), 1.28-1.21 (m, 2H), 1.05-0.91 (m, 6H). ^{13}C NMR (101 MHz, DMSO-d_6) δ 177.31, 175.32, 169.73, 157.94, 131.52, 123.61, 79.52, 75.47, 74.06, 64.57, 61.90, 60.34, 52.83,

51.65, 50.92, 49.60, 42.80, 29.54, 28.49, 28.42, 25.37, 23.57, 15.05, 10.79. Calculated $C_{28}H_{51}N_{10}O_7^+$ (*m/z*): 639.3786; found $(M+H)^+$: 639.3792.

LC Traces

DDD-**10skf**

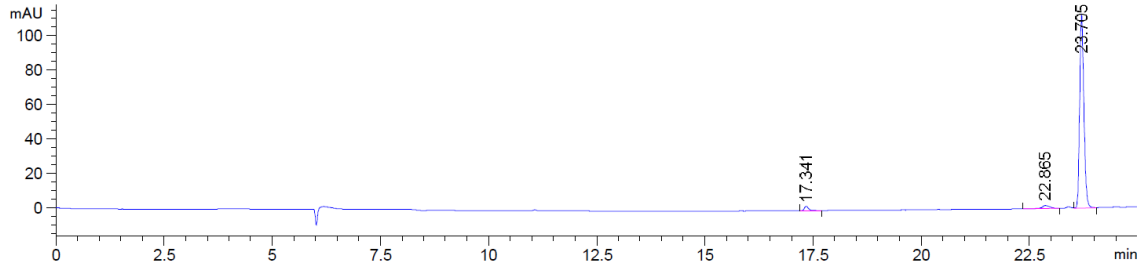

LDDL-**13sfks**

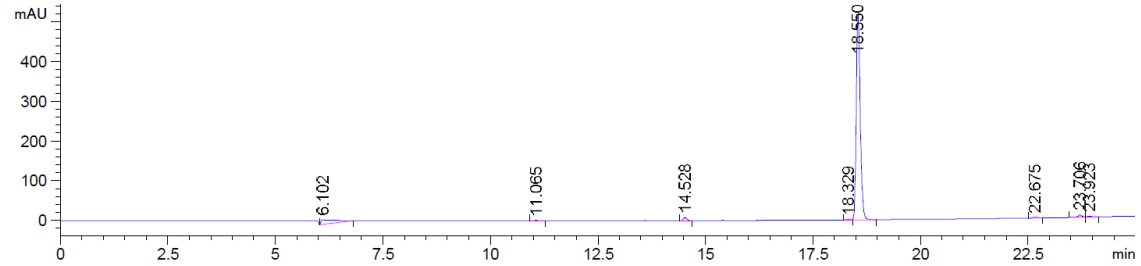

LLLL-**14kssi**

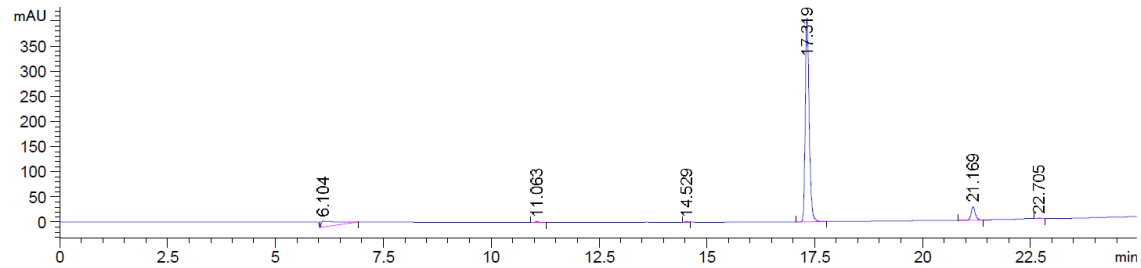

ELISA

96-well plates were incubated overnight at 4 °C with 100 µL of 2 µg/mL uPAR (from Dr. Mazar) in PBS for immobilization. The plate was then washed with 0.05% Tween-20 in PBS buffer between each step. A 1:1 mixture of Superblock buffer in PBS (ThermoFisher) with 0.04 M NaH2PO4 and 0.3 M NaCl buffer was used for blocking at room temperature for 1 h. Various concentrations of the compounds were added and incubated at room temperature for 1 h. Compounds were initially screened at 50 µM. For concentration-dependent studies, a range of compound concentrations from 0.5 µM to 1000 µM in PBS was used. After washing, 5 nM uPA-HRP (Molecular Innovations) in PBS was then added and incubated for 1 h. 3,3',5,5'-Tetramethylbenzidine (TMB; ThermoFisher) was added and incubated for an additional 20 min. Sulfuric acid is then incubated for 15 min acting as a stop solution. The signal was detected at 450 nm using a microplate reader.

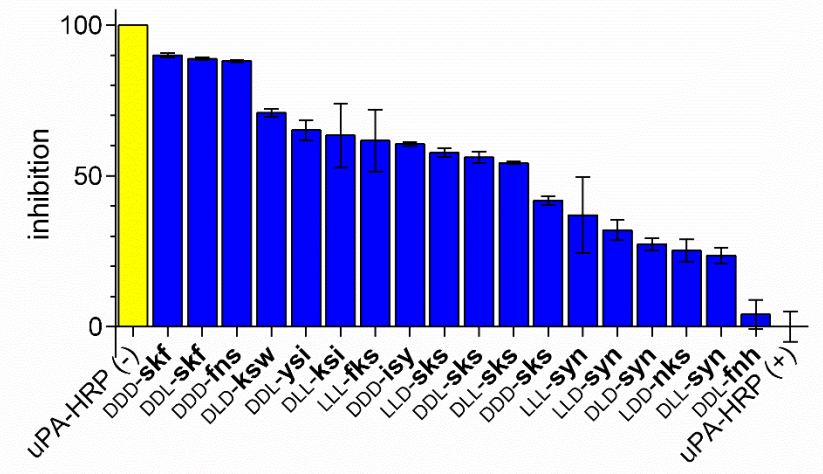

Figure B-1. Competitive ELISA of **10** at 50 µM.

Fluorescence Polarization Assay

Polarized fluorescence intensities were measured with excitation and emission wavelengths of 485 and 535 nm, respectively. To each well, 10 μL 50 nM of FITC-AE105 and 5 μM of uPAR in PBS were added. Various concentrations of the compounds were prepared (0.01 – 500 μM) and 10 μL were added to each well. The plate was shaken in the dark for 3 h before it was read. Controls included wells containing only the peptide and wells containing both protein and peptide each in triplicates.

Surface Plasmon Resonance

Direct binding of each compound to immobilize His-tagged uPAR (catalog no. 10925-H08H, SinoBiological) was measured by SPR using a Biacore T200 optical biosensor (Cytiva) at 25˚C. High density (8000-10000 RU) of anti-His antibody (His Capture Kit product no. 28995056, Cytiva) surfaces were created using CM5 sensor chips (Cytiva) using standard amine coupling chemistry. The mixture of equal volume of 0.1M N-hydroxysuccinimide and 0.4M 1-ethyl-3-(3-dimethylaminopropyl)-carbodiimide was injected for 8 min at 5 μl/min to activate the flow cell surface. Anti-His antibody stock (1 mg/mL) was diluted to 50 μg/mL with 10 mM sodium acetate pH 5.0 and injected for 10 min at 5 mL/min to the activated surface and immediately followed by a 5 min injection of 1M ethanolamine (pH 9.0) to deactivate the surface. uPAR stock (0.25 mg/ml) was diluted to 50 μg/ml in 1X PBS buffer containing 100 mM arginine and 10% glycerol (pH 7.5). Phosphate buffered saline (50 mM sodium phosphate pH 7.4, 150 mM NaCl) containing 0.01% (v/v) Tween-20 (PBST) was used for immobilization. A reference flow

cell was prepared with activation and deactivation steps but no anti-His antibody coupled. All binding experiments were performed in PBST containing 2% (v/v) DMSO at a flow rate of 50 µL/min. Each compound was dissolved in 100% DMSO to 20 mM and then diluted 50-fold in PBST to 550 µM concentration as working stock for further dilution in running buffer. To regenerate the sensor surface, bound molecule was removed by flowing 10 mM glycine-HCl (pH 2.2) over receptor surface for 30 sec and next cycle was performed on a fresh surface. For each compound kinetics run, the appropriate controls were used as described in text. The SPR sensorgrams were referenced, buffer subtracted, and evaluated using the Biacore T200 Evaluation Software (version 3.1).

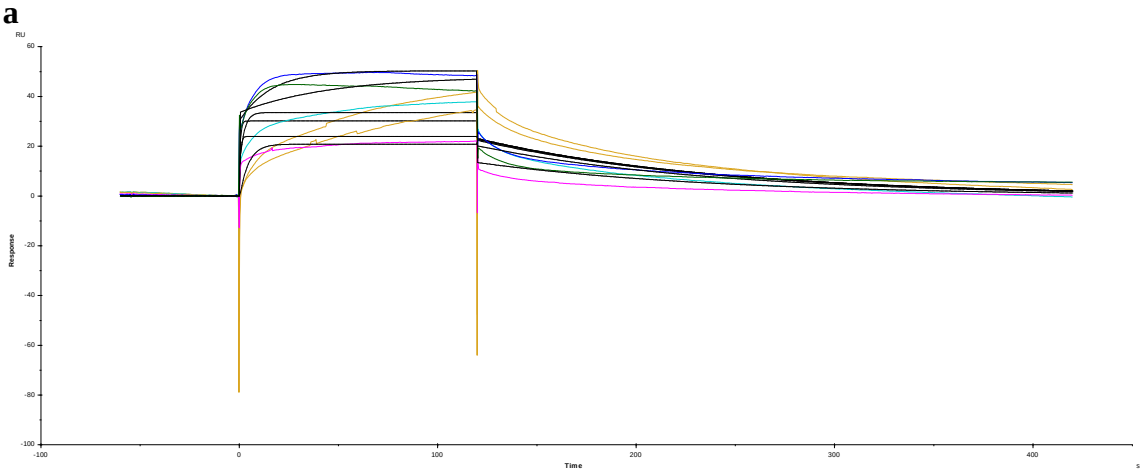

Figure B-2. Direct binding of compounds **a** DDD-**10skf**, **b** LLL-**12fsi**, **c** LDDL-**13sfks** and **d** LLLL-**14kssi** to uPAR immobilized on Biacore sensor chip surface (SPR) shown as a sensorgram.

b

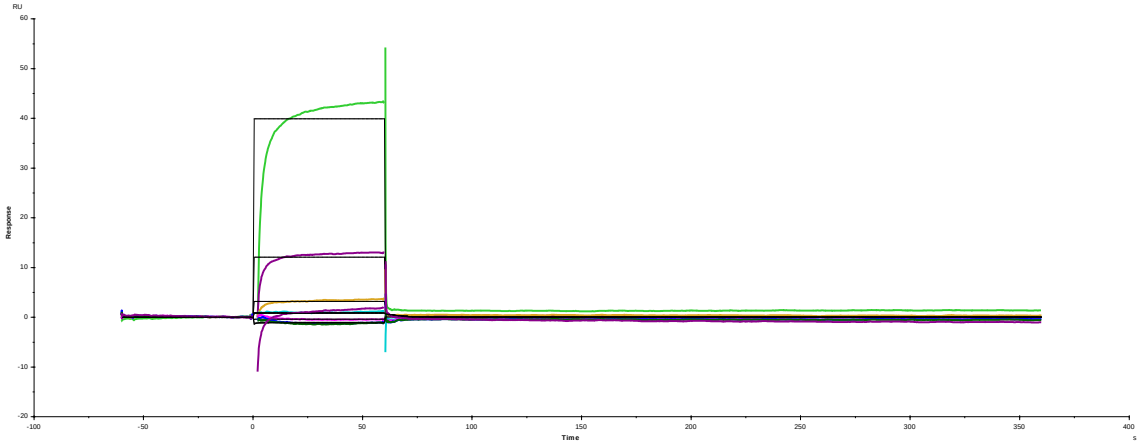

c

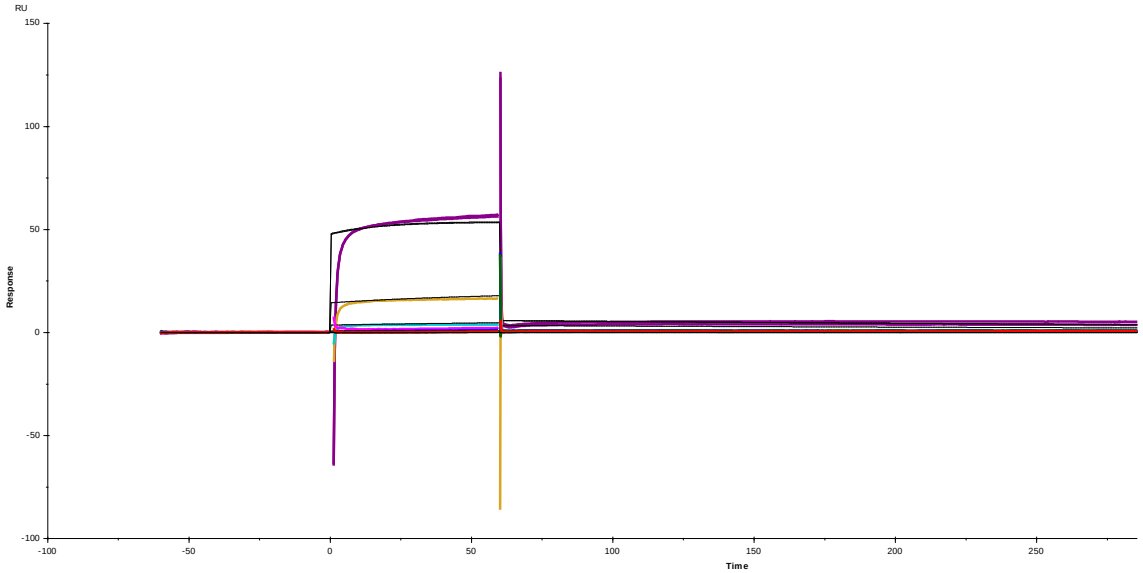

d

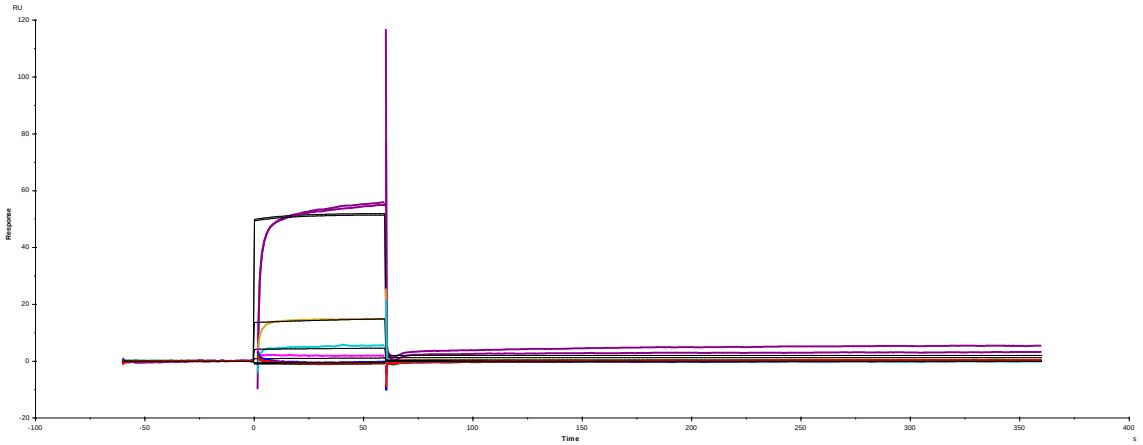

Figure B-2. Continued.

Cell Culture Procedure

MDA-MB-231 cells were cultured on 75 cm^2 tissue culture flasks in Dulbecco's Modified Eagle Medium (DMEM, Millipore Sigma) with 10% FBS. All cells were cultured in a humidified incubator at 37 °C with 5% CO_2 and 95% air.

Cell Viability Assay

MDA-MB-231 cells were seeded at 5000 cells/well (50 µL) on 96-well plates and incubated at 37 °C overnight. Various concentrations of the compounds were prepared in protein-free hybridoma medium (PFHM II) and added to cells to make final concentrations from 1 to 200 µM. After 48 h, 10 µL of AlamarBlue reagent (Invitrogen) was added and incubated for an additional 2 h. Fluorescence intensity (Ex/Em 495/519 nm) was measured on a microplate reader.

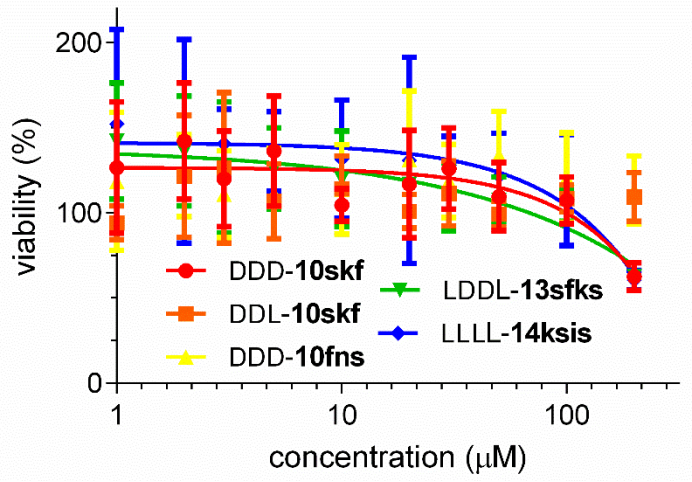

Figure B-3. MDA-MB-231 cell viabilities of compounds **10**, **13** and **14** as monitored using alamarBlue, where gefitinib is the positive control and LLL-**10faa** is the partial negative control.

Wound Healing

Culture-Insert 2 Wells (ibidi) were placed inside a 24-well plate. Using MDA-MB-231, 70 μL of a 3 x 10^5 cells/mL were added into each well of the insert. Plate was incubated for 24 hours at 37 ºC.

After incubation overnight, inserts were removed, and wells were gently washed with PBS to remove unattached cells. In each well, 0.5 mL of 0.1 % DMSO, 5 or 50 μM of the compounds with 1% FBS in 10% DMEM/F12 and PFHM II were added. Time-lapse imaging was recorded by EVOS (ThermoFisher) at 37 ºC and 5% CO_2, with images taken every 30 min for 45 hours. The results were evaluated using the ibidi software.[126]

Migration and Invasion Assay

Twenty-four well Transwell plates (Costar, Corning), with 8 μM pore size inserts, were used. To the lower compartment (in the well), 0.6 mL of 0.1 % DMSO, 5 or 50 μM of the compounds and 1% FBS in 10% DMEM/F12 and PFHM II was added before adding the insert to the well. To the upper compartment (inside the insert), 0.2 mL of 2 x 10^5 cells of MDA-MB-231 or HEK 293 with 0.1 % DMSO, 5 or 50 μM of the compounds and 1% FBS in 10% DMEM/F12 and PFHM II was added. Plates were incubated for 20 hours at 37 ºC.

After incubation overnight, inserts were taken out and washed with PBS 3 times. The upper side of the filter membrane is gently swiped with cotton swap to remove cell debris. The lower side of the insert filter was fixed with formaldehyde for 10 min, methanol for 10 min, and stained with Hematoxylin solution (Millipore Sigma) for 20 min, carefully

washing with PBS 3 times after each step. Cells on the insert were imaged and (manually) counted at 10x magnification (EVOS, ThermoFisher). Percent migration were normalized using the DMSO control (100%).

Invasion assay was similar except inserts were warmed to room temperature from -20 ^{o}C first. Serum-free DMEM was added to the inside of the insert and bottom of the wells and incubated for 2 h at 37 ^{o}C. The media was removed carefully before proceeding to add the solutions as described above.

APPENDIX C

UNCONVENTIONAL SECONDARY STRUCTURE MIMICS: LADDER-RUNGS*

Assays used to monitor the effects of small molecules on uPA•uPAR tend to test for parameters such as cell migration and invasion to reflect influence on metastatic spread; the work of Meroueh and co-workers on testing small molecules discovered by high-throughput screening on the same target was a good model for our studies[103, 105, 127-130] of compound **1** (same as compound **12** in the main chapters of this dissertation).

A competitive ELISA (uPAR anchored, uPA in solution) was first used to monitor binding to uPAR. At 50 μM, all ten candidate compounds from the EKO evaluation inhibited binding of uPA-HRP (5 nM; HRP is horse radish peroxidase) to some extent. The fact that all ten compounds passed the EKO evaluation speaks to the validity of this method for identification of binders. Three of these (LLL-**1fsi**, LDD-**1sfk**, DDL-**1sfk**) were selected for determination IC_{50} values; the values obtained were 8.35 ± 0.05, 13.5 ± 0.1, 25.4 ± 0.1 μM, respectively (Figure C-1b).

A fluorescence polarization assay was used to determine dissociation constants of the three lead compounds with respect to solubilized uPAR (Fig C-2c; Ploug's uPAR binding peptide AE105[108] was used as a competitor). The values obtained were in the range (7.5 – 22 μM), where LLL-**1fsi** was retained most strongly (7.5 ± 0.1 μM**)**.

---

* Reprinted with permission from "Unconventional Secondary Structure Mimics: Ladder-Rungs" by Chen-Ming Lin[+], Maritess Arancillo[+], Jonathan Whisenant, and Kevin Burgess, 2020. Angew. Chem., Int. Ed., 59, 9398–9402. DOI: 10.1002/anie.202002639. Copyright 2020 by Wiley-VCH Verlag GmbH & Co. KGaA, Weinheim.

[+] These authors contributed equally to this work.

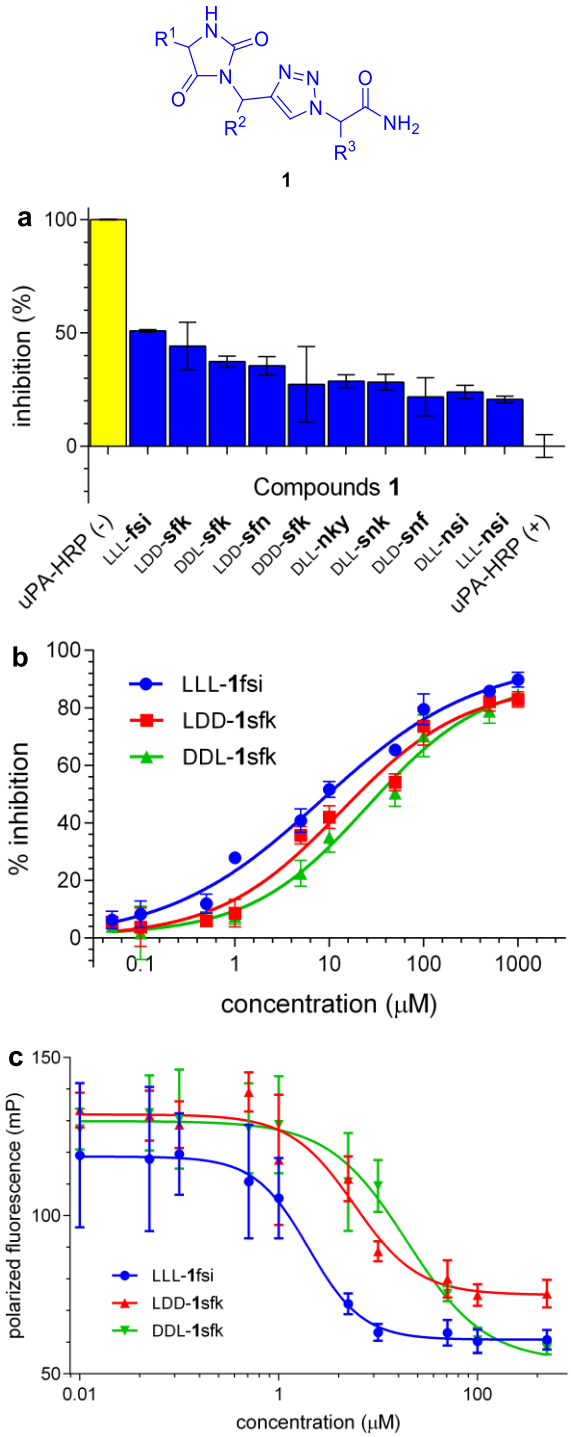

Figure C-1. a Competitive ELISA of all compounds at 50 μM. **b** Dose response of three (lead) compounds to obtain IC_{50} values. **c** Competitive fluorescence polarization to determine the binding, K_i, of the lead compounds **1**. Reprinted with permission from ref 106. Copyright 2020 Wiley-VCH Verlag GmbH & Co. KGaA, Weinheim.

Compounds that bind uPAR are not necessarily expected to be cytotoxic. Cytotoxicities of LLL-**1fsi**, LDD-**1sfk**, and DDL-**1sfk** on MDA-MB-231 ($uPAR^+$ metastatic, triple negative breast cancer cells;[107] Fig C-1d) were checked; only LLL-**1fsi** decreased in viability significantly at 200 μM. From this point forward, only the compound with highest affinity for uPAR, LLL-**1fsi**, was considered.

Mimic LLL-**1fsi** was evaluated in assays for wound healing, cell migration, and invasion; MDA-MB-231 cells were used throughout. Dose dependent effects were observed in all three assays (Figure C-2, images in Figure C-4 and C-5; AE105 was used as positive control;[88] the test compounds had no effect on invasion or migration of uPAR-negative HEK293 kidney embryonic cells[107]). Thus LLL-**1fsi** suppresses cell movement into a scratch, migration in response to a chemical gradient, and invasion across an extracellular matrix-analog; all characteristics of suppression of metastases.

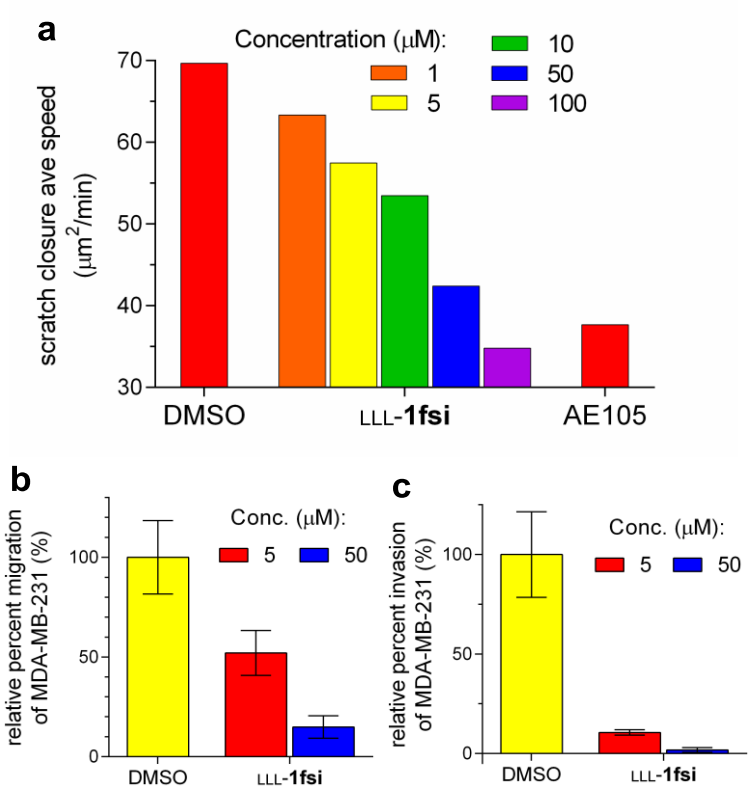

Figure C-2. a Dose response wound healing assay (peptide AE105 at 0.5 μM as a positive control). Data processed using ibidi software (available online).[126] **b** Normalized migration and **c** invasion assays using MDA-MB-231 compared with a DMSO control. Reprinted with permission from ref 106. Copyright 2020 Wiley-VCH Verlag GmbH & Co. KGaA, Weinheim.

Methods

ELISA

96-well plates were incubated overnight at 4 °C with 100 μL of 2 μg/mL uPAR (from Dr. Mazar) in PBS for immobilization. The plate was then washed with 0.05% Tween-20 in PBS buffer between each step. A 1:1 mixture of Superblock buffer in PBS (ThermoFisher) with 0.04 M NaH_2PO_4 and 0.3 M NaCl buffer was used for blocking at

room temperature for 1 h. Various concentrations of compound **1** were added and incubated at room temperature for 1 h. Compounds were initially screened at 50 μM. For concentration-dependent studies, a range of compound concentrations from 0.5 μM to 1000 μM in PBS was used. After washing, 5 nM uPA-HRP (Molecular Innovations) in PBS was then added and incubated for 1 h. TMB (ThermoFisher) was added and incubated for an additional 20 min. Sulfuric acid is then incubated for 15 min acting as a stop solution. The signal was detected at 450 nm using a microplate reader.

Fluorescence Polarization Assay

Polarized fluorescence intensities were measured with excitation and emission wavelengths of 485 and 535 nm, respectively. To each well, 10 mL 50 nM of AE105-FITC and 5 mM of uPAR in PBS were added. Various concentrations of **1** were prepared (0.01 – 500 mM) and 10 mL were added to each well. The plate was shaken in the dark for 3 h before it was read. Controls included wells containing only the peptide and wells containing both protein and peptide each in triplicates.

Cell Viability Assay

MDA-MB-231 cells were seeded at 5000 cells/well (50 μL) on 96-well plates and incubated at 37^{o}C overnight. Various concentrations of **1** were prepared in protein-free hybridoma medium (PFHM II) and added to cells to make final concentrations from 1 mM to 200 μM. After 48 h, 10 μL of AlamarBlue reagent (Invitrogen) was added and incubated

for an additional 2 h. Fluorescence intensity (Ex/Em 495/519 nm) was measured on a microplate reader.

Compounds that bind uPAR are not necessarily expected to be cytotoxic. Cytotoxicities of LLL-**1fsi**, LDD-**1sfk**, and DDL-**1sfk** on MDA-MB-231 ($uPAR^+$ metastatic, triple negative breast cancer cells; Figure C-3a) were checked; only LLL-**1fsi** decreased in viability significantly at 200 μM.

Table C-1. Summary of values (μM) for ELISA, FP, and cell viability (without PMA) with their corresponding standard deviation. Reprinted with permission from ref 106. Copyright 2020 Wiley-VCH Verlag GmbH & Co. KGaA, Weinheim.

	LLL-**1fsi**	LDD-**1sfk**	DDL-**1sfk**
ELISA (IC_{50})[a]	8.35 ± 0.05	13.5 ± 0.1	25.4 ± 0.1
FP (K_i)[a]	7.5 ± 0.2	12.1 ± 0.2	22.8 ± 0.4
Cell Viability (IC_{50}, no PMA)[b]	-	-	-

[a]Experiments were done in triplicates and repeated three times. [b]Cell viability was done in octuplicates and repeated for three times. Viability remained fairly constant throughout most of the experiment (Fig. C-3a), so no values are reported.

Another set of cells were seeded onto 96-well plates, this time with 100 nM phorbol 12-myristate 13-acetate (PMA, Alfa Aesar) added to increase the amount of uPAR in the cells.[131] Compounds **1** were added in the same procedure described above. Even with the increased amount of uPAR on the cells, the results in Fig. S2b show that only LLL-**1fsi** has significant cytotoxicity, with IC_{50} at about 31 μM.

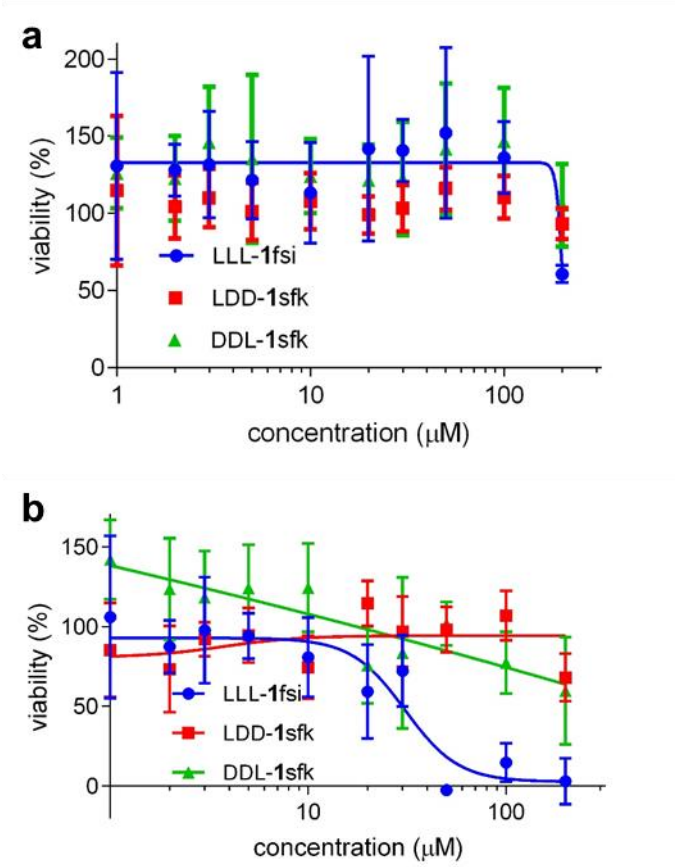

Figure C-3. a Cell viability for LLL-**1fsi**, LDD-**1sfk** and DDL-**1sfk** with respect to MDA-MB-231 cells. **b** Cell viability with PMA (phorbol 12-myristate 13-acetate, 100 nM) added to increase the expression of uPAR on the cell membrane.[131] Reprinted with permission from ref 106. Copyright 2020 Wiley-VCH Verlag GmbH & Co. KGaA, Weinheim.

Wound Healing

Culture-Insert 2 Wells (ibidi) were placed inside a 24-well plate. Using MDA-MB-231, 70 mL of a 3 x 10^5 cells/mL were added into each well of the insert. Plate was incubated for 24 hours at 37 ^oC.

After incubation overnight, inserts were removed, and wells were gently washed with PBS to remove unattached cells. In each well, 0.5 mL of 0.1 % DMSO, 5 or 50 μM of LLL-**1fsi** with 1% FBS in 10% DMEM/F12 and PFHM II were added. Time-lapse imaging was recorded by EVOS (ThermoFisher) at 37 ^oC and 5% CO_2, with images taken every 30 min for 45 hours. The results were evaluated using the ibidi software. [126]

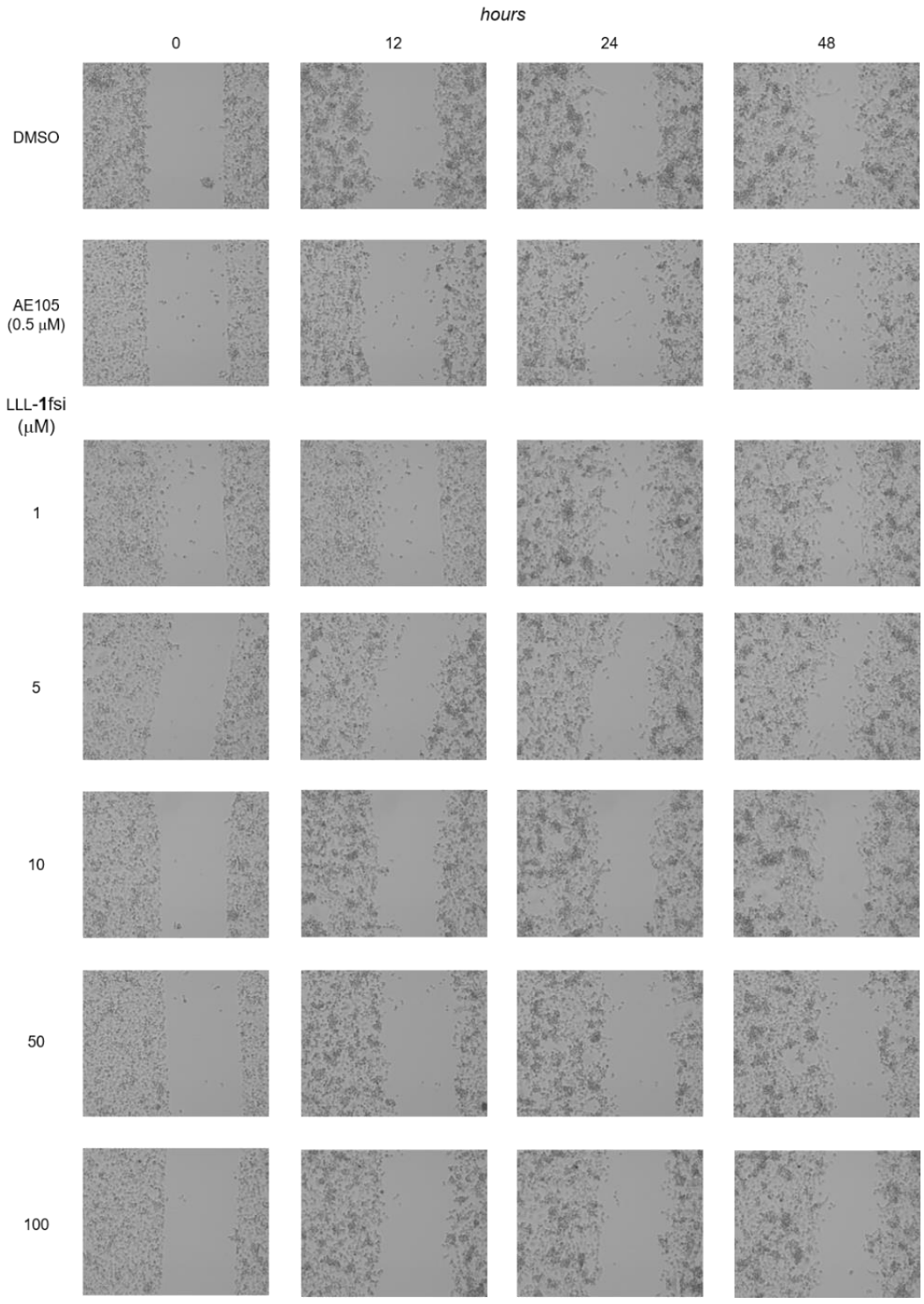

Figure C-4. During a 45-hour wound healing assay, images were taken every 30 minutes using a time-lapse microscope (EVOS, ThermoFisher). Representative pictures at 0, 12, 24 and 45 h are shown. Reprinted with permission from ref 106. Copyright 2020 Wiley-VCH Verlag GmbH & Co. KGaA, Weinheim.

Migration and Invasion Assay

Twenty-four well Transwell plates (Costar, Corning), with 8 μM pore size inserts, were used. To the lower compartment (in the well), 0.6 mL of 0.1 % DMSO, 5 or 50 μM of LLL-**1fsi** and 1% FBS in 10% DMEM/F12 and PFHM II was added before adding the insert to the well. To the upper compartment (inside the insert), 0.2 mL of 2 x 10^5 cells of MDA-MB-231 or HEK 293 with 0.1 % DMSO, 5 or 50 mM of LLL-**1fsi** and 1% FBS in 10% DMEM/F12 and PFHM II was added. Plates were incubated for 20 hours at 37 ^oC.

After incubation overnight, inserts were taken out and washed with PBS 3 times. The upper side of the filter membrane is gently swiped with cotton swap to remove cell debris. The lower side of the insert filter was fixed with formaldehyde for 10 min, methanol for 10 min, and stained with Hematoxylin solution (Millipore Sigma) for 20 min, carefully washing with PBS 3 times after each step. Cells on the insert were imaged and (manually) counted at 10x magnification (EVOS, ThermoFisher). Percent migration were normalized using the DMSO control (100%).

Invasion assay was similar except inserts were warmed to room temperature from -20 ^oC first. Serum-free DMEM was added to the inside of the insert and bottom of the wells and incubated for 2 h at 37 ^oC. The media was removed carefully before proceeding to add the solutions as described above.

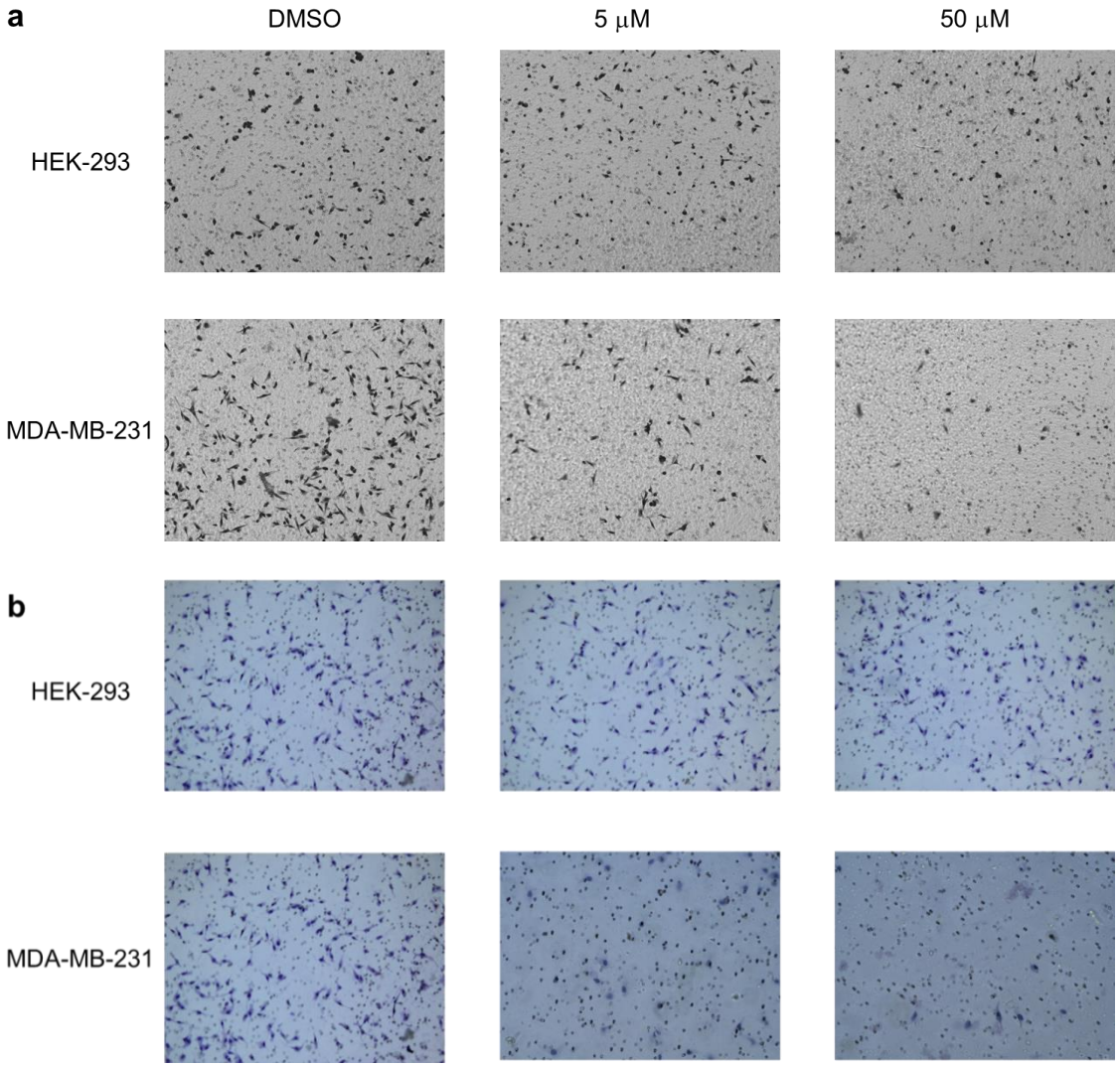

Figure C-5. Representative pictures of a Transwell® migration and **b** invasion assay for LLL-**1fsi**. Pores of the membranes could also be observed as the numerous small and round dots, while the cells are the larger and darker spots/streaks in the picture. Reprinted with permission from ref 106. Copyright 2020 Wiley-VCH Verlag GmbH & Co. KGaA, Weinheim.

APPENDIX D

EKO AND OTHER BIOINFORMATIC STUDIES

Design Criteria For Minimalist Mimics of Protein–Protein Interface Segments[*]

Data accumulated from EKO analyses

Figure D-2 plots the number of EKO alignments (referred to as "hits" later for simplicity) with RMSD < 0.35 Å for each hypothetical mimic, averaged over all stereoisomers. Mimic **1** gave significantly more hits than any other mimic. Mimics **1**–**4** gave more hits than our "control" A, whereas **5**–**8** gave less. Thus, **1**–**4** and **A** are fine interface mimics, and mimic **1** is a privileged design.

Figure D-2b breaks down the interface overlays according to stereochemistry of the mimics. All the mimics in Figure D-1 hypothetically could be obtained via synthesis from amino acids. It is tempting to assume the corresponding LLL-configurations should give the most overlays on PPI interfaces since natural proteins are derived exclusively from L-amino acids, but Figure D-2b shows this is not a valid assumption. Different stereochemical configurations can compensate for the unnatural backbones of minimalist mimics relative to the parent polyamide systems, to place side-chains in favorable orientations.

---

[*] Reprinted with permission from "Design Criteria For Minimalist Mimics of Protein–Protein Interface Segments" by Jaru Taechalertpaisarn, Rui-Liang Lyu, Maritess Arancillo, Chen-Ming Lin, Zhengyang Jiang, Lisa M. Perez, Thomas R. Ioerger and Kevin Burgess, 2019. *Org. Biomol. Chem.*, 17, 908–915. DOI: 10.1039/c8ob02901f. Copyright 2019 by The Royal Society of Chemistry.

We set out to rationalize the observations outlined above, but first it was necessary to test if they were just artifacts of the relative flexibilities of the mimics. The considerations used to do this is described in the following section.

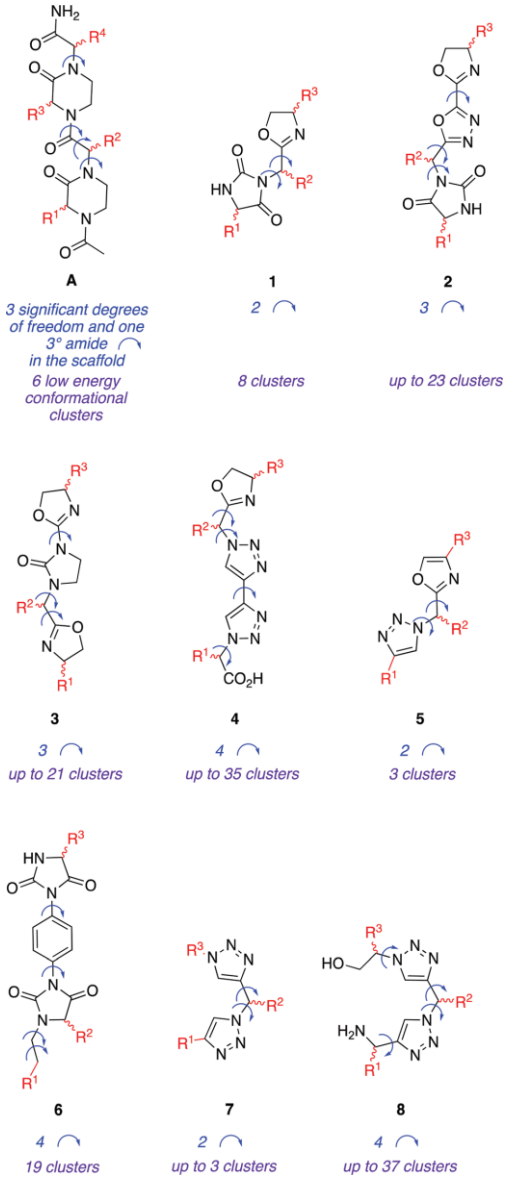

Figure D-1. Minimalist mimics featured in this study. Two indicators of compound flexibility are annotated below each structure. Since EKO was developed to evaluate minimalist mimics with three side-chains, we used only R^1, R^2, and R^4 of A in this work. Reprinted with permission from ref 50. Copyright 2019 The Royal Society of Chemistry.

The influence of relative flexibility on the EKO data

There are two simple quantitative indicators of flexibilities of minimalist mimics; both are indicated in Figure D-1. The first is "significant degrees of freedom", defined by the number of freely-rotating σ-bonds and by tertiary amides that flip between cis and trans conformations. The second indicator of conformational flexibility is based on assessment of preferred conformations generated by QMD simulation. The conformers are clustered based on Cα–Cβ orientations of the three side chains at the end of each QMD run. More flexible molecules tend to give more clusters in this process.

Mimics **A** and **1**–**8** were chosen partly because, in our estimation, they are more conformationally constrained than peptides; however, it is necessary to be mindful of their relative flexibilities. Flexible compounds may have more preferred conformers, thus have a better chance of aligning themselves with interface segments. Consequently, EKO evaluations are biased towards more flexible compounds, provided all other factors are equal, simply because a "match" is more likely to be found by screening more conformational partners. By examining the data, we found this was not the dominant consideration for minimalist mimic design. The following discussion elaborates on this conclusion.

Mimics **4**, **6** and **8** have both the most significant degrees of freedom in the series, and number of conformational clusters; these are the most flexible mimics. Conversely, **1**, **5**, and **7**, are the least flexible ones according to the two indicators discussed above. Comparing to Figure D-2 reveals the most flexible mimic (**8**) gave the least hits while (**1**),

being one of the least flexible ones, gave significantly more hits than any other; this is opposite to one might expect if the numbers of overlays at interfaces segments were governed predominantly by conformational flexibility. Structural parameters other than flexibility must be dominant in determining the numbers of hits since there is no apparent correlation between compound flexibility and number of hits. That conclusion cleared the way to search for other structural features that favor good minimalist mimic designs.

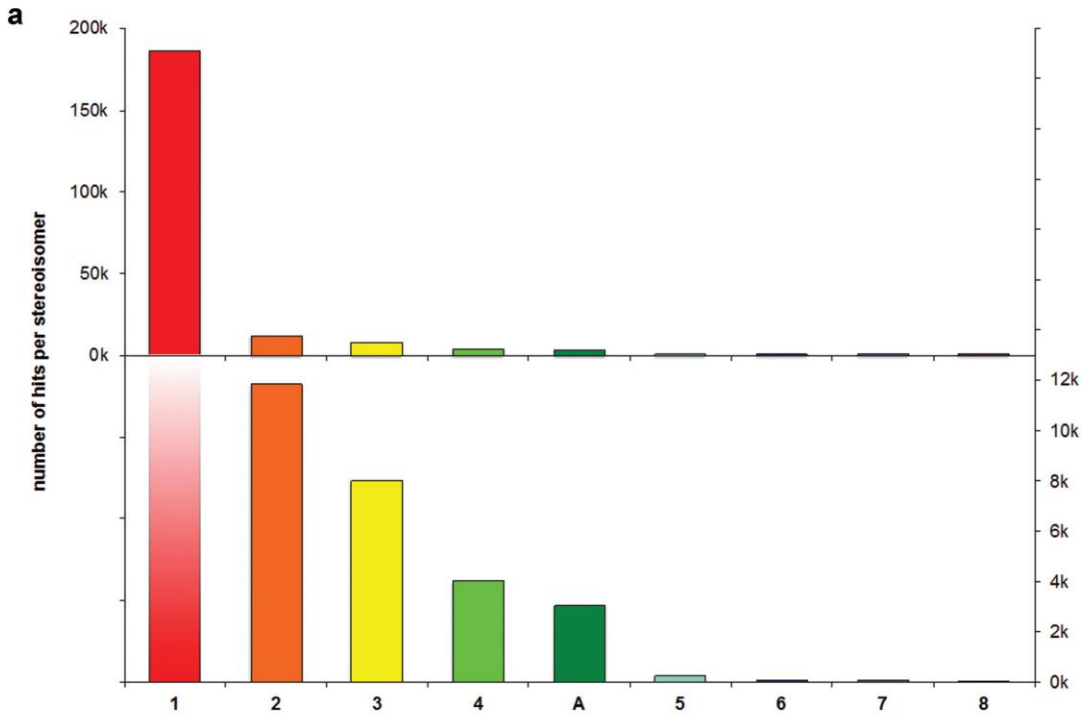

Figure D-2. Number of EKO hits with RMSD < 0.35 Å: **a** averaged over all stereoisomers for **1**–**8** and **A**; **b** breakdown to each stereoisomer for **1**–**4** and **A**. Reprinted with permission from ref 50. Copyright 2019 The Royal Society of Chemistry.

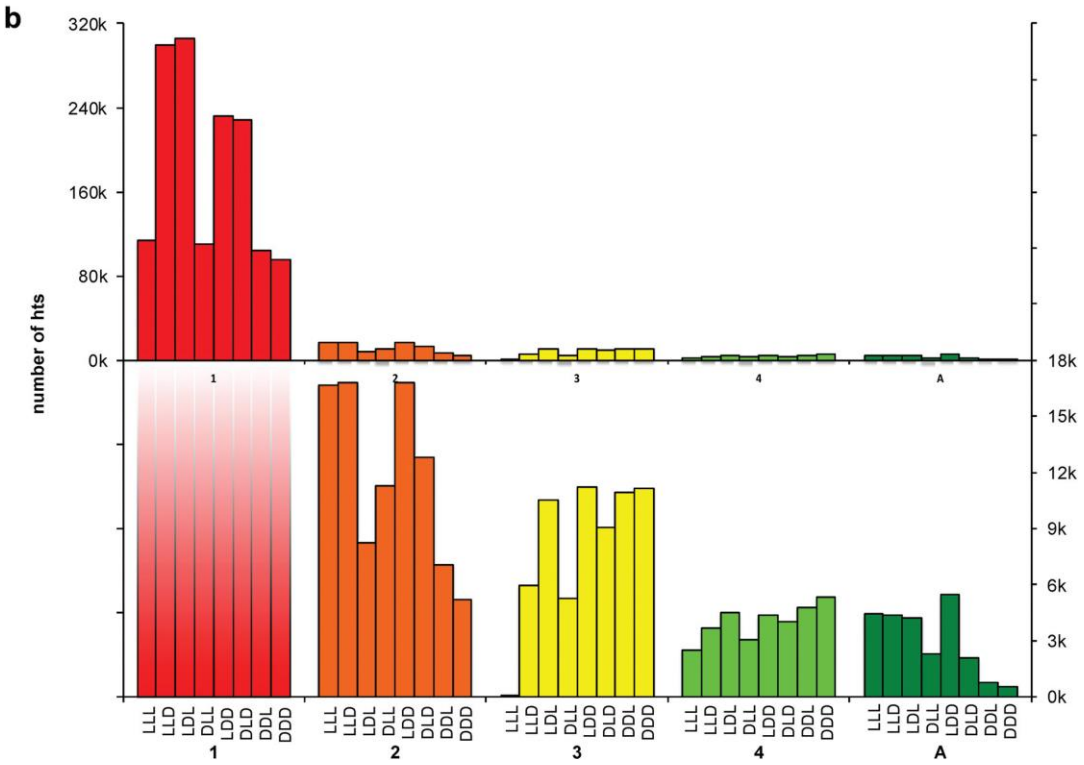

Figure D-2. Continued.

Correlations Between Secondary Structure- and Protein–Protein Interface-Mimicry: The Interface Mimicry Hypothesis[*]

Peptidomimetic A

EKOS analyses of the trimethyl-substituted chemotype LLL-**Aaaa** ("aaa" denotes three methyl side chains analogous to AlaAlaAla; the **aaa** nomenclature is often omitted in this paper for simplicity) indicates it tends to overlay select common secondary structures better than the most effective minimalist mimics as of 2014. Consequently, chemotype **A** is a useful benchmark for good interface mimic design.

Data from an EKOS analysis featuring all the isomers of **Aaaa** were obtained in the current study, whereas the original report only featured the LLL-isomer. Fig. D-3a shows how each of the eight possible stereoisomers (grouped on the x-axis) overlay on the ideal secondary structures, and D-3b arranges the best matching conformers in descending RMSD of the overlays irrespective of stereochemistry. The best overlay identified was for LDD-**A** on a parallel β-sheet (RMSD 0.21 Å). Fig. D-3c illustrates that best fit; the orientations of the side-chains in the ideal parallel β-sheet and the simulated conformer are indeed very close.

Fig. D-3a reveals LLL-**A** is a good mimic for helices, and LDD-**A** is better at mimicking extended structures. Consequently, it seemed likely that LLL-**A** would overlay more frequently on helices at PPI interfaces in the PDB, and LDD-**A** would overlay well

[*] Reprinted with permission from "Correlations Between Secondary Structure- and Protein–Protein Interface-Mimicry: The Interface Mimicry Hypothesis" by Jaru Taechalertpaisarn, Rui-Liang Lyu, Maritess Arancillo, Chen-Ming Lin, Lisa M. Perez, Thomas R. Ioerger and Kevin Burgess, 2019. *Org. Biomol. Chem.*, 17, 3267–3274. DOI: 10.1039/c9ob00204a. Copyright 2019 by The Royal Society of Chemistry.

more frequently on strands and sheets. To check if this is true, we selected the best overlays for each stereoisomer (RMSD < 0.25 Å based the three side-chains) from our previous EKO analysis on >240 000 PPI interfaces. This approach generated 312 and 320 PPI interface matches for LLL- and LDD isomer, respectively. Each match was then analyzed using the DSSP and STRIDE programs. To our surprise, only a small portion of these matches was on regions with clear secondary structures at all (Fig. D-3e and f). DSSP and STRIDE analyses

indicate most (>73%) of the matches were on segments (Fig. D-3f).

Consistent with the Secondary Structure Hypothesis, LLL-**A** does in fact overlay more frequently on helices than LDD-**A** (2.2 and 0.3% of the overlays, as determined by DSSP), while LDD-**A** more frequently matches well on sheets and strands (14.7 and 0%), but this only accounts for small fractions of the best overlays in each case.

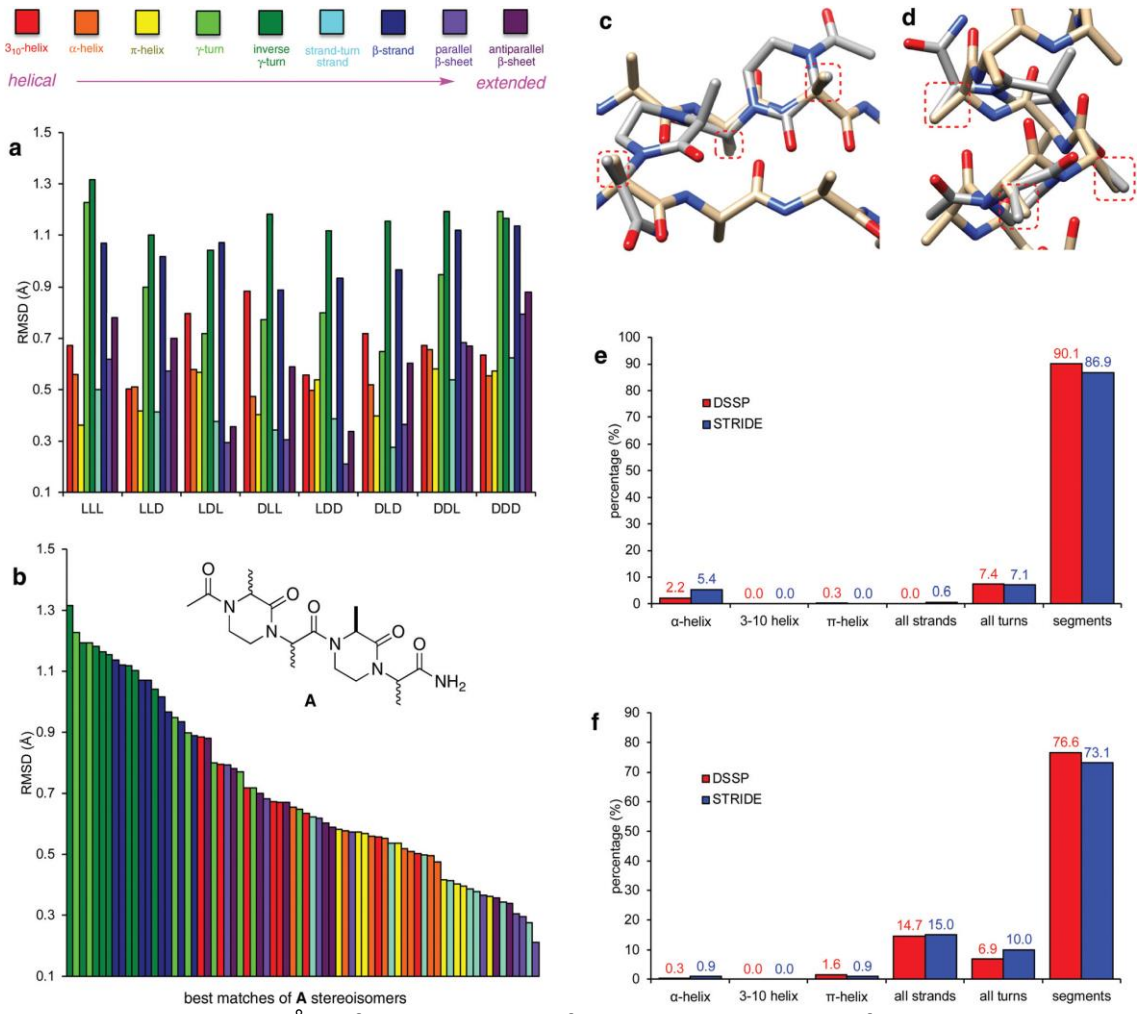

Figure D-3. RMSD (Å) of the overlays of mimics **A** on each of the ideal secondary structures, organized by stereochemistry (**a**) or by decreasing RMSD (**b**).Overlay of preferred conformers of LDD-**A** (silver) on a parallel β-sheet (gold), RMSD 0.21 Å (**c**); and, of LLL-**A** on a π-helix (also gold), RMSD 0.36 Å (**d**). Statistical distribution of secondary structures at PPI interfaces derived by DSSP and STRIDE calculations; **e** the best 312 overlays of LLL-**A** (all RMSDs < 0.25 Å); and **f** 320 overlays of LDD-**A** (RMSD < 0.25 Å). Note that calculations do not differentiate strand-turn-strand, parallel- and antiparallel-sheets. Reprinted with permission from ref 51. Copyright 2019 The Royal Society of Chemistry.

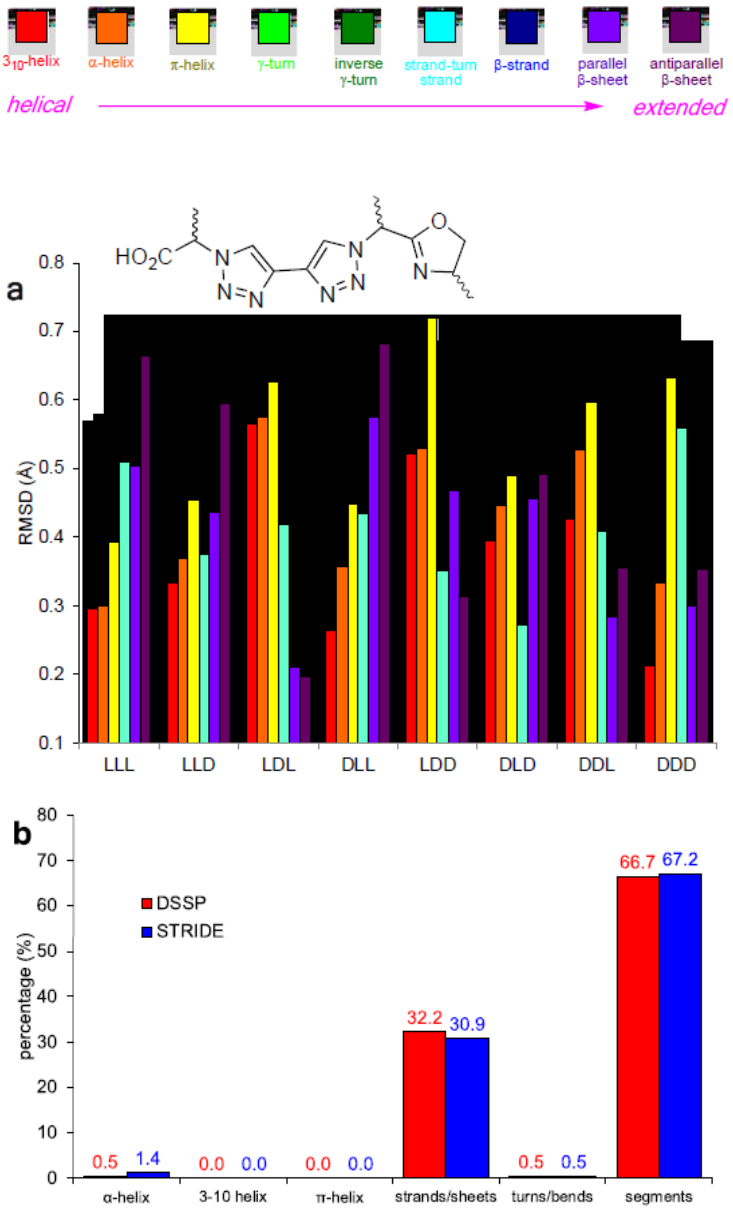

Figure D-4. a RMSD (Å) of the overlays of mimics **4** on each of the ideal secondary structures, organized by stereochemistry. Statistical distribution of secondary structures at PPI interfaces derived by DSSP and STRIDE calculations; **b** the best 369 overlays of LDL-**4**; **c** the best 308 overlays of LLL-**4**. Reprinted with permission from ref 51. Copyright 2019 The Royal Society of Chemistry.

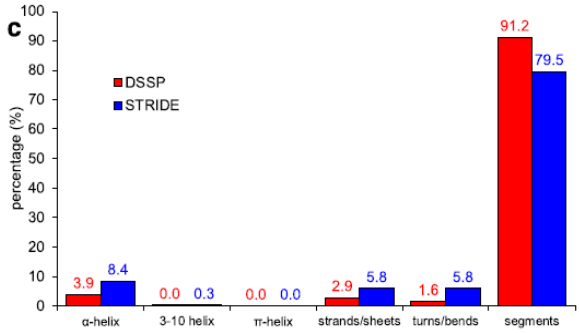

Figure D-4. Continued.

PPI Summary Table

The Burgess' group has designed several chemotypes to potentially perturb different PPIs using EKO. Below are several chemotypes (Figure D-5) ran through several different PPIs. Table D-1 and D-2 show the lowest RMSD of the chemotype matched on the protein given by EKO, with the number of hits below 0.5 Å in parentheses.

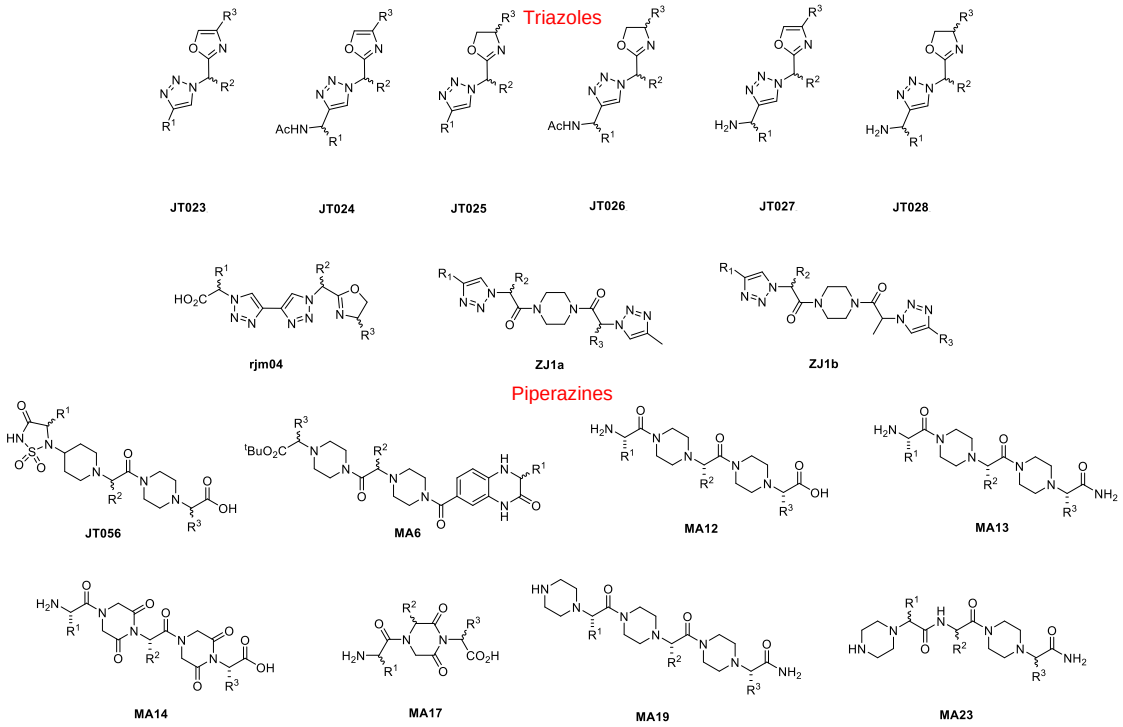

Figure D-5. Different chemotypes with 3 possible side chains.

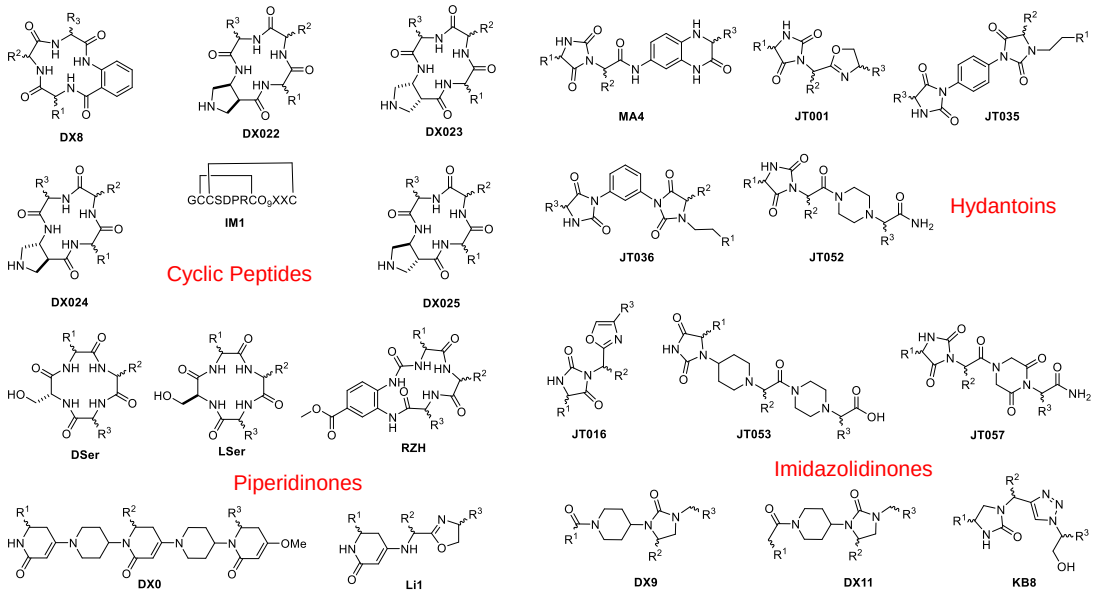

Figure D-5. Continued.

Table D-1. Chemotypes Matching on PPI Cancer Targets.

	PDB	Match	Triazoles										Piperazines							
			JT023	JT024	JT025	JT026	JT027	JT028	MA9	rjm04	ZJ1a	ZJ1b	JT055	MA6	MA12	MA13	MA14	MA17	MA19	MA23
EGFR●EGFR	1MOX	EGFR	0.42 (8)	0.40 (6)	0.34 (21)	0.26 (36)	0.34 (5)	0.26 (39)	0.44 (12)	0.24 (41)	0.36 (14)	0.26 (56)	0.47 (1)	0.43 (2)	0.43 (15)	0.42 (15)		0.33 (20)	0.45 (3)	0.30 (39)
EGFR●TGF-α	1MOX	EGFR	0.37 (4)	0.35 (5)	0.27 (8)	0.34 (9)	0.39 (4)	0.28 (7)	0.49 (1)	0.50 (1)		0.35 (18)	0.37 (8)		0.38 (4)	0.34 (5)		0.24 (7)	0.49 (1)	0.28 (6)
		TGF-α	0.33 (5)	0.37 (12)	0.18 (13)	0.26 (30)	0.37 (12)	0.27 (34)	0.45 (6)	0.29 (17)	0.41 (11)	0.24 (25)	0.31 (11)	0.43 (1)	0.36 (28)	0.36 (27)	0.46 (4)	0.37 (14)	0.37 (12)	0.26 (17)
GDNF●GDNFR-1	3FUB	GDNF	0.33 (6)	0.46 (3)	0.25 (15)	0.33 (14)	0.49 (1)	0.32 (17)	0.43 (1)	0.37 (2)		0.34 (18)		0.42 (2)				0.24 (15)		0.25 (10)
	2V5E	GDNF	0.45 (5)	0.38 (4)	0.32 (14)	0.24 (22)	0.33 (4)	0.22 (21)	0.45 (1)	0.33 (2)	0.45 (1)	0.36 (16)		0.49 (1)	0.49 (2)	0.50 (1)	0.42 (1)	0.26 (24)		0.40 (7)
Mcl-1●Bim BH3	2NL9	Bim BH3		0.49 (1)	0.39 (9)	0.40 (15)		0.41 (17)		0.23 (16)		0.34 (13)							0.47 (1)	0.43 (5)
NEDD8●APPBP1	1R4N	APPBP1										0.50 (1)								
		NEDD8		0.31 (2)	0.47 (2)	0.29 (7)	0.42 (2)	0.38 (5)		0.39 (4)		0.44 (3)								0.40 (6)
NEDD8●UBA3	1R4N	UBA3	0.40 (7)	0.38 (3)	0.29 (14)	0.32 (7)	0.37 (3)	0.34 (7)		0.36 (7)	0.38 (5)	0.25 (9)	0.39 (1)		0.42 (4)	0.42 (5)	0.41 (4)	0.36 (12)	0.43 (3)	0.30 (18)
		NEDD8	0.50 (1)		0.33 (8)	0.40 (14)		0.42 (15)				0.26 (4)						0.31 (14)		0.38 (7)
p53●MDM2	1YCR	p53	0.40 (8)	0.40 (4)	0.27 (20)	0.40 (27)	0.42 (4)	0.36 (30)	0.50 (1)	0.21 (14)	0.41 (3)	0.31 (22)			0.38 (3)	0.37 (3)		0.35 (15)		0.34 (20)
		MDM2		0.49 (2)		0.43 (3)		0.43 (3)		0.45 (3)		0.34 (7)		0.38 (2)	0.47 (1)	0.48 (1)				
PD-1●PD-L1	3BIK	PD-L1			0.39 (10)	0.29 (11)		0.27 (12)		0.25 (19)	0.37 (6)	0.39 (11)	0.47 (2)		0.46 (2)	0.47 (1)	0.41 (3)	0.28 (19)		0.29 (13)
		PD-1	0.29 (2)	0.46 (1)	0.26 (8)	0.39 (7)	0.47 (2)	0.37 (7)			0.42 (2)	0.35 (12)						0.28 (8)		0.36 (1)
	4ZQK	PD-L1													0.45 (1)	0.45 (1)		0.39 (10)		0.41 (2)
		PD-1																0.32 (4)		0.33 (3)
RAS●PI3K	1HE8	RAS	0.40 (4)		0.25 (12)	0.43 (9)		0.43 (10)		0.49 (1)		0.40 (5)						0.22 (19)		0.37 (4)
		PI3K	0.48 (3)		0.33 (13)	0.28 (20)		0.25 (20)	0.47 (1)	0.48 (1)		0.32 (12)						0.27 (19)		0.34 (11)
RAS●SOS	1BKD	RAS	0.31 (5)	0.42 (11)	0.23 (17)	0.31 (32)	0.43 (10)	0.34 (35)		0.25 (25)		0.26 (30)			0.45 (4)	0.47 (5)			0.44 (3)	0.31 (14)
		SOS	0.29 (8)	0.39 (14)	0.26 (25)	0.35 (32)	0.40 (11)	0.34 (29)	0.46 (8)	0.24 (21)	0.42 (5)	0.33 (35)			0.48 (5)	0.47 (8)		0.38 (5)	0.29 (4)	0.29 (14)
uPA●uPAR	2I9B	uPA	0.38 (2)	0.37 (6)	0.27 (27)	0.26 (45)	0.37 (7)	0.29 (39)	0.47 (30)	0.17 (25)	0.25 (36)	0.28 (48)	0.40 (3)	0.40 (9)	0.32 (18)	0.31 (13)	0.41 (3)	0.21 (29)	0.46 (3)	0.22 (58)
	3U73	uPA	0.38 (4)	0.21 (12)	0.28 (20)	0.22 (53)	0.22 (14)	0.19 (49)	0.34 (14)	0.13 (17)	0.22 (28)	0.31 (40)	0.44 (3)	0.50 (1)	0.44 (6)	0.36 (6)	0.37 (6)	0.40 (19)		0.24 (28)
	3BT1	uPA			0.29 (11)	0.34 (20)	0.46 (1)	0.31 (17)	0.45 (2)	0.39 (2)	0.22 (16)	0.30 (21)	0.44 (2)		0.47 (7)	0.46 (6)	0.40 (4)	0.41 (13)		0.22 (42)

Table D-1. Continued.

	PDB	Match	Cyclic Peptides									Hydantoins								Piperidinones		Imidazolidinones		
			DX8	DX022	DX023	DX024	DX025	Dser	IM1	Lser	RZH	JT001	JT016	JT035	JT036	JT052	JT053	JT057	MA4	DX0	Li1	DX9	DX11	KB8
EGFR•EGFR	1MOX	EGFR	0.34 (2)	0.44 (1)	0.42 (2)	0.48 (2)	0.33 (2)	0.38 (2)	0.50 (1)	0.37 (2)	0.45 (1)	0.11 (40)	0.35 (18)	0.36 (4)	0.29 (26)	0.35 (14)	0.46 (3)	0.36 (13)	0.27 (29)	0.40 (9)	0.29 (58)	0.36 (4)	0.33 (5)	0.26 (36)
EGFR•TGF-α	1MOX	EGFR	0.42 (4)	0.28 (2)	0.23 (2)	0.41 (3)	0.30 (3)				0.29 (2)	0.22 (14)	0.26 (7)		0.41 (3)	0.36 (5)	0.47 (3)	0.41 (6)	0.20 (2)	0.38 (3)	0.38 (9)	0.33 (1)	0.38 (2)	0.30 (10)
		TGF-α	0.22 (5)	0.18 (7)	0.17 (7)	0.16 (6)	0.27 (7)	0.30 (4)	0.34 (1)	0.26 (4)	0.15 (7)	0.22 (25)	0.31 (9)		0.39 (9)	0.31 (7)	0.29 (9)	0.42 (10)	0.39 (5)	0.36 (24)	0.25 (42)	0.45 (4)	0.32 (7)	0.29 (35)
GDNF•GDNFR-1	3FUB	GDNF	0.30 (4)	0.29 (3)	0.24 (4)	0.43 (2)	0.27 (6)	0.37 (3)	0.48 (1)	0.43 (2)	0.34 (3)	0.15 (32)	0.33 (13)	0.45 (2)	0.34 (3)				0.33 (2)	0.42 (6)	0.30 (23)	0.41 (2)	0.41 (5)	0.33 (14)
	2V5E	GDNF	0.33 (2)							0.48 (2)	0.36 (5)	0.14 (28)	0.36 (12)	0.48 (2)	0.38 (3)		0.48 (1)		0.44 (1)	0.37 (9)	0.32 (20)	0.34 (2)	0.38 (2)	0.18 (21)
Mcl-1•Bim BH3	2NL9	Bim BH3	0.28 (4)	0.33 (3)	0.36 (1)	0.38 (3)		0.48 (1)	0.47 (1)	0.43 (3)	0.47 (1)	0.29 (14)	0.40 (5)		0.38 (12)	0.46 (2)	0.47 (2)	0.42 (2)	0.30 (15)	0.40 (5)	0.30 (18)			0.43 (14)
NEDD8•APPBP1	1R4N	APPBP1																					0.39 (1)	
		NEDD8		0.47 (1)	0.49 (1)		0.50 (1)	0.46 (1)		0.49 (1)		0.49 (1)	0.50 (1)		0.30 (5)	0.45 (5)		0.41 (2)			0.23 (10)			0.38 (3)
NEDD8•UBA3	1R4N	UBA3	0.25 (1)	0.33 (5)	0.26 (5)	0.39 (4)	0.31 (5)			0.48 (1)	0.28 (6)	0.28 (18)	0.31 (10)	0.37 (6)		0.35 (7)	0.42 (6)	0.46 (2)	0.40 (2)	0.27 (12)	0.27 (14)	0.25 (4)	0.40 (8)	0.26 (8)
		NEDD8										0.13 (13)	0.41 (3)						0.40 (1)		0.30 (13)		0.30 (4)	0.44 (8)
p53•MDM2	1YCR	p53	0.36 (5)	0.43 (1)	0.37 (1)	0.47 (2)	0.42 (4)	0.48 (2)	0.39 (1)		0.44 (1)	0.18 (33)	0.35 (15)	0.37 (6)	0.40 (6)	0.43 (5)	0.48 (1)	0.42 (8)	0.26 (16)	0.38 (5)	0.22 (45)	0.27 (3)	0.31 (4)	0.26 (22)
		MDM2										0.49 (2)		0.48 (1)	0.43 (2)	0.47 (3)		0.40 (2)	0.30 (2)	0.36 (3)	0.44 (4)			0.46 (4)
PD-1•PD-L1	3BIK	PD-L1	0.41 (1)	0.48 (1)	0.46 (1)		0.42 (2)	0..45 (2)	0.41 (1)	0.46 (1)	0.44 (1)	0.35 (12)	0.38 (5)	0.30 (10)	0.29 (11)	0.45 (5)	0.45 (6)	0.47 (2)	0.26 (8)	0.29 (17)	0.29 (19)	0.26 (3)		0.35 (6)
		PD-1		0.22 (2)	0.13 (2)	0.33 (2)	0.27 (2)			0.48 (1)	0.25 (1)	0.13 (16)	0.27 (8)							0.49 (1)	0.36 (6)		0.33 (4)	0.36 (9)
	4ZQK	PD-L1	0.40 (2)	0.48 (1)	0.47 (1)		0.39 (2)																	
		PD-1		0.20 (2)	0.18 (2)	0.34 (2)	0.34 (2)										0.49 (1)							
RAS•PI3K	1HE8	RAS		0.46 (2)	0.48 (1)	0.49 (1)	0.49 (1)				0.44 (4)	0.25 (16)	0.25 (8)		0.50 (1)				0.45 (1)		0.32 (15)		0.31 (4)	0.47 (6)
		PI3K	0.33 (2)	0.39 (1)	0.36 (1)		0.29 (2)	0.39 (2)		0.46 (1)		0.26 (20)	0.38 (7)	0.46 (1)	0.36 (3)				0.41 (2)		0.33 (29)		0.37 (3)	0.34 (11)
RAS•SOS	1BKD	RAS	0.33 (8)	0.37 (7)	0.39 (6)	0.31 (5)	0.34 (2)	0.43 (3)	0.38 (1)	0.39 (3)	0.37 (4)	0.19 (26)	0.23 (7)		0.38 (11)	0.36 (6)	0.50 (1)	0.37 (9)	0.33 (9)	0.30 (8)	0.24 (54)	0.32 (4)	0.42 (2)	0.35 (25)
		SOS	0.32 (4)	0.36 (9)	0.28 (8)	0.33 (5)	0.38 (6)	0.47 (2)	0.42 (1)	0.38 (1)	0.36 (5)	0.24 (29)	0.27 (16)	0.49 (1)	0.39 (8)	0.44 (12)	0.46 (1)	0.38 (13)	0.35 (8)	0.36 (9)	0.27 (41)	0.40 (3)	0.39 (3)	0.31 (26)
uPA•uPAR	2I9B	uPA	0.30 (7)					0.36 (3)		0.34 (3)	0.34 (6)	0.17 (58)	0.27 (18)	0.30 (14)	0.28 (17)	0.30 (18)	0.43 (7)	0.29 (20)	0.24 (28)	0.32 (20)	0.21 (53)	0.29 (6)	0.21 (13)	0.27 (28)
	3U73	uPA	0.16 (9)	0.33 (6)	0.33 (9)	0.33 (5)	0.19 (6)	0.29 (3)	0.32 (2)	0.35 (3)	0.28 (9)	0.17 (38)	0.29 (9)	0.42 (2)	0.33 (11)	0.33 (16)	0.42 (8)	0.26 (13)	0.16 (16)	0.20 (22)	0.25 (60)	0.47 (4)	0.18 (5)	0.20 (41)
	3BT1	uPA	0.28 (5)					0.38 (4)		0.37 (4)	0.31 (5)	0.17 (34)	0.28 (8)		0.37 (4)	0.39 (12)	0.42 (8)	0.30 (15)	0.38 (4)	0.33 (2)	0.28 (23)	0.42 (4)	0.37 (3)	0.29 (16)

Table D-2. Chemotypes Matching on Other PPI Targets.

	PDB	Match	Triazoles											Piperazines							
			JT023	JT024	JT025	JT026	JT027	JT028	MA9	rjm04	ZJ1a	ZJ1b	JT055	MA6	MA12	MA13	MA14	MA17	MA19	MA23
Nef•AP-1	4EMZ	AP-1	0.43 (4)		0.30 (12)	0.43 (9)		0.43 (8)	0.45 (1)	0.31 (5)	0.29 (3)	0.33 (23)					0.44 (1)	0.26 (8)		0.30 (12)
		Nef	0.30 (6)		0.19 (14)	0.40 (7)		0.40 (9)		0.35 (7)	0.38 (1)	0.32 (15)			0.50 (1)	0.39 (2)		0.27 (18)		0.38 (9)
Nef•MHC-I	4EMZ	MHC-I			0.42 (3)				0.44 (1)			0.32 (5)								0.47 (1)
NS5A•NS5A	1ZH1	NS5A	0.41 (2)		0.29 (5)	0.44 (7)		0.41 (7)				0.39 (12)				0.49 (1)				0.41 (2)
PCSK9•LDLR	3GCX	PCSK9	0.40 (2)		0.28 (9)	0.38 (12)		0.36 (11)		0.24 (15)		0.25 (8)						0.21 (13)		0.29 (5)
		LDLR	0.33 (3)	0.43 (6)	0.28 (16)	0.37 (22)	0.46 (4)	0.40 (18)	0.38 (5)	0.35 (13)	0.42 (3)	0.29 (13)		0.36 (6)			0.36 (2)	0.25 (9)		0.27 (17)
TNF-α•TNF-α	3ALQ	TNF-α	0.45 (2)	0.33 (2)	0.32 (16)	0.20 (26)	0.32 (2)	0.19 (25)		0.40 (3)		0.38 (10)	0.35 (2)		0.42 (4)	0.41 (3)		0.24 (29)	0.46 (1)	0.36 (8)
TNF-α•TNFR2	3ALQ	TNF-α	0.39 (3)	0.39 (5)	0.26 (11)	0.38 (19)	0.40 (5)	0.38 (18)		0.22 (5)	0.46 (2)	0.33 (14)		0.29 (4)	0.50 (1)			0.34 (7)		0.27 (7)
		TNFR2	0.49 (2)	0.39 (2)	0.43 (2)	0.42 (3)	0.39 (2)	0.38 (3)		0.43 (7)		0.33 (7)								0.25 (7)

	PDB	Match	Cyclic Peptides									Hydantoins								Piperidinones		Imidazolidinones		
			DX8	DX022	DX023	DX024	DX025	Dser	IM1	Lser	RZH	JT001	JT016	JT035	JT036	JT052	JT053	JT057	MA4	DX0	Li1	DX9	DX11	KB8
Nef•AP-1	4EMZ	AP-1	0.30 (6)	0.32 (3)	0.29 (4)	0.35 (4)	0.28 (2)		0.44 (1)	0.47 (3)	0.25 (3)	0.31 (21)	0.34 (12)		0.40 (4)	0.43 (5)		0.45 (2)	0.37 (2)	0.42 (1)	0.35 (20)	0.29 (2)	0.39 (5)	0.41 (9)
		Nef	0.28 (2)					0.28 (2)		0.28 (2)	0.18 (1)	0.22 (19)	0.29 (10)	0.39 (1)	0.40 (3)				0.35 (10)	0.36 (2)	0.18 (19)	0.39 (2)	0.33 (4)	0.43 (7)
Nef•MHC-I	4EMZ	MHC-I	0.33 (4)					0.34 (1)	0.44 (3)	0.38 (2)		0.38 (4)	0.45 (2)											
NS5A•NS5A	1ZH1	NS5A	0.46 (1)					0.46 (1)				0.23 (9)	0.37 (4)							0.49 (2)	0.33 (10)			0.47 (3)
PCSK9•LDLR	3GCX	PCSK9		0.39 (2)	0.37 (2)		0.40 (1)				0.39 (1)	0.19 (12)	0.36 (7)		0.25 (7)	0.48 (2)			0.38 (5)	0.44 (2)	0.27 (17)	0.45 (1)	0.44 (4)	0.43 (8)
		LDLR	0.15 (4)	0.24 (4)	0.30 (3)	0.29 (5)	0.36 (4)	0.42 (4)		0.35 (5)	0.39 (3)	0.21 (21)	0.28 (11)		0.24 (4)	0.39 (12)		0.21 (8)	0.33 (13)		0.32 (19)	0.45 (1)	0.28 (2)	0.39 (15)
TNF-α•TNF-α	3ALQ	TNF-α	0.34 (4)	0.41 (7)	0.43 (6)	0.39 (3)	0.34 (6)	0.38 (2)	0.50 (1)	0.46 (3)	0.45 (2)	0.20 (31)	0.32 (14)		0.29 (5)	0.38 (6)		0.28 (4)	0.41 (3)	0.28 (26)	0.30 (31)	0.35 (2)	0.35 (5)	0.23 (16)
TNF-α•TNFR2	3ALQ	TNF-α	0.18 (6)	0.22 (8)	0.21 (7)	0.17 (7)	0.28 (6)	0.23 (2)	0.44 (2)	0.24 (2)	0.20 (2)	0.14 (16)	0.27 (13)	0.34 (4)	0.48 (1)	0.30 (7)		0.40 (3)	0.27 (6)		0.29 (21)	0.46 (1)		0.41 (15)
		TNFR2											0.41 (1)	0.37 (7)		0.36 (3)		0.46 (2)	0.36 (4)	0.45 (2)	0.33 (10)	0.45 (1)	0.31 (1)	0.36 (5)

APPENDIX E

ASSAYS DONE FOR OTHER PROJECTS

Relative Toxicities of Tumor-seeking Dyes

Effects On Cell Migration and Wound Healing

Experiments to assess the effects of compounds on cell migration and wound healing are dynamic. Video clips of representative data are linked in the supporting material and quantitative measures of these effects are shown in Figure 3. Six compounds were selected for these experiments, three with *meso*-Cl functionality and three without. Dyes **4**-Cl, **5**-Cl, and **1**-Ph were excluded because their relatively high cytotoxicities preclude measurement of cell migration and wound healing at 30 μM; less effects were observed if these experiments were performed using concentrations of 10 μM. Surprisingly, presence of meso-Cl functionality (in **1**-Cl - **3**-Cl) correlates with reduced migration and wound healing, indicative of potential inhibition of metastatic spread.

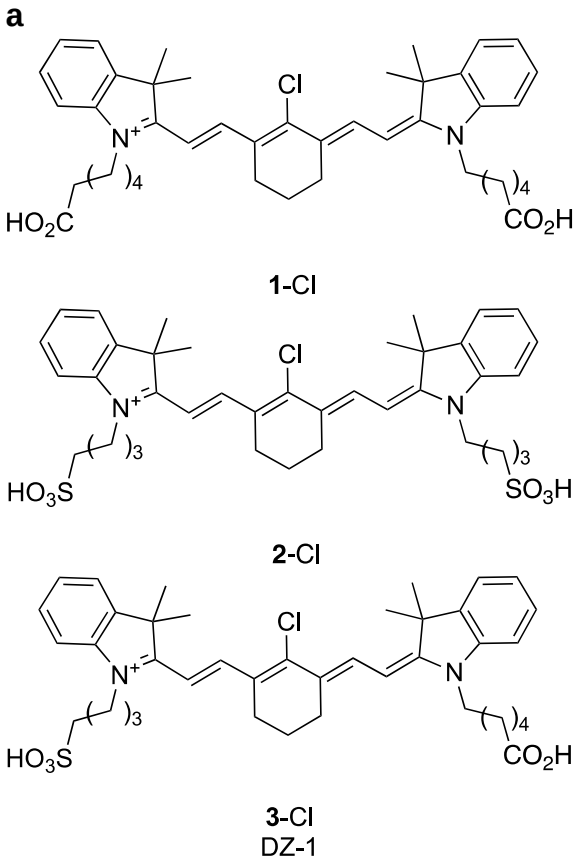

Figure E-1. a Structures of **1**-Cl, **2**-Cl, and **3**-Cl. **b** Migration assay using MDA-MB-231, incubated for 20 hours at 37 ºC with 30 μM of the dyes and 1% FBS in 10% DMEM/F12 and PFHM II. Cells were counted at 10x magnification (EVOS), averaged, and normalized with the DMSO blank to get the relative percent migration shown above. Error bars show standard deviation. **c** Wound healing assay using MDA-MB-231 was incubated for 24 hours at 37 ºC, replacing the media with 30 μM of the dyes and 1% FBS in 10% DMEM/F12 and PFHM II afterwards. Scratch closure average speeds were calculated using the Automated Cellular Analysis System (ACAS) from ibidi,[126] with images taken every 30 min for 45 hours.

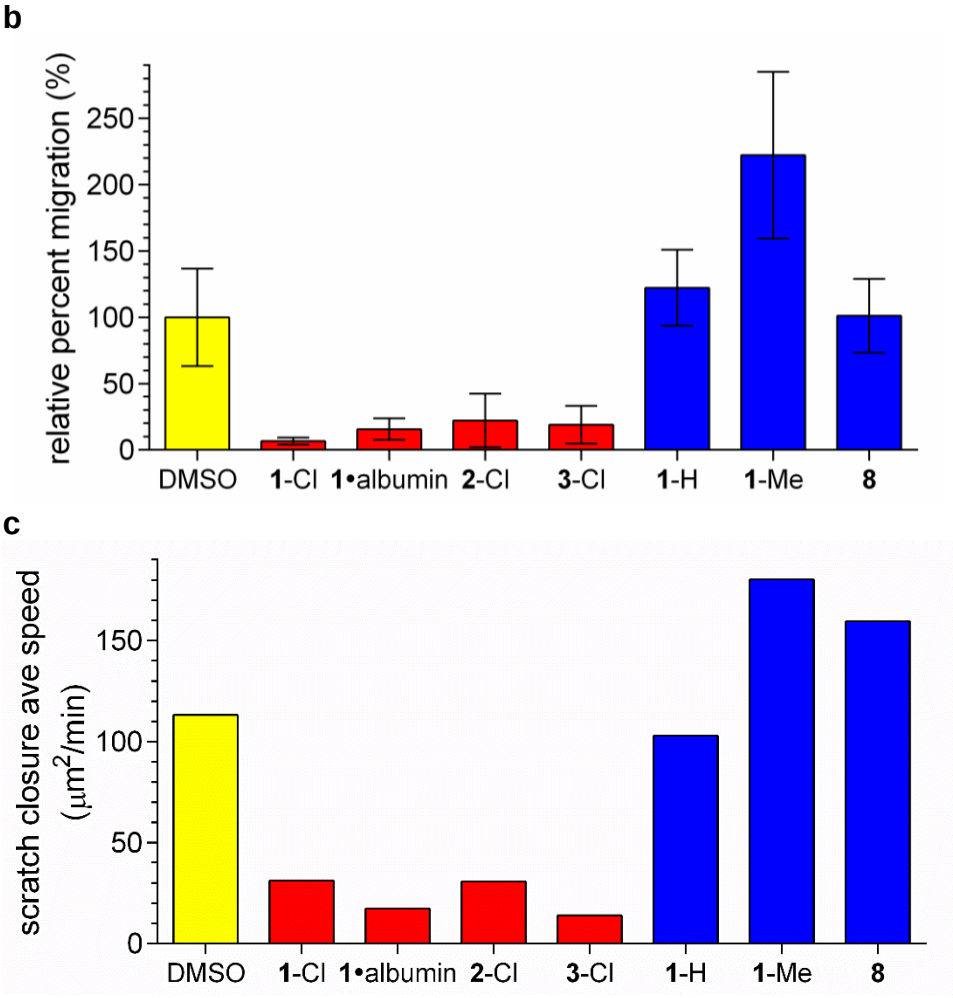

Figure E-1. Continued.

Methods

Wound Healing

Culture-Insert 3 Wells (ibidi) were placed inside a 24-well plate. Using MDA-MB-231, 70 μL of a 3 x 10^5 cells/mL were added into each well of the insert. Plate was incubated for 24 hours at 37 ^oC.

After incubation overnight, inserts were removed, and wells were gently washed with PBS to remove unattached cells. In each well, 500 μL of DMSO or 30 μM of the corresponding dye with 1% FBS in 10% DMEM/F12 and PFHM II were added. Time-lapse imaging was done (EVOS, ThermoFisher) at 37 ºC and 5% CO_2, with images taken every 30 min for 45 hours.

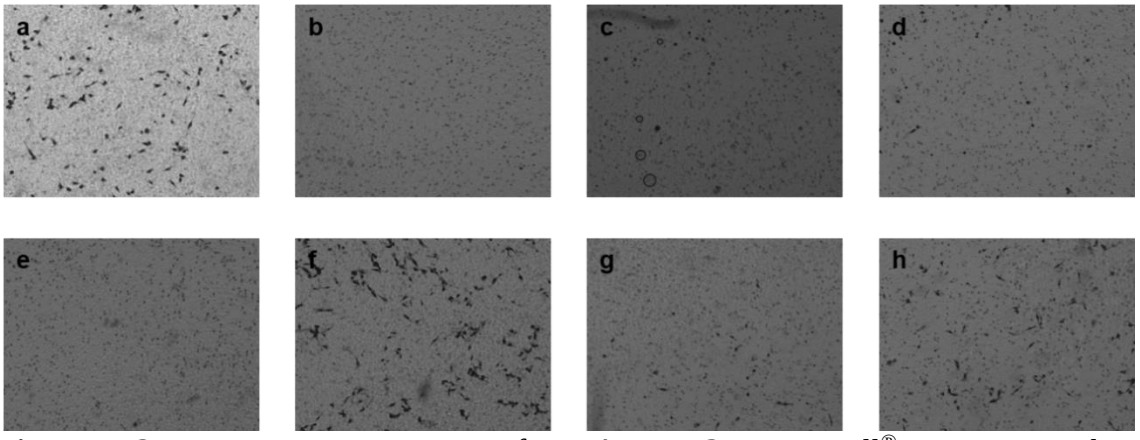

Figure E-2. Representative pictures of MDA-MB-231 Transwell® migration with **a** DMSO and 30 μM of the following dyes: **b 1**-Cl, **c 1**•albumin, **d 2**-Cl, **e 3**-Cl, **f 1**-H, **g 1**-Me, and **h 8**. Pores of the membranes could also be observed as the numerous small and round dots, while the cells are the larger and darker spots/streaks in the picture.

Migration Assay

Twenty-four well Transwell plates (Costar, Corning), with 8 μM pore size inserts, were used. To the lower compartment (in the well), 0.65 mL of DMSO or 30 μM dye and 1% FBS in 10% DMEM/F12 and PFHM II was added before adding the insert to the well. To the upper compartment (inside the insert), 0.2 mL of 2 x 10^5 cells of MDA-MB-231

with 30 μM dye and 1% FBS in 10% DMEM/F12 and PFHM II was added. Plates were incubated for 20 hours at 37 ^{o}C with 30 μM of the dyes and 1% FBS in 10% DMEM/F12 and PFHM II.

After incubation overnight, inserts were taken out and washed with PBS for 3 times. The upper side of the filter membrane is gently swiped with cotton swap to remove cell debris. The lower side of the insert filter was fixed with formaldehyde for 10 min, methanol for 10 min, and stained with Hematoxylin solution (Millipore Sigma) for 20 min, carefully washing with PBS 3 times after each step. Cells were imaged and counted at 10x magnification (EVOS, ThermoFisher).

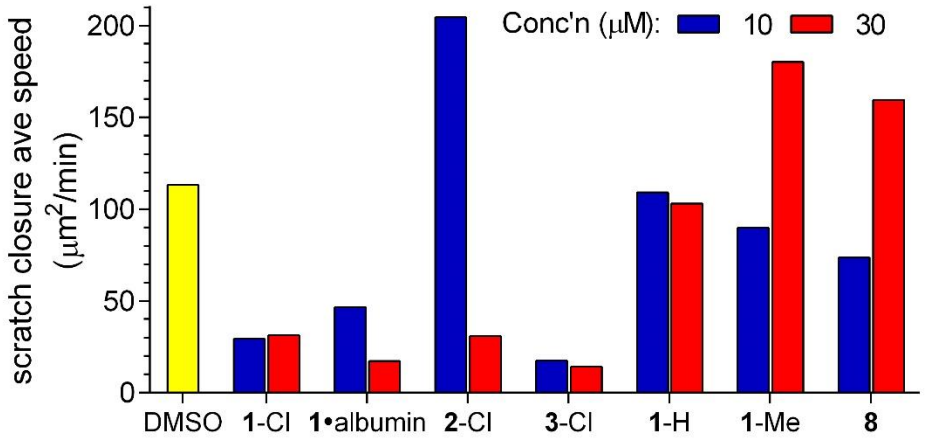

Figure E-3. Wound healing assay using MDA-MB-231 was incubated for 24 hours at 37 ^{o}C, replacing the media with 30 μM of the dyes and 1% FBS in 10% DMEM/F12 and PFHM II afterwards. Scratch closure average speeds were calculated using the Automated Cellular Analysis System (ACAS) from ibidi, with images taken every 30 min for 45 hours.

Small Molecules Targeting the NEDD8•NAE Protein–Protein Interaction[*]

K_i determination via fluorescence polarization

A series of experiments were performed to determine the dissociation constant for binding of LLL-**1lvl** to NAE via fluorescence polarization.[132-133] However, direct labeling of small molecules like LLL-**1lvl** with relatively large fluors tends to impact their K_i values, so a different approach was used. Consequently, the K_i determination was performed in two steps: (i) measure K_d for fluorescein-N8 (labeled positive control peptide) with NAE via directing binding; then, (ii) determine the K_i of LLL-**1lvl** for NAE via competitive binding versus fluorescein-N8. A Z-factor[132] was measured for the assay in step (i) to check its validity; the value was acceptable (0.52). Additionally, NAE binding affinities of two more compounds (DLLL-**3klvl** and LLL-**fsi**) were evaluated; DLLL-**3klvl,** which is similar to the featured lead LLL-**1lvl**, but only containing an extra lysine**,** and a negative control LLL-**fsi** designed for another target,[106] wherein the side chains do not match the NEDD8 *C*-terminus.

Addition of detergent in FP assays can be important to avoid some false positive outcomes.[134] Here the FP assay was carried out with and without addition of 0.01% Tween-20 in buffer; the FP without 0.01% Tween-20 shown in Figure E-4 is essentially identical to that with addition of 0.01% Tween-20 (Figure S8).

---

[*] Reprinted with permission from "Small Molecules Targeting the NEDD8•NAE Protein–Protein Interaction" by Chen-Ming Lin, Zhengyang Jiang, Zhe Gao, Maritess Arancillo, and Kevin Burgess, 2021. *Chem. Sci.*, 12, 1535-1543. DOI: 10.1039/d0sc00958j. Copyright 2021 by The Royal Society of Chemistry.

In the direct binding assay, the K_d of fluorescein-N8 to NAE was determined to be 162 ± 16 nM. Subsequently, the competitive binding assay indicated LLL-**1lvl** binds to NAE with a K_i of 6.4 ± 0.3 μM (Figure E-4), *i.e.* about an order of magnitude less than the labeled peptide *C*-terminus (fluorescein-N8). DLLL-**3klvl** and LLL-**1lvl** have the side-chains and orientations that EKO predicts will bind, but the partial control LLL-**fsi** has different side chains. In the event, both LLL-**1lvl** and the extended sequence DLLL-**3klvl** exhibited micromolar binding to NAE, but the partial negative control LLL-**fsi** did not bind, as expected.

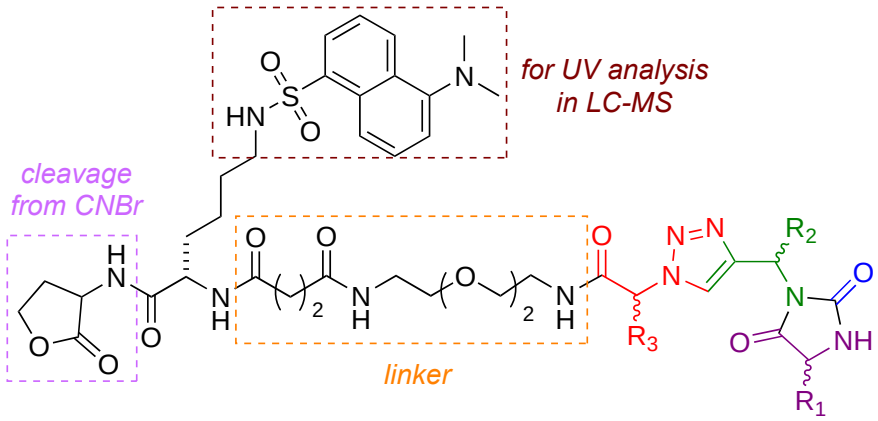

1

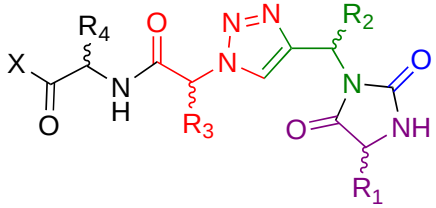

3

X = OH or NH_2

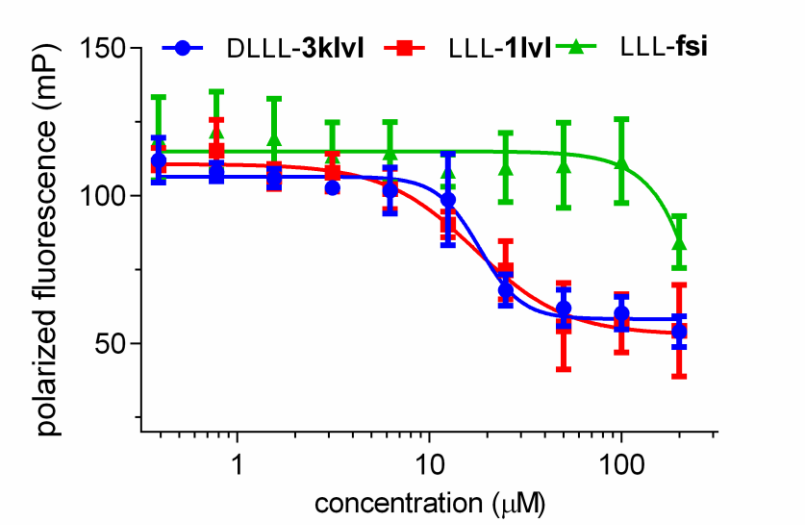

Figure E-4. Fluorescence polarization binding assay for binding to NAE. Competitive binding of the three mimics indicated each with fluorescein-N8. Error bars represent standard deviations based on n = 6. Reprinted with permission from ref 111. Copyright 2019 The Royal Society of Chemistry.